

REPUBLIQUE ALGERIENNE DÉMOCRATIQUE ET POPULAIRE

وزارة التعليم العالي و البحث العلمي

MINISTÈRE DE L'ENSEIGNEMENT SUPÉRIEUR ET DE LA RECHERCHE SCIENTIFIQUE

جامعة غليزان

UNIVERSITE DE RELIZANE

FACULTÉ DES SCIENCES ET TECHNOLOGIES

DÉPARTEMENT DE GÉNIE MÉCANIQUE



THESE DE DOCTORAT LMD 3^{ème} cycle

Filière : Génie mécanique

Spécialité : Energétique

Intitulé de la thèse :

Transfer thermique dans une cavité contenant un cylindre rotatif et rempli de nano-fluide.

Présenter par :

Mr BELHADJ MAHAMMED Amine

Président	KAID-AMEUR Djilali	MCA	Université de Relizane
Directeur de la thèse	FARES Redouane	MCA	Université de Relizane
Co-directeur de la thèse	LOUNIS Mourad	Pr	Université de Kemis Meliana
Examineurs	HABIBI Samir	Pr	UDL-Sidi Bel Abbas
	NAIM Houcine	MCA	UST- Oran
	BENDAOUZI Seif Eddine	MCA	Université de Relizane

Année universitaire : 2023/2024

PEOPLE'S DEMOCRATIC REPUBLIC OF ALGERIA

وزارة التعليم العالي و البحث العلمي

MINISTRY OF HIGHER EDUCATION AND SCIENTIFIC RESEARCH

جامعة غليزان

RELIZANE UNIVERSITY

FACULTY OF SCIENCE AND TECHNOLOGY

MECHANICAL ENGINEERING DEPARTMENT



LMD 3rd cycle DOCTORATE THESIS

Specialty: Mechanical engineering

Option: Energetic

Thesis title:

Thermal transfer in a cavity containing a rotating cylinder and filled with nanofluid.

Presented by:

Mr. BELHADJ MAHAMMED Amine

President	KAID-AMEUR Djilali	MCA	Relizane University
Thesis director	FARES Redouane	MCA	Relizane University
Thesis co-director	LOUNIS Mourad	Pr	Khemis Meliana University
Examiners	HABIBI Samir	Pr	Sidi Bel Abbes University
	NAIM Houcine	MCA	USTO-MB University
	BENDAOU DI Seif Eddine	MCA	Relizane University

2023/2024

Acknowledgments

In the name of ALLAH, the Most Gracious and Merciful, Alhamdulillah, all thanks to ALLAH for His strength and grace in finishing this thesis. Without His guidance and mercy, the achievement of this objective would not have been possible.

I'd like to express my gratitude to everyone who helped make this study feasible. My supervisor, **Dr. FARES Redouane**, in the mechanical engineering department at University of Relizane, Algeria, has provided me with invaluable assistance and advice, for which I am truly grateful. He has been incredibly understanding and patient as my thesis has developed. His encouraging words and recommendations encouraged me to carry out more investigation. His outstanding guidance and support throughout my PhD studies allowed me to acquire a wealth of information and experience that will be useful to me going forward. Without his help, I never would have been able to accomplish the aim.

I would like to thank **Pr. LOUNIS Mourad** for her invaluable support, advice and help in my thesis. I am very grateful to the president and the members of jury who agreed to read and judge my work. I would like to warmly thank all those who, near or far, have shown me their concern to accomplish this work.

And finally, my family has had a major influence in my academic career. I owe everything to my parents, who I would like to thank them for always having faith in me. I want to express my gratitude to everyone who has assisted me, whether directly or indirectly, in finishing my thesis.

Dedications

*With heartfelt gratitude, I extend my appreciation to my beloved **parents**. Their unwavering encouragement and steadfast support echo in my ears.*

*This work is dedicated to my love, **my wife**, and my heart, **my daughter Line**. Their energy and unwritten joy fueled me throughout this remarkable journey.*

*To my sweet sisters **Imane** and her lovely daughter **Assil**, and to my two cherished pieces of heart—my sisters **Douaa & Insaf**—who stood by my side, unwavering and ever-present, this dissertation is dedicated.*

*I also extend this dedication to my first friend, my brother **Oualid**, whose unwavering support sustained me through this process. To my friends and my entire family, your encouragement has been invaluable.*

*Special thanks go to my professors, **Dr. Fares Redouane & Pr. Mourad Lounis**, my greatest cheerleaders during my doctoral program.*

Thank you all

Abstract

Heat transfer is a fundamental concept in engineering, crucial for various industries. It involves the exchange of thermal energy between physical systems. One common application is using a solid-fluid heat transfer medium to either add or remove heat from a system. While traditional heat transfer fluids (HTFs) have been widely used, they often fall short due to their limited thermal properties. Nanofluids (NFs) and hybrid nanofluids (HNFs) are HTFs that have gained attention in recent years. These engineered fluids offer improved thermal characteristics, making them promising candidates for future heat transfer applications.

Researchers have been particularly interested in understanding entropy generation in nanofluid natural convection flow. A mathematical model has been developed to describe this phenomenon, utilizing the Galerkin weighted residual finite element method to discretize the resulting non-dimensional equations.

In this study, we explore steady-state, incompressible free convection flow of nanofluids within different enclosures using computational fluid dynamics (CFD) software. The shape of the enclosure varies, including different configurations of hot and cold walls, straight and wavy sidewalls, and the presence or absence of in-situ barriers.

The study examines the impact of Rayleigh numbers (Ra), Hartman numbers (Ha), Darcy numbers (Da), solid volume fractions (ϕ), and multiple geometrical parameters, on isotherm, streamline, average Nusselt number (Nu_{avg}), and the total entropy generation.

We analyze the impact of these factors on various aspects, including isotherms, streamlines, average Nusselt number (Nu_{avg}), and total entropy generation. Notably, introducing nanofluids enhances heat transfer efficiency under specific conditions. The most significant improvement occurs in conduction-dominated flow regimes, where the enhanced thermal properties of nanofluids play a crucial role. However, when convection dominates heat transfer, nanofluids do not significantly enhance efficiency. Additionally, the buoyant force increases with temperature.

This study of heat transfer in nanofluids reveals intriguing insights. Ra enhances both average Nusselt numbers and natural convection flow. Furthermore, high Ra values make the average

Nusselt number more sensitive to external factors. Flow velocity is lowered by applying Lorentz force in the opposite direction of natural flow. The flow cross-section enters the cavity and circulates more effectively as the Da value rises. The geometrical design of the chamber has a considerable impact on heat transfer performance. Furthermore, installing internal barriers and altering the cavity's size and their walls arrangement were extremely critical.

In summary, nanofluids hold great promise for advancing heat transfer technology. However, a comprehensive understanding of the interplay among various factors is crucial to fully harness their potential in practical applications.

Keywords: Convective heat transport, magnetohydrodynamics, CFD, nanofluids, porous media, Galerkin finite element approach.

ملخص

نقل الحرارة هو مفهوم أساسي في الهندسة، وهو أمر بالغ الأهمية للعديد من الصناعات. يتضمن نقل الحرارة تبادل الطاقة الحرارية بين الأنظمة الفيزيائية. تطبيق شائع هو استخدام وسط نقل الحرارة الصلب-سائل لإضافة أو إزالة الحرارة من نظام ما. على الرغم من استخدام السوائل التقليدية لنقل الحرارة على نطاق واسع، إلا أنها غالبًا ما تكون غير كافية بسبب خصائصها الحرارية المحدودة.

تعتبر النانوسوائل والنانوسوائل المختلطة وسائط نقل الحرارة التي اكتسبت اهتمامًا في السنوات الأخيرة. توفر هذه السوائل المهندسة خصائص حرارية محسنة، مما يجعلها مرشحين مميزين لتطبيقات نقل الحرارة المستقبلية. أظهر الباحثون اهتمامًا خاصًا بفهم توليد الانتروبيا في تدفق الحمل الطبيعي للنانوسوائل.

تم تطوير نموذج رياضي لوصف هذه الظاهرة، باستخدام طريقة العنصر المحدود المتبقي المرتبط بجاليركين لتقسيم المعادلات غير البعدية الناتجة. في هذه الدراسة، نستكشف تدفق الحمل الحراري الحر في حالة الثبات وعدم الانضغاط للنانوسوائل داخل حاويات مختلفة باستخدام برامج الديناميكا السائلية الحاسوبية.

تتفاوت شكل الحاوية، بما في ذلك تكوينات مختلفة للجدران الساخنة والباردة، والجدران الجانبية المستقيمة والموجبة. وجود أو عدم وجود حواجز الموقع. يدرس البحث بالموازاة مع ذلك تأثير أعداد رايلي وأعداد هارتمان، وأعداد دارسي، وعدة معلمات هندسية مختلف.

تكشف هذه الدراسة عن رؤى مثيرة حول نقل الحرارة في النانوسوائل. عدد نوسلت المتوسط وتدفق الحمل الطبيعي يتحسنان بفضل عدد رايلي. علاوة على ذلك، تجعل القيم العالية لعدد رايلي العدد المتوسط لنوسلت أكثر حساسية للعوامل الخارجية يتم تخفيض سرعة التدفق عن طريق تطبيق قوة لورنتز في الاتجاه المعاكس للتدفق الطبيعي. علاوة على ذلك، كان تثبيت الحواجز الداخلية وتغيير حجم الحاوية وترتيب جدرانها أمرًا بالغ الأهمية.

الكلمات الرئيسية: نقل الحرارة، المغناطيسية الهيدروديناميكية، الديناميكا السائلية الحاسوبية، النانوسوائل، وسائط مسامية، النهج العنصري المحدود المرتبط بجاليركين.

Résumé

Le transfert de chaleur est un concept fondamental en ingénierie, essentiel pour diverses industries. Il implique l'échange d'énergie thermique entre des systèmes physiques. Une application courante consiste à utiliser un milieu de transfert de chaleur solide-fluide pour ajouter ou retirer de la chaleur d'un système. Bien que les fluides de transfert de chaleur traditionnels (HTF) aient été largement utilisés, ils sont souvent limités par leurs propriétés thermiques restreintes. Les nanofluides (NF) et les nanofluides hybrides (HNF) sont des HTF qui ont attiré l'attention ces dernières années. Ces fluides non conventionnels offrent des caractéristiques thermiques améliorées, ce qui en fait des candidats prometteurs pour les futures applications de transfert de chaleur.

Les chercheurs se sont particulièrement intéressés à la génération d'entropie dans l'écoulement naturel de nanofluides par convection. Un modèle mathématique a été développé pour décrire ce phénomène, utilisant la méthode des éléments finis résiduels pondérés de Galerkin pour discrétiser les équations sans dimension résultantes. Dans cette étude, nous explorons l'écoulement de convection libre en régime permanent et incompressible de nanofluides à l'intérieur de différentes enceintes à l'aide d'un logiciel de dynamique des fluides computationnelle (CFD). La forme de l'enceinte varie, comprenant différentes configurations de parois chaudes et froides, de parois latérales droites et ondulées, ainsi que la présence ou l'absence de barrières in situ.

L'étude examine l'impact des nombres de Rayleigh (Ra), des nombres de Hartmann (Ha), des nombres de Darcy (Da), des fractions volumiques solides (ϕ) et de multiples paramètres géométriques sur les isothermes, les lignes de courant, le nombre de Nusselt moyen (Nu_{avg}) et la génération de l'entropie totale.

Nous analysons l'impact de ces facteurs sur divers aspects, notamment les isothermes, les lignes de courant, le nombre de Nusselt moyen (Nu_{avg}) et la génération de l'entropie totale. Notamment, l'introduction de nanofluides améliore l'efficacité du transfert de chaleur dans des conditions spécifiques. L'amélioration la plus significative se produit dans les régimes d'écoulement dominés par la conduction, où les propriétés thermiques améliorées des

nanofluides jouent un rôle crucial. Cependant, lorsque la convection domine le transfert de chaleur, les nanofluides n'améliorent pas significativement l'efficacité. De plus, la force de flottabilité augmente avec la température.

Cette étude du transfert de chaleur dans les nanofluides révèle des perspectives intrigantes. Le nombre de Rayleigh (Ra) améliore à la fois les nombres de Nusselt moyens et l'écoulement naturel par convection. De plus, des valeurs élevées de Ra rendent le nombre de Nusselt moyen plus sensible aux facteurs externes. La vitesse d'écoulement est réduite en appliquant la force de Lorentz dans la direction opposée à l'écoulement naturel. La section transversale de l'écoulement pénètre dans la cavité et circule de manière plus efficace à mesure que la valeur de Darcy (Da) augmente. La conception géométrique de la chambre a un impact considérable sur les performances de transfert de chaleur. De plus, l'installation de barrières internes et la modification de la taille de la cavité et de l'agencement de leurs parois étaient extrêmement critiques.

En résumé, les nanofluides offrent de grandes perspectives pour l'avancement de la technologie de transfert de chaleur. Cependant, une compréhension complète de l'interaction entre les différents facteurs est essentielle pour exploiter pleinement leur potentiel dans les applications pratiques.

Mots-clés : *Transport de chaleur par convection, magnétohydrodynamique, CFD, nanofluides, milieux poreux, méthode des éléments finis de Galerkin.*

Nomenclature

List of symbols

Symbols

K	Thermal conductivity [$\text{W. m}^{-1}.\text{K}^{-1}$]
Ra	Rayleigh number
Ha	Hartmann number.
Nu	Nusselt number
Da	Darcy number
Pr	Prandtl number
p	Pressure [Pa]
P	Dimensionless pressure
T	Temperature [K]
g	Gravity acceleration vector [m/s^2]
u, v	Velocity components [m/s]
U, V	Nondimensional velocity components
x, y	Coordinate [m]
X, Y	Dimensionless coordinate
K	Permeability [m^2]
Fc	Forchheimer coefficient
B_0	Intensity of magnetic field
Cp	Heat capacity ($\text{J.kg}^{-1}.\text{°C}^{-1}$)
S_{gen}	Dimensionless entropy generation
Ri	Richardson number
Re	Reynolds number
Gr	Grashof number

Greek symbols

ε	Porosity
α	Thermal diffusivity [m^2/s]
ν	Kinematic diffusivity [$\text{m}^2.\text{s}^{-1}$]
ϕ	Solid volume fraction

β	Thermal expansion coefficient [K^{-1}]
μ	Dynamic viscosity [$\text{W. m}^{-1}.\text{K}^{-1}$]
ρ	Density [kg.m^{-3}]
σ	Electrical conductivity [$\Omega. \text{m}$]
θ	Dimensionless temperature
ψ	Non-dimensional stream function
ω	Rotational speed [m/s]

Subscripts

f	Fluid
bf	Basic fluid
nf	Nanofluid
hnf	Hybrid nanofluid
np	Solid particles
avg	Average
loc	Local
h	Hot
c	Cold
p	Porous medium

Others

a	Length (m)
L, H	Dimension of the cavity [m]
r_{ob}	Radius of cylinder [m]
r_p	Radius of porous media [m]
λ	length of the baffle [m]
ξ	Baffle thickness [m]
dm	Diameter of cylinder (m)
N, und	Undulation number

List of figures

Chapter I	
Figure I.1. heat energy mechanisms	3
Figure I.2. Natural convection	5
Figure I.3. Forced convection	9
Figure I.4. Mixed convection.....	13
Figure I.5. Porous media.....	18
Chapter II	
Figure II. 1. Buoyancy force.....	23
Figure II. 2. Example of FME discretization.....	30
Figure II. 3. Flow diagram illustrating FEM computational process	31
Chapter III	
Figure. III. 1. A schematic representation (a) of the physical scheme and grid distribution (b) of the calculational domain.....	33
Figure III. 2. Comparison of current work (a) with Ref. [93] (b) at Ra=105 and Ha=0.	36
Figure III.3.a. Evolution of the ψ_{\max} , and T for multiple amounts of Ra.....	38
Figure. III.3.b. Evolution of Nu_{avg} with Ra for diverse Ha	39
Figure. III. 3.c. Evolution of Nu_{avg} with Ra for diverse ε	39
Figure. III.3.d. Evolution of Nu_{avg} with Ra for diverse Da	39
Figure. III.3.e. Evolution of Nu_{avg} with Ra for diverse r_p	39
Figure. III.3.g. Evolution of Nu_{avg} with Ra for diverse r_{ob}	39
Figure. III.3.f. Evolution of Nu_{avg} with Ra for diverse ω	39
Figure III.4. a. Evolution of ψ_{\max} and T for various Ha	41
Figure. III.4.b. Evolution of Nu_{avg} with Ha for diverse Da.....	41
Figure. III.4.c. Evolution of Nu_{avg} with Ha for diverse ε	41
Figure. III.4.d. Evolution of Nu_{avg} with Ha for diverse r_p	41
Figure. III.4.e. Evolution of Nu_{avg} with Ha for diverse Φ	41
Fig.III.5 Graphic illustration of the mesh distribution (a) and physical model (b) of the studied geometry.....	43
Figure.III.6. a Evolution of the streamlines and isotherms for multiple amounts of Ra.....	46

Figure. III.6.b Evolution of Nu_{avg} with Ra for different Ha values.....	47
Figure. III.6.c Evolution of Nu_{avg} with Ra for different porosity values.....	47
Figure. III.6.d Evolution of Nu_{avg} with Ra for different Da values.....	48
Figure. III.6.e Evolution of Nu_{avg} with Ra for various nanoparticles concentrations	48
Figure. III.6.f Evolution of Nu_{avg} with Ra for different baffle thickness	48
Figure. III.6.g Evolution of Nu_{avg} with Ra for different baffle length	48
Figure. III.6.h Evolution of Nu_{avg} with Ra for different baffle undulation number.....	49
Figure. III.6.i Evolution of Nu_{avg} with Ra for different values of the empty square sides' length (a).....	49
Figure.III.7. a Evolution of the streamlines and isotherms for multiple amounts of Ha	50
Figure. III.7.b Evolution of Nu_{avg} with Ha for different porosity values.....	51
Figure. III.7.c Evolution of Nu_{avg} with Ha for different Da values.....	51
Figure. III.7.d Evolution of Nu_{avg} with Ha for various nanoparticles concentrations.....	51
Figure. III.7.e Evolution of Nu_{avg} with Ha for different baffle thickness	51
Figure. III.7.f Evolution of Nu_{avg} with Ha for different baffle length.....	52
Figure. III.7.g Evolution of Nu_{avg} with Ha for different baffle undulation number.....	52
Figure. III.7.h Evolution of Nu_{avg} with Ha for different values of the empty square sides' length.....	52
Figure. III.8.a Evolution of Nu_{avg} with the nanoparticles volume fraction for various values of porosity	53
Figure. III.8.b Evolution of Nu_{avg} with the nanoparticles volume fraction for various values of Darcy number	53
Figure. III.8.c Evolution of Nu_{avg} with the nanoparticles volume fraction for various values of baffle thickness	54
Figure. III.8.d Evolution of Nu_{avg} with the nanoparticles volume fraction for various values of baffle length.....	54
Figure. III.8.e Evolution of Nu_{avg} with the nanoparticles volume fraction for various values of the empty square sides' length.....	54
<hr/> Chapter IV <hr/>	
Figure. IV.1: Evolution of ψ_{max} and T for various r_p values.....	57
Figure. IV.2. Evolution of Nu_{avg} with r_p for various ω values	58
Figure. IV.3.a Evolution of ψ_{max} and T for multiple values of ω	60
Figure. IV.3.b. Evolution of Nu_{avg} with ω for various values of r_{ob}	61
Figure. IV.3.c. Evolution of Nu_{avg} with ω for various values of r_p	61

Figure. IV.3.d. Evolution of ψ_{\max} and T for various values of r_{ob}	62
Figure. IV.4.b. Evolution of Nu_{avg} versus the length (a)	63
Figure.IV.5. a Evolution of isotherms and streamlines for various values of Da	65
Figure.IV.5. b Evolution of Nu_{avg} with Da for different nanoparticles volume fraction values	66
Figure.IV.5. e Evolution of Nu_{avg} with Da for different values of undulated baffle length ...	66
Figure.IV.5. f Evolution of Nu_{avg} with Da for different values of undulation number.....	67
Figure.IV.5. g Evolution of Nu_{avg} with Da for different values of the empty square sides length (a)	67
Figure.IV.6. a Evolution of the isotherms and streamlines for various values of porosity	68
Figure.IV.6. b Evolution of Nu_{avg} with porosity for different values of baffle thickness.....	69
Figure.IV.6.c Evolution of Nu_{avg} with porosity for different values of baffle length.....	69
Figure.IV.6. d Evolution of Nu_{avg} with porosity for different values of undulation number .	69

Chapter V

Figure.V.1 Graphical representation of the studied geometry in 2D (a) and 3D (b).	72
Figure V.2. Evolution of S_{gen} with various values of Ra.....	73
Figure V.3. Evolution of S_{gen} with various values of Ha	74
Figure V.4. Evolution of S_{gen} with various values of Da	75
Figure V.5. Evolution of S_{gen} with various values of rotational speeds (ω)	75
Figure V.6. Evolution of S_{gen} and Nu_{avg} for various values of undulation number (N).....	76

List of tables

Table I.1: Examples of recent experiment studies in natural convection.	6
Table I.2: Examples of recent numerical studies in natural convection.	8
Table I.3: Examples of recent experimental studies in forced convection.	11
Table I.4: Examples of recent numerical studies in forced convection.	12
Table I.5: Examples of recent studies in mixed convection... ..	15
Table. III. 1. Effect of the mesh size on average Nusselt number.....	15

Contents

Acknowledgments.....	I
Dedications	II
Abstract.....	III
ملخص.....	V
Résumé.....	VI
Nomenclature.....	VIII
List of Figures.....	IX
List of tables.....	XII
Contents	XIII
Introduction.....	XVII
Context
Aim and objectives
Thesis layout.....

Chapter I

Chapter I Generalities & literature review.....	3
I.1 Overview on convection heat transfer	3
I.1.1 Introduction to convection heat transfer.....	3
I.1.2 Natural convection.....	4
I.1.3 Forced convection.....	8
I.1.4 Mixed convection	13
I.2 Magnetohydrodynamics	16
I.2.1 Definition.....	16
I.2.2 MHD Fluid Mechanics Aspect.....	17
I.3 Porous media.....	17
I.3.1 Definition.....	17
I.3.1 Fluid Flow Models in porous media	18

Chapter II

Chapter II Mathematical Modeling & Computational Technique	22
II.1 Introduction.....	22
II.2 Mathematical modeling.....	22

II.2.1	Definitions of key parameters	23
II.2.2	Governing Equations.....	26
II.2.3	Governing equations for porous media.....	27
II.2.3	Boundary Conditions	28
II.2.4	Non-dimensional formulations	28
II.3	Computational procedures	29
II.3.1	Computational Fluid Dynamics	29
II.3.2	Discretization Approaches	29
II.3.3	Finite Element Method.....	29
II.3.4	Mesh Generation	30

Chapter III

Chapter III Influence of the thermos-physical properties of nanofluids and hybrid-nanofluids	32
III.1 Introduction.....	32
III.2 Case 01: MHD natural convection of a hybrid nanofluid involved in a complex triangular enclosure.....	32
III.2.1 Abstract	32
III.2.2 Characterization of problem	32
III.2.3 Formulation of the Mathematical Model.....	33
III.2.3.1 Mathematical Formulation	33
III.2.3.2 Thermo-physical Aspects of the working fluid	34
III.2.3.3 Validation and test of mesh independency	35
III.2.3.3 Results discussion.....	35
a- Influence of Rayleigh number.....	36
b- Influence of Hartmann number	39
III.3 Case 02: MHD natural convection of a nanofluid involved in a complex C-shaped enclosure	42
III.3.1 Abstract	42
III.3.2 Characterization of problem	42
III.3.3 Formulation of the Mathematical Model.....	43
III.3.3.1 Mathematical Formulation	43
III.3.3.2 Thermophysical Characteristics of the hybrid nanofluid	44
III.3.3.3 Boundary conditions.....	45

III.3.3.4 Results discussion.....	45
a- Influence of Rayleigh number.....	45
b- Influence of Hartmann number.....	49
c- Influence of nanoparticles concentration.....	53
III.4 Conclusions.....	55

Chapter IV

Chapter IV Influence of the geometrical parameters of the cavity.....	56
IV.1 Introduction.....	56
IV.2 Case 01: MHD natural convection of a hybrid nanofluid involved in a complex triangular enclosure.....	56
IV.2.1 Abstract.....	56
IV.2.2 Results discussion.....	56
a- Influence of the porous medium proportion.....	56
b- Influence of the cylindrical barrier radius and its velocity.....	58
c- Influence of modifying the triangular cavity shape.....	62
IV.3 Case 02: Case 02: MHD natural convection of a nanofluid involved in a complex C-shaped enclosure.....	64
IV.3.1 Abstract.....	64
IV.3.2 Results discussion.....	64
a- Influence of permeability.....	64
b- Influence of porosity.....	67
IV.4 Conclusions.....	70

Chapter V

Chapter V Entropy generation analysis in case of MHD natural convection.....	71
V.1 Introduction.....	71
VI.2 Case study: Entropy generation in case of MHD natural convection within a complex cubic cavity filled with a hybrid nanofluid.....	71
V.2.1 Abstract.....	71
V.2.2 Characterization of problem.....	71
V.2.3 Formulation of the Mathematical Model.....	72
V.2.4 Results discussion.....	73
a- Entropy generation versus Rayleigh number.....	73

b- Entropy generation versus Hartmann number..... 74

c- Entropy generation versus Darcy number..... 74

d- Entropy generation versus the rotation speed of the inner cylinder..... 75

e- Entropy generation versus undulation number..... 76

V.3 Conclusions..... 76

Chapter VI

Chapter VI Final conclusions & Way Forward..... 77

V.1 Summary of major conclusions..... 77

V.1 Further works & Way forward..... 79

References.....

ANNEX & Publications.....

Introduction

Context:

In the realm of engineering practice, comprehending the mechanisms of heat transfer has become increasingly vital. Heat transfer plays a pivotal role in designing various instruments and equipment, including power plants, refrigerators, and electronic devices-items that are fundamental to our daily lives. Enhancing heat transfer efficiency remains a central challenge for engineers. The numerous varieties of heat transfer processes are reflected by the heat input into a system, or the removal of heat produced in a process [1].

Heat transfer applications have an impact on people's daily lives, directly or indirectly, and they drive the invention of new research to increase their performance. In recent decades, several enhancement strategies have been developed, including surface vibration, rotating an obstructing item inside a hollow, and changing the roughness of the heat transfer surface. However, these technologies have certain drawbacks, including much higher-pressure loss and increased power needs [1].

Conventional heat transfer fluids with low thermal conductivity, such as water, oil, and ethylene glycol mixes, provide a substantial barrier to improving the performance and efficiency of numerous engineering systems, including exchangers and electronic devices. To address this issue, there is a strong motivation to create innovative heat transfer fluids with much higher conductivity. Minuscule solid particles can be suspended in fluids to increase their heat conductivity. The particles of many types, including metallic, nonmetallic, and polymeric particles, can be combined with fluids to produce more efficient fluids. These limits prompted much inquiry [2].

Maxwell [3] proposed in 1873 the idea of developing an energy-efficient fluid by enhancing the thermophysical properties of conventional fluids. He increased the heat transfer performance of a classic, poor conventional fluid by mixing it with solid particles, which have higher thermal conductivity than conventional liquids. This led to the invention of a new coolant with superior heat transfer capabilities. Nevertheless, Maxwell's theory is out of date and has certain disadvantages, such as erosion, clogging, sedimentation, and a large pressure decrease. As a result, it is incompatible with microchannel flow. Ahuja [4] continued to work on this concept in 1975, investigating polystyrene suspensions. He conducted a series of tests using spheres of polystyrene particles ranging in diameter from 50 to 100 micrometers and mixed with water. The effective thermal conductivity of liquid coolants was discovered to have improved considerably. Nonetheless, due to a lack of technology at the time, the particles were not sufficiently small (on the microscale) to be used properly, particularly in small devices.

Following that, fast advancements in both manufacturing techniques and nanotechnology are viewed as the most important factor driving the main industrial and engineering revolution of the twenty-first century. Nanoparticles with particle sizes of 100 nm or less may currently be

produced. Choi [5] made the most progress on improving the thermal properties of heat transfer fluids in 1995. He discovered that adding a small number of metal nanoparticles to a fluid called "Nanofluid" dramatically increased its heat transmission ability. This idea addresses many of the challenges connected with micron-sized particles floating in a fluid. Because the particles are an order of magnitude smaller, their colloidal stability is significantly higher.

A nanofluid is made up of a base fluid with low conductivity, such as water, ethylene, or mineral oil, and suspended metallic nanoparticles with higher conductivity, such as Al_2O_3 , CuO , and TiO_2 [6]. The use of an optimal nanoparticle volume percentage appears to produce greater than expected effective thermal conductivity, resulting in a higher heat transfer coefficient [7]. Researchers have also investigated the use of nanoparticles as additives to improve heat transfer and thermal performance in conventional fluids. Nanofluids can be homogeneous one-phase or two-phase fluids; A "single-phase flow" occurs when the temperature and velocity of the base fluid and nanoparticles are both the same. A "two-phase flow" occurs when the velocity and temperature of the nanoparticles and the base fluid vary [8].

Furthermore, the form of the cavity and the sort of fluid have a considerable impact on heat convection. To establish the heat transfer convection issue, it has been required to understand geometric shapes, fluid types, and boundary conditions [9] [10]. Both conventional fluids and nanofluids have been used in various research to examine natural, forced, and mixed convective heat transfer types in an enclosure or a moving wall cavity. All types of convective heat transfer have been the focus of extensive investigation until today. On top of that, due to the combined relevance of nanofluids and porous materials in improving heat transfer, extensive research has been conducted to explore the thermal properties of nanofluids in pipes, non-porous cavities, and inside porous media [11] [12].

Aim and objectives:

Although convective heat transfer in enclosures has been extensively researched in recent years, it encompasses a wide range of heat transfer and fluid flow situations within various types of cavities. In recent years, there has been an increased focus in improving heat transfer rates in convective instances. Convection heat transfer may be used in a variety of technical and industrial applications, including electronic cooling, solar energy, and oil extraction. Several elements have been addressed in the literature, including varied enclosure forms, boundary conditions, coolants, laminar and turbulent approaches, and models.

To examine the natural convective heat transfers and flow patterns, innovative designs with a central static or rotating barriers, fins, and baffles were constructed in this study. Furthermore, various heating sources and settings have been developed, and partially or completely porous cavities have been studied. On the other hand, the thermophysical properties of the working fluids have been improved. Nanofluids and hybrid nanofluids are studied under a variety of situations.

This study focuses on natural convective heat transport and fluid dynamics within novel enclosures that are either partly or totally porous. The following objectives guided the research and shaped the content of each chapter. The research aims are as follows:

- Improving heat transfer performance in various applications.
- Investigating nanofluid processes that promote heat transmission and the effects of nanoparticles with variable volume fractions and thermal characteristics.
- Assessing the influence of enclosure geometry and various internal obstacles.
- Understanding how changing the rotating speed and direction of the central cylinder inside the chamber can impact the energy transport.
- Studying the case of implementing inner baffles within the cavities.
- By proposing different cases of heating source configurations, evaluate the heat transfer efficiency and flow patterns inside the geometry.
- Compare average Nusselt number values and total entropy across all analyzed cases.
- Define encouraging prospective and clear forward-looking path for further works.

Thesis layout:

The current thesis has been constructed as follows:

Chapter I: In this chapter, we delve into the literature related to fluid models employed in the PhD thesis. The primary objective is to provide an overview of the key ideas driving this thesis. We begin by discussing porous materials, magnetohydrodynamics, and first natural convection. Subsequently, we explore nanofluids, scrutinizing their origin, production methods, and potential applications and benefits.

Chapter II: We explore the nuances of dimensionless parameters and fundamental ideas that are central to our theory in this part. We first go over the governing equations that explain nanofluid flow in terms of mathematics when porous media and a magnetic field are present. We also investigate the relationships between the non-dimensional numbers pertinent to our investigation and the thermo-physical characteristics of nanofluids.

In addition, we explore methods for numerical solutions and highlight their use in computational fluid dynamics (CFD). Finally, we offer a thorough description of the mesh, form, and validation processes of the computational domain.

Chapter III: The thesis research concerning the thermos-physical characteristics of hybrid nanofluids and nanofluids and their results are the main topic of this chapter. This chapter will examine two distinct cases. First case is a triangular cavity with inner rotative cylinder; filled with a hybrid-nanofluid and including a partial porous media. Second case is a C-shaped porous cavity with inner baffles involving a nanofluid.

Chapter IV: In this section, we delve into the effects of various geometrical configurations on the previously discussed cases. Specifically, we explore the impact of cavity walls, the installation of different types of barriers and the presence of porous media with various values of porosity and permeability.

Chapter V: In addition to the previous chapters, we focused in this section on the calculation of entropy by studying a complex geometry filled with a hybrid nanofluid.

Chapter VI: This final section synthesizes the research findings and suggests potential avenues for future investigation.

Chapter I

Generalities & Literature review

Chapter I: Generalities & Literature review

I.1. Overview on convection heat transfer.

I.1.1. Introduction to convection heat transfer

The field of thermodynamics is focused on the quantification of energy transfer as a system transition between equilibrium states, without consideration for the duration of the process. However, in engineering, there is often a keen interest in the rate at which heat is transferred, which is the primary focus of heat exchange research [1].

Heat transfer plays a crucial role in various industrial applications, encompassing both macroscopic and microscopic scales. Scientists are currently striving to predict and optimize heat transfer rates in a wide array of practical scenarios. The three fundamental mechanisms of heat transfer that are recognized are conduction, convection, and radiation [1].

Conduction refers to the transfer of energy from regions of higher energy within a material to regions of lower energy, because of particle interactions. Conduction heat transfer is characterized by more intense molecular energy at higher temperatures [1].

Radiation, on the other hand, is the emission of energy from materials at nonzero temperatures. Although our focus will be on radiation emitted from solid surfaces, it is also possible for liquids and gases to emit radiation. This emission can be attributed to changes in the electron configurations of the constituent molecules or atoms, irrespective of the material's nature. The energy of the radiation field is propagated through electromagnetic waves, also known as photons. Unlike conduction and convection, radiation does not rely on the presence of a material medium to transmit energy. In fact, radiation transfer is most efficient in a vacuum [1].

Convective heat transfer entails the examination of heat transmission mechanisms brought about by the movement of fluids. The human desire to comprehend and forecast the way fluid flow operates as a "carrier" or "conveyor belt" for energy and substance has resulted in the advancement of convective heat transfer within the realm of contemporary science. Heat transfer and fluid mechanics, two more established scientific fields, converge with convective heat transfer, forming an undeniable nexus. Consequently, the analysis of each convective heat transfer scenario must be founded upon a firm grasp of fundamental principles in fluid mechanics and heat transfer. The objective of this chapter is to elucidate these principles [2].

Natural convection and forced convection are the two branches of convective heat transfer. Forced convection denotes the transmission of heat through induced fluid motion that is compelled to occur. This induced flow necessitates a consistent mechanical power. On the other hand, natural convection differs from forced convection as it is driven by the fluid flow driving force caused by a density gradient and a gravitational field. The buoyancy forces are responsible for driving the flows due to the presence of a density differential. The buoyancy effects caused by this density differential are what lead to flow occurrence. Buoyancy is

caused by the combination of a fluid density differential and body force. The temperature distribution in natural convection is dependent on the intensity of the fluid currents, which are driven by the temperature potential. There are various ways in which these two mechanisms can interact. The simultaneous presence of a buoyancy-driven flow (natural convection) and an imposed flow (forced convection) is referred to as a mixed convection mechanism. Furthermore, convection heat transfer can be categorized as either exterior or internal. In external convection, the fluid surrounds a surface, such as flow across a flat or curved surface. On the other hand, in internal convection, the fluid is surrounded by a surface, such as a pipe conveying steam or a water-filled cooling tube in an internal combustion engine. Fluid flows can be classified as laminar, turbulent, or transitory (transition from laminar to turbulent) [2].

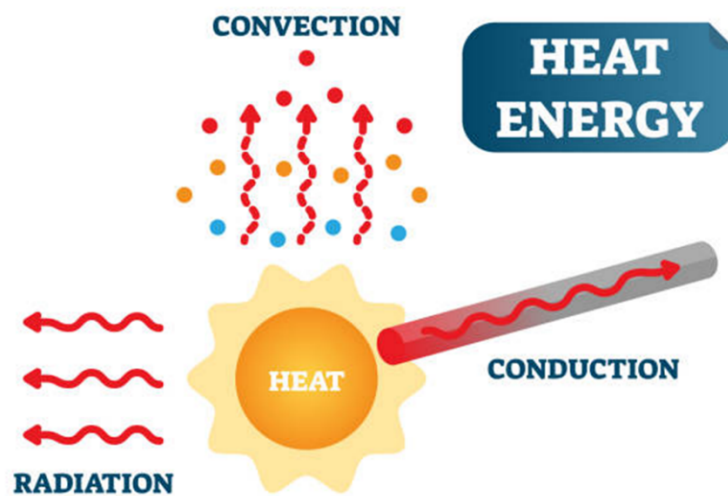


Figure I.1: Heat energy mechanisms

I.1.2. Natural convection

Natural convection is a process that uses the combined forces of conduction and fluid motion to transfer energy from a solid surface to a flowing liquid or gas. The fluid velocity increases with increasing convective heat transfer. In many electronic devices, nuclear reactor cooling and others, natural convection flow is taken into consideration. Natural convection happens when a fluid that is close to a heat source absorbs heat, becomes less dense, and rises because of thermal expansion. Then, the surrounding, cooler fluid flows in to take its place. Academics are interested in it because of its growing importance in technological and environmental applications [13].

Temperature gradient, heat flow, geometry, fluid density, fluid viscosity, fluid heat capacity, fluid thermal conductivity, fluid direction, and enclosure pivot are all known to affect natural convection. In porous materials, porosity and permeability have a significant role in the effectiveness of natural convection. Natural convection has a more complicated reaction, particularly in conjugated domains. Temperature has an impact on a fluid's physical

characteristics. This influence is expressed as streamlines and isothermal lines rather than the thermal boundary layer expression utilized in forced convection. Whether the surfaces are heated isothermally or with a continuous heat flow, the free convection process can be altered. Natural convection in cavities has been analyzed experimentally and numerically, and research has produced increasingly reliable results over time, up to the present day [13].

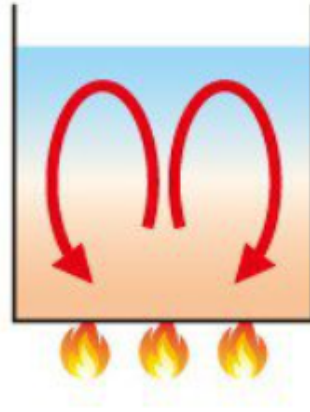


Figure I.2: Natural convection

Many experimental experiments have been conducted in the past. Free convection heat transfer in a horizontal cylindrical enclosure with fluids including water, air, and several silicone oil types was studied by Fand et al. [14] in 1977. The fluids varied in Rayleigh number (Ra) from 2.5×10^2 to 1.8×10^7 . The goal of their research was to ascertain whether the Nusselt number (Nu) depends just on Ra or on both Ra and Pr . Nu is a function of Pr and Ra , as demonstrated by the following correlation:

$$Nu_u = 0.478 Ra_f^{0.5} Pr_f^{0.25} \quad (1)$$

Sparrow and Charmcill [15] investigated in 1983 how temperature changes affected the free convection response of a vertical annulus gap (cylindrical enclosure of an internal cylinder) between two concentric cylinders. Air with a Rayleigh number between 1.5×10^3 and 10^5 used as the working fluid. The experimental results were contrasted with previous work correlations, which included the following correlation (AR , or aspect ratio, confined to a range of [0.1-0.2]) with a 1% validation error:

$$Nu_u = 0.754 Ra_f^{0.204} Pr_f^{0.052} \quad (2)$$

The impact of inclination angle on free convection heat transport in an inclined cylindrical annulus was investigated by Hamad [16] in 1989. It was discovered that the free convection heat transfer coefficient was independent of the inclination degree. Kitamura et al. [17] studied free convection in 1999 by viewing flow patterns around a cylinder's exterior surface and monitoring the temperature distribution on the outside wall surface. The researchers noticed that three-dimensional flow segregation began at the cylinder's irregular borders and progressed until the turbulent transition. It was discovered that local Nusselt numbers

increase considerably in transitional and turbulent flow zones, even though these regions only cover a small part of the cylinder's outer surface.

In 2008, Abu Nada [18] investigated how Rayleigh number, inclination angle, and aspect ratio affect free convection heat transfer in a concentric cylindrical container. The inner cylinder was heated, while the outer cylinder was cooled with cold fluid flowing at a rapid rate. The findings revealed that increasing the aspect ratio greatly reduces the heat transfer rate, while increasing the inclination degree marginally improves the heat transfer rate, and that the heat transfer rate is directly proportional to the Rayleigh number.

In 2011, Yesiloz and Aydin [19] investigated the effect of Ra and inclination on natural convection behavior in a quadrant enclosure. The observations of the vortexes produced by free convection have been discussed. The experimental results coincided well with the streamlines obtained from CFD simulation. In 2016, Ghodsinezhad et al. [20] conducted an experiment to investigate the natural convection of Al₂O₃-water nanofluids inside a rectangular chamber heated differently on two opposed vertical walls. Malvern Zeta sizer, Zeta potential, and UV-visible spectroscopy were all utilized to investigate the nanofluid's characteristics and stability over several volumes Rayleigh numbers (Ra) and viscosity.

In 2020, Toriki and Etesami [21] concentrated on the heat transfer that occurs through the natural convection between SiO₂/water nanofluids at different concentrations and degrees of inclination within a rectangular enclosure. They observed that at low concentrations of nanofluid, the effect of tilt angle on Nusselt number is more pronounced. Nusselt number is less affected by nanofluid concentration as the cavity's inclination angle increases or the heated wall gets closer to its vertical state. The largest values of the Nusselt number were determined for tilt angles of zero degree or level state. The heat transfer rate decreased with increasing inclination angle.

Numerous recent experimental papers have been published in the last few years, discussing various scenarios related to the optimization of natural convection of hybrid-nanofluids and nanofluids.

Table I.1: Examples of recent experiment studies in natural convection.

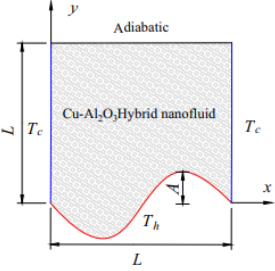
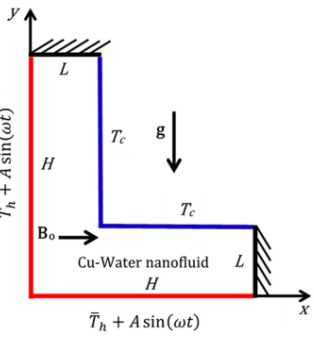
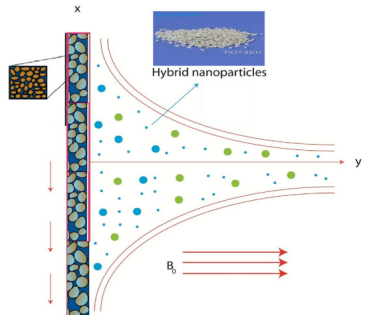
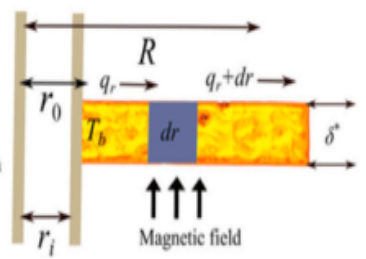
Authors /Year	Subject	Nanofluid	Outcomes
Ammar M. Abdulateef [22] /2023	Experimental Approach for Improving Natural Convection Heat Transfer using Nanofluid in a Porous Heat Exchanger Unit.	Nanofluid : Cu	Porous triplex tube heat exchanger (TTHX) has a lower Nu number compared to pure TTHX, with a ratio 24%. The porous construction led to slower fluid circulation and reduced buoyant forces.

Debashis Dey and Sukanta K. Dash [23] /2023)	An experimental study of natural convection nanofluids in a cavity with and without a rotating magnetic field.	Nanofluid : Al ₂ O ₃ Nanofluid : Fe ₃ O ₄	When there is a magnetic bead in the cavity, the rotational electromagnetic field improves heat transmission for non-magnetic nanofluids.
T.O. Scott et al. [24] /2023	experimental investigation using Al ₂ O ₃ -MWCNT/water hybrid nanofluids on the effect of volume concentration on natural convection heat transfer.	Hybrid-nanofluid: Al ₂ O ₃ -MWCNT	At a volume concentration of 0.10%, heat transmission increased by 49.27% compared to the base fluid.
Nazarahari et al. [25]/2024	Experiments focus on the natural convection heat transport of nanofluids in different shaped holes of porous media.	Nanofluid : Al ₂ O ₃ Nanofluid : Ti ₂ O ₃	Heat transfer efficiency and Nusselt numbers for nanofluids and porous media are maximum at a chamber angle of 30° and lowest at 0°.

likewise, several of numerical studies have been carried out with the goal of optimizing natural convection's efficiency and comprehending the influence of any prospective characteristics on the performance of heat transfer. Keyhani et al. [26] examined flush-heated and alternatively unheated partitions of equal measurement on the divergent standing wall, as well as free convection heat transmission within a rectangular enclosure with an isothermal vertical cold wall in 1988. According to the results, stratification was the primary factor regulating the heated compartments' temperature, and turbulent flow happened when the local modified Rayleigh number (Ra) varied between 9.3×10^{11} and 1.9×10^{12} . Solutions for the natural convection situation in a square chamber with distinct heat sources were found by Ahmed and Yovanovich [27] in 1992. The aspect ratio defined in this study (A) = 1, $0 < Ra < 10^6$, and $Pr = 0.72$ (air as the working fluid), numerical modeling was completed. The aspect ratio (A) divided by the height of the heat source (S) yielded the Rayleigh number. Validation of this work was attained at $Ra = 0$ (conduction limit). The link between the Nusselt number and the Rayleigh number was examined over a range of scale lengths. To investigate natural convection in buildings, Kulkarni [28] looked at putting a sidewall heater behind a chilly window in 1998. The aim of the study was to investigate transitory free convection in a rectangular container sustained under various Ra values. Ra is often raised to cause Nu to increase in $[8 \times 10^{10} - 2 \times 10^{11}]$ range.

More recent numerical studies are summarized in the table below.

Table I.2: Examples of recent numerical studies in natural convection.

Authors/year	Geometry	Nanofluid	Outcomes
Hakim T. Kadhim et al. [29]/2022		Hybrid nanofluid: Cu-Al ₂ O ₃	Major impacts of local thermal non-equilibrium are seen for high Darcy number and low modified conductivity ratio values.
Khalid B. Saleem et al. [30]/2023		Nanofluid: Cu	The higher the temperature oscillation amplitude applied to the hot walls, the greater the peak Nusselt number. The frequency at which the peak Nu occurs remains almost constant as the oscillation amplitude increases, in contrast to the square cavity case.
Mumtaz Khan et al. [31]/2023		Hybrid nanofluid: TiO ₂ -SiO ₂	As the buoyancy forces increase, the hybrid nanofluid's heat transfer rate at the permeable vertical surface increases by 56,51%.
ALBAIDANI, Mashaal M., et al. [32]/2023.		Nanofluid: Al ₂ O ₃ Nanofluid: Cu Nanofluid: CuO	The fin is made more efficient by considering Al ₂ O ₃ , CuO, and Cu by using ternary nanomaterial with concentration factors up to 2.0%.

I.1.3. Forced convection.

The task of enhancing convective heat transfer, together with the accompanying theoretical and practical obstacles, is currently emerging as a distinct and rapidly developing area of heat exchange research. Major of the apparatus, tools, and technology necessary for the various

types of heat exchangers that may be used to remove intense heat. The relevance of this issue is determined by the objective of achieving maximum compactness with minimal material consumption, improving heat exchange performance factor, and decreasing energy prices. Several experimental and numerical investigations of forced convection have been conducted over time [33].

The notion of "forced convection" refers to when the fluid's motion is sustained by a force in the form of a pressure difference supplied by an external device. Forced convection is one of the most efficient techniques of heat transfer since it induces fluid motion by an external source such as a suction device, pump, fan, and so on. The process is widely employed in highly high-temperature systems, including surface optimization for increased heat transfer, electric circuitry cooling, cooling channels, nuclear power systems, heating and cooling applications, and petrochemicals. External forces drive the fluid to flow across a surface, through a vented chamber, or via a duct. Because forced convection produces more fluid motion than free convection, it is used in a wide range of technologies and technical applications [34].

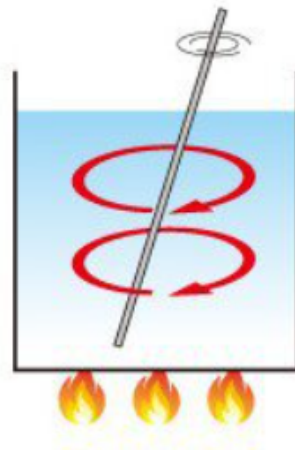


Figure I.3: Forced convection.

Several experimental investigations have been conducted thus far on the forced convective heat transfer of nanofluids. Experimental studies of the flow properties and convective heat transfer of water-based nanofluids based on TiO_2 and Al_2O_3 through a horizontal tube were conducted in 1998 by Pak and Cho [35]. They presented the first regression correlation that predicts the Nusselt number of nanofluid independently of the solid volume percentage of nanoparticles. An experimental study on the convective heat transfer of copper-water nanofluids in a straight tube with a constant heat flux wall was reported in 2003 by Xuan and Li [36]. Their sponsorship proved that the heat transfer rate of nanofluid was greater than that of pure water. In 2004, Wen and Ding [37] conducted experiments to investigate the convective heat transport of alumina-water nanofluids via a copper tube in a laminar flow regime. Their findings clearly demonstrate that the use of nanofluids, especially at higher Reynolds numbers, considerably enhances convective heat efficiency. In 2010, Chandrasekar

et al. [38] reported a 51% increase in the convective heat transfer coefficient for thermally completely developed turbulent tube flow of Al_2O_3 -water nanofluid at 0.2 vol.% compared to pure water. Fotukian et al. [39] investigated the turbulent convective heat transfer performance and pressure drop of a 0.24% volume Copper oxide-water nanofluid traveling through a circular tube. The experimental results reveal that a 25% increase in heat transfer coefficient is associated with a 20% increase in pressure drop. In 2012, Kanjirakat and Raza [40] conducted an experiment to investigate the effect of these factors on heat transfer during the flow of water and aqueous nanofluid in a microchannel with a constant wall temperature boundary condition at the bottom surface and an insulated boundary condition on the top and sides. The purpose of their work is to explore the heat transfer performance of nanofluids in an industrial model heat exchanger. This study examined the laminar flow of SiO_2 -water nanofluids within a rectangular microchannel flow assembly. The influence of flow rate on thermal performance of this nanofluid is explored, as well as fluctuations in thermophysical characteristics under different experimental conditions. Ho and Lin [41] conducted an experimental investigation in 2014 to examine how using alumina-water nanofluid over pure water in an iso-flux heated horizontal circular tube at a constant heating power affects the effectiveness of turbulent forced convective heat transfer. In 2017, Ghasemi et al. [42] conducted an experiment to investigate the forced convective heat transfer of nanofluid as a coolant running through a heat sink. The researchers found that using nanofluid as a coolant instead of pure fluid enhances heat transfer performance by increasing the amount of heat loss. Furthermore, the impacts of various key factors, such as Reynolds number and nanoparticle concentration, on the heat sink's thermal and hydrodynamic characteristics are comprehensively investigated. In addition, the pressure drop across the nanofluid heat sink is just slightly higher than that of the pure water-cooled heat sink. Salari et al. [43] investigated the forced convection heat transfer of a nanofluid in a heat exchanger filled with partly porous material in 2020. The results indicated that the performance evaluation criteria (PEC) parameter rose considerably. The highest PEC was 1.19 at a nanoparticle concentration of 1.0%. The influence of porosity in porous materials on EPC was also investigated. The results showed that decreasing the porosity enhanced the PEC. The Nusselt number was very sensitive to variations in porosity. As a result, using partial porous media to improve the thermal performance of heat exchangers in industrial applications is recommended. New correlations are shown for estimating the Nusselt number and friction factor in empty tubes and tubes containing partially porous material. Talebi et al. [44] carried out an experimental study in 2022 to examine the heat transfer effects of hybrid nanofluids on the flow around a vertical rod with a cosine heat flux. Hybrid nanofluids are made by mixing TiO_2 and Al_2O_3 nanoparticles with deionized water. There are turbulence experiments as well as laminar flow tests conducted. based on the findings. There is over 20% between 1.5% Al_2O_3 and water.

The following are few recent experimental works focused on the behavior of nanofluids and hybrid nanofluids under the effect of forced convection.

Table I.3: Examples of recent experimental studies in forced convection.

Authors /Year	Subject	Nanofluid	Outcomes
M. Ziad Saghir and Mohammad M. Rahman [45]/2022	Experimental study of forced convection using Al ₂ O ₃ , Fe ₃ O ₄ , ND-Fe ₃ O ₄ , and (MWCNT-Fe ₃ O ₄) hybrid-nanofluid in rectangular channels.	Nanofluids: Al ₂ O ₃ , Fe ₃ O ₄ , ND-Fe ₃ O ₄ Hybrid nanofluid: MWCNT-Fe ₃ O ₄	0.2% vol Al ₂ O ₃ transfers heat more effectively than 0.3% vol Al ₂ O ₃ . And 0.2% vol Fe ₃ O ₄ nanofluid is the best fluid for heat extraction.
S.H. Abdel-Latif et al. [46] /2022	Experimental examination of forced convection heat transfer with CNTs and CuO water-based nano-fluids.	Nanofluid: CNTs Nanofluid: CuO	A nanofluid made with 0.1% vol. CNTs showed a maximum heat transfer coefficient boost of 26.55%, whereas 0.5% vol. CuO produced a 20.6% increase.
Vinay Singh et al. [47] /2023	An Experimental Study Putting Forward a Novel Correlation to study thermophysical Properties and Convective Heat Transfer of nanofluids in a Copper Tube.	Nanofluid: Al ₂ O ₃ Nanofluid: CuO	The average heat transfer coefficient increased by up to 50.62% when Al ₂ O ₃ nanofluids were utilized at 0.5 wt%, while CuO nanofluids at 0.5 wt% concentration and a Reynolds number of 2200 indicated a 52.74%
A Pouranfard et al. [48] /2023	Forced convection heat transfer in an upward two-phase air-water/SiO ₂ nanofluid flow with a slug flow regime.	Nanofluid: SiO ₂	Greater Nusselt numbers and heat transfer coefficients (HTC) for two-phase air/water flow under the same regime in comparison to air/aqueous nanosilica nanofluids.

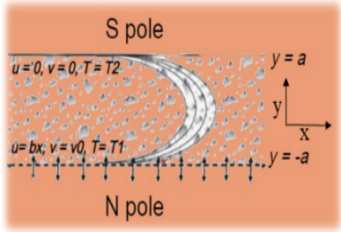
It has become more convenient to use computational methods to investigate heat transfer characteristics with nanofluids because of the rising expense of NPs and the instability of real nanofluids. To date, many numerical studies have been undertaken to acquire a better understanding of the impacts of diverse properties such as different shaped non-circular ducts and nanofluids. The vast bulk of these numerical studies have been conducted to compare simulation situations to previous experimental examples. Numerical analysis is an effective method for investigating forced convection applications at a reasonable cost and with the most exact findings. The outcomes of numerical investigations contribute to the enhancement of present and future experimental works [49].

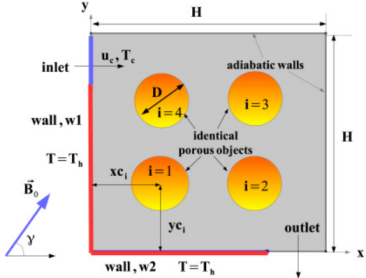
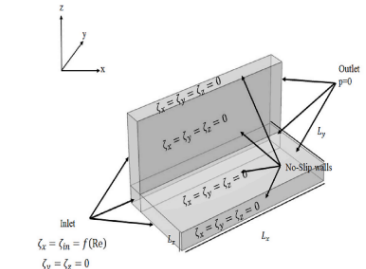
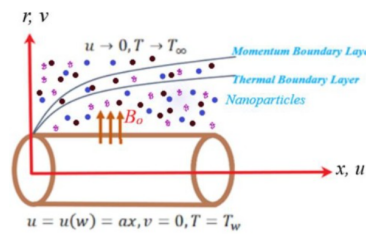
In 2005, Maiga et al. [50] conducted a computational analysis to investigate the forced convection flow of water-Al₂O₃ and ethylene glycol- Al₂O₃ nanofluids inside a uniformly

heated tube with a constant and uniform heat flux at the wall. The results showed that adding nanoparticles considerably improved heat transfer at the tube wall in both the laminar and turbulent regimes. Heat transfer improves with increased particle concentration. However, the presence of particles has had a detrimental influence on wall friction, which increases with particle volume concentration. In 2009, Praveen et al [51] numerically investigated the turbulent flow and heat transfer of three unique nanofluids CuO, Al₂O₃, and SiO₂ traveling through a circular tube filled with ethylene glycol and water under continuous heat flux. In 2010, Vajjha et al [52] conducted a numerical analysis of three-dimensional laminar flow and heat transfer using two different nanofluids, Al₂O₃ and CuO, in an ethylene glycol and water mixture circulating through the flat tubes of an automobile radiator to determine their superiority over the base fluid. In 2012, Choi and Zhang [53] used the finite element technique to study the laminar forced convection heat transport of Al₂O₃-water nanofluid in a conduit with a return bend. According to the findings, when the Reynolds and Prandtl numbers grow, so does the average Nusselt number, and an increase in specific heat in the nanofluid adds to improved heat transmission. Secondary flows cause the average Nusselt number in the return bend to be larger than that in the inlet and exit pipes. Mashaei et al. [54] conducted numerical research in 2016 to investigate the forced convection behavior of water-Al₂O₃ nanofluid in a tiny annulus filled with porous medium with variable properties. It is determined how heat load and particle concentration levels impact the thermophysical properties, velocity, pressure, and temperature fields, as well as the heat pipe's thermal performance. In 2019, Selimefendigil et al [55] conducted a numerical analysis of the behavior of a CNT-water nanofluid used as a working fluid to examine forced convection in a three-dimensional conduit featuring an elliptic cross-section. In 2021, Alsabery et al. [56] released a numerical study that described the motion of the particles in a laminar nanofluid flow in a wavy channel using the second Newton's law. The effects of dimensionless time, waviness number, and Reynolds number on flow structures and heat transmission have been studied.

More recently, Serval numerical studied have been published to provide deeper understanding on the forced convection heat transfer and the associated behavior of nanofluids.

Table I.4: Examples of recent numerical studies in forced convection.

Authors	Geometry	Nanofluid	Observations
B. Jalili et al. [57] /2023		Nanofluid: CuO	As the nanofluid volume percentage increased, the temperature profile shrank, and the maximum Nusselt number was produced by platelet-shaped nanoparticles.

<p>Fatih Selimefendigil and Hakan F. Öztop [58] /2023</p>		<p>Hybrid-nanofluid : Ag-MgO</p>	<p>The PCs (porous cylinders) can be used to regulate the quantity and magnitude of vortices. When the cylinders with the lowest permeability are considered, the average Nu values increase.</p>
<p>Nevzat Akkurt et al. [59] /2023</p>		<p>Hybrid-nanofluid : Cu-Al₂O₃</p>	<p>Increasing the volume % of copper and aluminum oxide both raises the average Nusselt number near the center of the channel, but the rate of growth due to copper is the highest.</p>
<p>Ahmed Jan et al. [60] /2024</p>		<p>Ternary hybrid-nanofluid : Al₂O₃ - Fe₂O₃ - SiO₂</p>	<p>The effect of (Al₂O₃ + Fe₃O₄ + SiO₂) on the thermal profile is greater than (Al₂O₃ + Fe₃O₄) or Al₂O₃, and the thermal profile increases when the radiation parameter values grow.</p>

I.1.4. Mixed convection.

Mixed convection flows arise when forced convection and natural convection combine. Mixed convection in a lid-driven enclosure is a fascinating subject in engineering and related industries, such as electronic equipment cooling. The design of solar collectors, furnaces, building thermal systems, drying and air conditioning technologies, and so on. Several scholars investigated the effects of mixed convective fluxes in cavities and channels using computational, experimental, and analytical techniques [61].

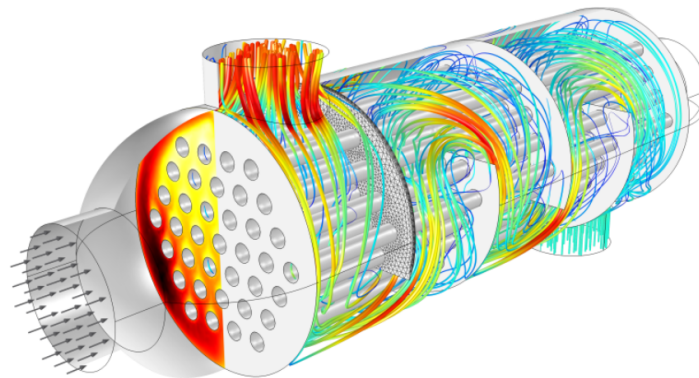


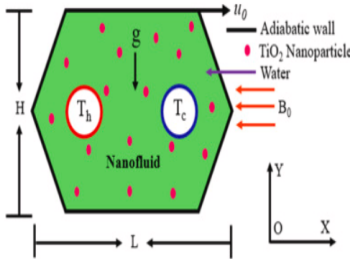
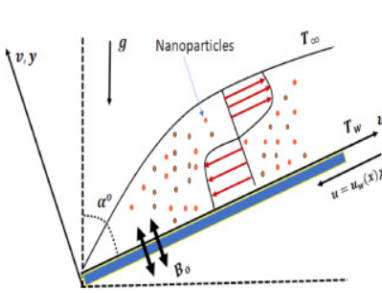
Figure I.3: Mixed convection

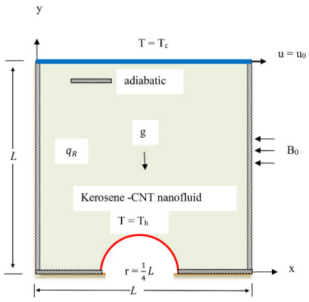
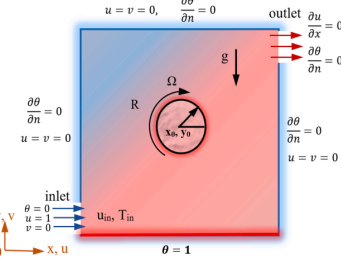
In 1980, Merkin [62] explored how a uniform stream travels through an impermeable vertical barrier enclosed in saturated porous media and constantly feeds heat to the porous medium in the situation of mixed heat convection. Numerous examples have been researched. In the first scenario, the flow transitions from mostly forced convection at the leading edge to predominantly free convection further downstream. In both cases, series solutions are obtained, and the flow in the intermediate area is characterized by a numerical solution to the equations. Another example demonstrates how the flow separates downstream of the leading edge, and the nature of the solution around this separation point is discussed. In 1985, Osborne and Incropera [63] conducted an experiment to explore the influence of buoyancy on convection heat transfer in transitional and turbulent water flows between horizontal parallel plates. They discovered that when heat flux increased in transitional flow, the Nusselt values at the top and bottom plates decreased and increased, respectively. The bottom plate's results are explained by increased heat transfer via free convection, whereas the top plate's results are explained by boundary-layer laminarization. Top plate heat transfer data in turbulent flow are correlated using a pure forced convection expression, whereas bottom plate data are correlated using a mixed convection expression. In 1995, Aldoss et al. [64] investigated the behavior of mixed convection in a vertical plate immersed in porous material. The impact of magnetic field strength on the local Nusselt number and local wall shear stress was investigated, and a non-Darcian model including inertia and boundary effects was employed. Within two limited limits, a particular modification of the governing equations has been investigated to cover the full mixed convection regime. In the mixed convection regime, magnetic field strength had a considerable impact on both the local Nusselt number and the local wall shear stress. In 2000, Aydin and Yang [65] conducted a computational investigation of the laminar mixed convection transport mechanism in a hollow driven by shear and buoyancy, with moving chilled sidewalls and a locally heated lower wall. The study focused on the interplay between forced and natural convection. To model localized heating scenarios, a centrally positioned heat source on the bottom wall was used, along with varying values of the dimensionless heat source length. In 2005, Abu-Mulaweh [66] investigated the influence of step height on turbulent mixed convection flow over a forward-facing step. The intensity of temperature variations downstream of the step, as well as streamwise and transverse velocity fluctuations, were shown to increase as the step height rose. Furthermore, it was revealed that increasing step height increases both reattachment length and heat transfer rate from the downstream heated wall. Mirmasoumi and Behzadmehr [67] did a numerical analysis in 2008 to evaluate the link between mixed convection heat transfer in nanofluids and the average diameter of nanoparticles in horizontal tubes. The computed outcomes demonstrate that when the mean diameter of the nanoparticles lowers, the convection heat transfer coefficient rises significantly. However, the hydrodynamic properties are not much changed. When using bigger nanoparticles and/or assuming relatively high Grashof numbers, the nanoparticle distribution at the tube cross section becomes more non-uniform. In 2010, Mansour et al. [68] investigated mixed convection flows in a square lid-driven hollow that was partially heated from below and filled with water-based nanofluids. To solve the problem's dimensionless governing equations, the finite difference method was applied. The effects of the governing parameters Reynolds number, solid volume fraction, various heat source length values, and different heat source locations were

considered for the streamlines and isotherm contours, as well as the Nusselt number and average Nusselt number along the heat source. In 2014, Sourtiji et al. [69] conducted a numerical study of mixed convection flow and heat transfer within a square cavity with different input and output port locations. In 2016, Selimefendigil and Oztop [70] used a finite element technique with Galerkin weighted residuals to investigate the mixed convection of a nanofluid-filled cavity driven by an oscillating lid under the influence of an inclined uniform magnetic field. It has been observed that for large Hartmann and Richardson values, the heat transfer technique is useless. When compared to base fluid, the solid volume fraction of nanoparticles rises, resulting in average heat transfer augmentation. The main focus of the study conducted in 2021 by Wahid et al [71] is the magnetohydrodynamic (MHD) radiative flow of a hybrid alumina-copper/water nanofluid via a permeable vertical plate with mixed convection. In this paper, they tested at the hybridization of two distinct types of nanoparticles, Cu and Al₂O₃. With the adaption of standard similarity transformations, the controlling flow and heat transfer equations are reduced to ordinary differential equations (ODEs), which are then evaluated to get the numerical solutions. They found that the increase in copper concentration volume is seen to hasten boundary layer separation while decreasing the physical quantities of interest. The mixed convection parameter improves skin friction and heat transfer rate, particularly for the realizable solution.

In recent years, a lot of research investigations have focused on the mixed convection heat transfer of nanofluids. Due to its prevalence in both our everyday lives and a wide spectrum of innovative industrial applications, that issue has been the focus of several computational and experimental research. Some recent papers are presented below.

Table I.5: Examples of recent studies in mixed convection.

Authors	Geometry	Nanofluid	Observations
Saiful Islam et al [72] /2023		Nanofluid: TiO ₂	Increasing Re and ϕ improves nanofluid thermal performance, while increasing Ha decreases it. Furthermore, ϕ and have positive sensitivity to Nu_{avg} , whereas Ha has negative sensitivity.
M. Yasir et al. [73] /2023		Hybrid nanofluid : Zn-TiO ₂	Increased magnetic strength and inclination angle improve fluid velocity and heat dispersion. Thermal distribution improves with increased thermal radiation, temperature ratio parameter, and heat source/sink.

<p>Md. J. Hassan et al [74] /2024</p>		<p>Nanofluid: CNT</p>	<p>Under unstable circumstances, velocity, average temperature, bulk temperature, fluid temperature gradient, drag force, and pressure all rise with dimensionless time (τ). However, mean heat transfer falls for both natural and induced convection regimes.</p>
<p>F.A. Abood et al. [75] / 2024</p>		<p>Hybrid nanofluid : Ag-MgO</p>	<p>Nu gradually increases by 20% with larger Richardson numbers and opposing rotating speeds. Counterclockwise rotation results in a 15% drop in thermal boundary layer thickness.</p>

I.2. Magnetohydrodynamics

I.2.1. Definition.

The term magnetohydrodynamics (MHD) combines the terms dynamics, hydro, and magneto, where dynamics is movement, hydro is a liquid or fluid, and magneto is a magnetic field. The movement of electrically conducting fluids in electric and magnetic fields is the focus of this branch of magneto fluid dynamics. It looks at the dynamics of a material moving in an electromagnetic field, where an induction-modified field causes currents to flow through the material and connects the flow field and dynamics equations [76].

It is described as a field of physics that integrates concepts from fluid dynamics and magnetism to investigate the behavior of electrically conducting fluids, including plasmas, liquid metals, and some ionized gases. The fundamental focus of MHD is the interaction between fluid motion and the magnetic fields it produces or is exposed to. However, a comprehensive theory known as magnetohydrodynamics (MHD) did not arise until the 20th century. The term Magnetohydrodynamics (MHD) was originally used in 1942 by the scientist Hannes Olof Gösta Alfvén (born 30 May 1908 in Norrköping, Sweden – died 2 April 1995 in Djursholm, Sweden). For his work on this topic, he was granted the 1970 Nobel Prize in Physics. The main goal of MHD is to understand how an electrically conducting fluid—a liquid or an ionized gas known as plasma—moves when exposed to a magnetic field. Electromagnetic effects and the velocity of the conductive fluid are coupled "[76].



Hannes Alfvén (1908-1995)

The basic equations of MHD explain magnetic induction, mass, momentum, and energy in a conducting fluid. The effects of electromagnetic forces are considered in these often-complicated calculations. To put it briefly, the electromagnetic Maxwell's equations and the Navier-Stokes equations for fluid dynamics are combined to provide the equations that characterize MHD. It is possible to simultaneously solve these partial differential equations analytically and numerically. A conducting fluid traveling across a magnetic field and its mutual influence generate MHD. This creates an electromagnetic force in a fluid flowing over a transverse magnetic field, and the resulting magnetic field and current combine to create a workforce that opposes the flow of the fluid. Furthermore, the magnetic field created by the current modifies the initial magnetic field [76].

I.2.2. MHD Fluid Mechanics Aspect.

Magnetohydrodynamic (MHD) fluids have electrical conductivity but no inherent magnetism; instead, the interaction with magnetic fields is created by electric currents running through them. This conductivity results from the presence of movable free charges, such as ions or electrons, which may move freely. According to non-relativistic electromagnetic principles, a charged particle, such as an electron, encounters three unique forms of forces. Magnetism, represented by the magnetic field (B), arises from the motion of charged particles and magnetic materials. The force acting upon a charged particle (q) in motion with a velocity (v) within an electric field (E) and a magnetic field (B) is termed the Lorentz force, named after the Dutch physicist Hendrik A. Lorentz. This force is mathematically described as [77]:

$$F = qE + qv \times B \quad (3)$$

For simplified cases, the Lorentz force may be described as:

$$F = qv \times B \quad (4)$$

I.3. Porous media

I.3.1. Definition.

Porous materials, or porous media, are solid solids that contain voids or pores. These materials are characterized by their capacity to permit fluid movement under external influences, resulting in categorization as permeable or non-permeable porous media. Porous media can display a variety of features, including pore dispersion or non-dispersion, internal structure homogeneity or heterogeneity, and the ability to mix numerous structural components [78].



Figure I.4: Porous media

One essential feature that distinguishes porous medium is porosity. It is given as a value between 0 and 1 and measures the percentage of empty space within a material relative to its overall volume. The porosity of naturally porous materials is usually about 0.6. On the other hand, metal foams and other manufactured materials may reach extraordinarily high porosity values of almost 0.99. A material's porosity is determined by both its natural properties and the manufacturing process it goes through [78].

The investigation of heat transfer properties in porous media is a subject of great significance in several technical domains and businesses, including heat exchangers, heat storage systems, geothermal applications, and drying techniques. One passive method of increasing heat transfer efficiency in mechanical systems is to use porous materials. This is because the presence of porous materials alters fluid flow patterns and raises the system's thermal conductivity overall [79].

I.3.2. Fluid Flow Models in porous media

The choice of the fluid flow model depends on the specific characteristics of the porous medium, the flow regime (e.g., laminar, or turbulent), and the research or engineering application. Researchers and engineers select the most appropriate model to accurately represent the flow and heat transfer behavior in each porous medium. The modeling of convective heat transfer within porous media relies on various fluid flow models. Some of the most important and commonly used fluid flow models for convective heat transfer in porous media include [79]:

- Darcy's Law:

A fundamental equation for fluid flow in porous medium is Darcy's law. It describes the relationship between fluid velocity and pressure gradient in a porous media. It's useful for depicting sluggish, viscous flows through porous materials.

Darcy's law relates the rate of flow (Q) of a fluid through a porous medium to the pressure gradient (ΔP) and the permeability (K) of the medium [80]:

$$Q = -KA (\Delta P / \mu) \quad (5)$$

Where :

- Q is the rate of flow (volume per unit time).
- K is the permeability of the porous medium.
- A is the cross-sectional area through which the fluid flows.
- ΔP is the pressure drop across the porous medium.
- μ is the dynamic viscosity of the fluid.

- Hazen Darcy equation :

Darcy's experiments were carried out under constant temperature conditions with a single type of fluid. As a result, Darcy's equation in its original version does not account for the fluid's viscosity (μ). Darcy's equation, however, is reconfigured to include viscosity as a determining factor by incorporating a specific permeability relation, represented as $K = k \mu$, resulting in the viscosity-dependent form shown below [80]:

$$v = \left(\frac{K}{\mu} \right) \frac{\Delta P}{\Delta x} \quad (6)$$

Specific permeability K is regarded as a hydraulic parameter that is unaffected by the properties of the fluid. The formula given above is the Hazen-Darcy equation, also referred to as Darcy's law.

- Forchheimer's Law:

An extension of Darcy's law that accounts for the nonlinear effects of fluid flow through porous media, including inertial effects, is Forchheimer's law. When the flow velocities are relatively high or the flow is turbulent, it is used.

Forchheimer's Law introduces an additional term to account for non-linear effects that become significant at high flow velocities. The modified equation is as follows [80]:

$$Q = -KA \left(\frac{\Delta P}{\mu} \right) - B\rho u \quad (7)$$

Where :

- Q, K, A, ΔP , and μ have the same meanings as in Darcy's law.
- B is the Forchheimer coefficient, which represents the non-linear resistance to flow.
- ρ is the fluid density.
- u is the fluid velocity

- Hazen–Dupuit–Darcy Equation :

The investigation of steady-state, open-channel flows led to the development of the quadratic Hazen-Dupuit-Darcy equation. The following definition of the equation is based on an equilibrium between the gravitational force and the shearing resistance [80]:

$$0 = \frac{\partial p}{\partial x} + \frac{\mu}{k} u - C \rho u^2 \quad (8)$$

- Brinkman's Extension:

To describe fluid flow in porous media, Brinkman's extension incorporates both Darcy's and Forchheimer's terms, resulting in a more comprehensive model that accounts for both viscous and inertial forces.

The general form of the Brinkman formula is as follow [80]:

$$\Delta P = -\mu \nabla^2 u - \rho g \nabla z + \mu \alpha \nabla T \quad (9)$$

Where:

- ΔP is the pressure drop across the porous medium.
- μ is the dynamic viscosity of the fluid.
- $\nabla^2 u$ represents the Laplacian of the velocity field within the porous medium.
- ρ is the density of the fluid.
- g is the acceleration due to gravity.
- ∇z represents the gradient of the elevation.
- α is the thermal diffusivity of the fluid.
- ∇T is the gradient of temperature within the porous medium.

- Brinkman–Hazen–Dupuit–Darcy Equation:

Brinkman noticed that the shearing tension of the fluid's viscosity could be insignificant in compared to the viscous drag when the permeability is low. The Brinkman-Hazen-Dupuit-Darcy equation is thus obtained by including the shearing tension term, a Laplacian term [80].

$$0 = -\nabla p + \mu \nabla^2 u + \frac{\mu}{k} \phi u + \frac{C_F}{k^{1/2}} \rho \phi^2 |u| u \quad (10)$$

where $|u|$ is the velocity's magnitude. Regardless of the viscous drag, the fluid could change the viscous shearing tension. In the engineering disciplines, porous media can take many different forms, such as packed beds, windowing environments, metal foams, and aerodynamic gels.

- Brinkman–Forchheimer Equation :

The Brinkman–Forchheimer Equation, often referred to as the Brinkman-Forchheimer extension of Darcy's Law, is a modified version of the Darcy's Law equation that accounts for additional resistance to fluid flow in porous media. It is particularly useful when dealing with porous materials that exhibit non-negligible inertia and viscous effects. The equation is named after the scientists H.C. Brinkman and Paul Forchheimer.

The general form of the Brinkman-Forchheimer Equation is as follow [80]:

$$\Delta P = -\mu \nabla^2 u - \rho_f \nabla \phi - \rho_f \alpha u \quad (11)$$

Where:

- ΔP represents the pressure drop across the porous medium.
- μ is the dynamic viscosity of the fluid.
- $\nabla^2 u$ represents the Laplacian of the fluid velocity vector.
- ρ_f is the density of the fluid.
- $\nabla \phi$ is the gradient of the fluid pressure.
- α is the Forchheimer coefficient, which accounts for the additional resistance in the porous medium due to inertial effects.

Chapter II

Mathematical Modeling Computational Technique

Chapter II: Mathematical Modeling & Computational Technique

II.1 Introduction

The increasing need to nanofluids for energy conservation has resulted in a strong demand for nanofluid-based heat transfer devices, necessitating the gathering of experimental data. However, the expense of testing has an inherent drawback in that it restricts one's ability to gather sufficient knowledge. One significant problem is the insufficiency of the experimental techniques in establishing the numerous components influencing and their strength of influence on the system. All these challenges with experimental techniques have led to the development of computer modeling for nanofluid research [81].

The description of the nanofluid system based on a few assumptions yields a set of differential equations known as transport equations, which are then solved using various computer methods. Because the governing equations are nonlinear, solving nanofluid flow problems analytically is very difficult [81].

Computational fluid dynamics (CFD) is a computer-based modeling approach for analyzing systems including fluid flow and heat transport processes. It includes fundamental operations like as input, solving, and output. The flow issue to be solved acts as an input for CFD applications. It essentially comprises information on the physical phenomena described by the model, the geometry of the flow domain (also known as the computational domain), and the properties of the working fluid phases [82].

The requirements for generated grids and boundary conditions are also included. The described problem is then resolved numerically using a method based on solvers that employ standard computer codes. Applying an appropriate numerical technique, such as the finite difference method (FDM), finite volume method (FVM), finite element method (FEM), or other techniques, makes this achievable. The CFD application can produce output of results that are visualized in the form of the specified geometry and mesh by vectors, contours, surface plots, graphics, and animations once the problem has been solved [82].

II.2 Mathematical Modeling

In the present work, we explored the physical nature of buoyancy-induced flows and heat transfer in cavities in the presence of a magnetic field. Furthermore, because of its critical relevance in many applications, cavity geometry has been investigated in heat transmission. The convective heat transfer behavior of nanofluids and hybrid-nanofluids in various enclosures with variable geometrical forms and heat source configurations is investigated. The governing equations for the current problems, along with the relevant boundary conditions, are first translated into a non-dimensional form, and the resulting nonlinear system of partial differential equations is then numerically solved using the finite element technique.

This section presents numerical solutions for nondimensional parameters such as the Rayleigh number (Ra), Hartmann number (Ha), and Prandtl number (Pr). The findings are

shown as streamlines and isothermal lines. Finally, the mean Nusselt numbers and entropy generation are calculated.

II.2.1. Definitions of key parameters

Most important dimensionless variables and factors that are pertinent to the mathematical modeling of convective heat transport are as follows:

Buoyancy Force

The gravitational field contains a net force that pushes the lighter fluid upward from the heavier fluid. The buoyancy force is the upward force produced by a fluid on a body that is fully or partially submerged in it. The buoyancy force is proportional to the weight of fluid displaced by the body [83].

$$F_{\text{buoyancy}} = \rho_{\text{fluid}} g V_{\text{body}} \quad (12)$$

Where ρ_{fluid} is the average density of the fluid, g is gravity's acceleration, and V_{body} is the volume of the body immersed in the fluid. In the absence of other effects, the net vertical force acting on the body is equal to the difference between the body's weight and buoyancy force.

$$F_{\text{net}} = mg - F_{\text{buoyancy}} = \rho_{\text{body}} g V_{\text{body}} - \rho_{\text{fluid}} g V_{\text{body}} = (\rho_{\text{body}} - \rho_{\text{fluid}}) g V_{\text{body}} \quad (13)$$

The net force (F_{net}) is related to the disparity in densities between the body submerged in the fluid and the fluid itself. As a result, a body submerged in a liquid loses weight equivalent to the weight of the fluid it replaces. It is the Archimedes principle.

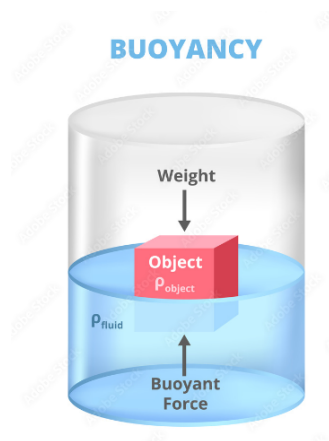


Figure II. 1 : Buoyancy force.

Volumetric Expansion Coefficient

The density of a fluid varies in proportion to its temperature. Therefore, knowing how density varies with temperature while keeping a constant pressure is critical. The coefficient of thermal (or volumetric) expansion is what relates these qualities.

It is defined as the fractional change in volume to temperature change at constant pressure, represented by (β) and written as [83].

$$\beta = -\frac{1}{v} \left(\frac{\partial v}{\partial T} \right)_p \quad \text{with } v = \frac{1}{\rho} \quad (14)$$

$$\text{Then } \beta = \rho \left[\frac{\partial(1/\rho)}{\partial T} \right]_p = \rho \left[-\frac{1}{\rho^2} \frac{\partial \rho}{\partial T} \right]_p \quad \text{and} \quad \beta = -\frac{1}{\rho} \left(\frac{\partial \rho}{\partial T} \right)_p \quad (15)$$

For an ideal gas:

$$\rho = \frac{P}{RT} \quad \text{and} \quad \left(\frac{\partial \rho}{\partial T} \right)_p = -\frac{P}{RT^2} \quad \text{therefore, } \beta = \frac{1}{T} (k^{-1}) \quad (16)$$

Where T is the absolute temperature.

Grashof Number

The Grashof number, defined as the ratio of buoyant force to viscous force exerted on the fluid, describes the flow regime in natural convection. It is designated as (Gr) and represents [83]:

$$Gr = \frac{\text{Buoyancy force}}{\text{Viscous force}} = \frac{g\Delta\rho V}{\rho\nu^2} = \frac{g\beta\Delta T V}{\nu^2} \quad (17)$$

where $\beta\Delta T = \Delta\rho/\rho$, the fraction of volume change of fluid with the temperature change ΔT at constant pressure. Grashof Number can be expressed as:

$$Gr = \frac{g\beta(T_s - T_\infty)L^3}{\nu^2} \quad (18)$$

Prandtl number

The Prandtl number (Pr) refers to Ludwig Prandtl, who created the boundary layer idea in 1904 and made fundamental contributions to boundary layer theory. Fluids have Prandtl values ranging from less than 0.01 for liquid metals to more than 100,000 for heavy oils. It's worth mentioning that water has a Prandtl number of around 7. The Prandtl values of gases are near to one, suggesting that momentum and heat dissipate at approximately the same rate through the fluid. As a result, for liquid metals, the thermal boundary layer is considerably thicker than the velocity boundary layer, whereas for oils, it is much thinner [84].

The Prandtl number is defined as the ratio of kinematic viscosity to thermal diffusivity. Kinematic viscosity describes impulse transfer by molecular friction, whereas thermal diffusivity represents heat transport via conduction. The Prandtl number refers to the relative speed at which momentum and energy travel through a fluid [83].

$$Pr = \frac{\text{Kinematic viscosity}}{\text{Thermal diffusivity}}$$

$$Pr = \frac{\nu}{k/\rho C_p} = \frac{\rho\nu C_p}{k} = \frac{\mu C_p}{k} \quad \text{and} \quad \rho\nu = \mu \quad (19)$$

$$\text{Simplified as } Pr = \nu/\alpha \quad (20)$$

where $\alpha = k / \rho C_p$ known as the thermal diffusivity

Rayleigh number

Rayleigh number is the most important independent parameter. It describes the balance of thermal force to viscous and thermal dissipation and provides an estimate of the intensity of the thermal driving force in natural convection. The Rayleigh number can alternatively be calculated as the ratio of buoyant forces to the product of heat and momentum diffusivities. It is influenced by the problem's geometrical parameters. When Ra exceeds a threshold Rayleigh number, heat transmission in the medium changes from conduction to convection. It is the product of the Grashof and Prandtl numbers [83].

$$Ra = GrPr = \frac{g\beta}{\nu\alpha}(Ts - T\infty)x^3 \quad (21)$$

Hartmann number

The Hartmann number is the ratio of electromagnetic force to viscous force, named after a German engineer who oversaw significant studies in the 1930s. The definition is as follows [85]:

$$Ha = B_0L \sqrt{\frac{\sigma}{\mu}} \quad (22)$$

Where Bo is the magnetic field, L is the length scale (m), σ is electrical conductivity, and μ is the dynamic viscosity of the working fluid.

Nusselt number

Wilhelm Nusselt invented the Nusselt number, also known as the dimensionless convection heat transfer coefficient, after making significant discoveries about convective heat transfer in the first part of the twentieth century. A higher Nusselt number indicates a high heat transfer by convection and a significant temperature differential at the surface. A fluid layer with a Nusselt number equal to 1 implies that heat is transported entirely via conduction. When the Nusselt number > 1 , convective heat transfer takes precedence [86].

The Nusselt Number is defined as the ratio of heat flow rate by convection to heat flow rate by conduction across a unit temperature gradient and a characteristic length 'L'. It quantifies the increase in heat transfer across a fluid layer due to convection as opposed to conduction through the same fluid layer [83].

The local Nusselt number at the cavity's heated surface is defined by the following expression:

$$Nu = \frac{\text{Convection heat transfer}}{\text{Conduction heat transfer}} = \frac{hL}{K} \quad (23)$$

$$Nu_{Loc} = \begin{cases} \frac{k_{nf}}{k_f} \frac{\partial T}{\partial x} \\ \frac{k_{nf}}{k_f} \frac{\partial T}{\partial y} \end{cases} \quad (24)$$

The heat transfer coefficient is denoted by h , whereas the thermal conductivity of the fluid is represented by k .

The expression of the average Nusselt number is the following:

$$Nu = \int_0^L Nu \, dx \quad (25)$$

Reynolds number

The dimensionless number (Re) represents the ratio of inertial and viscous forces. Laminar flow occurs when the fluid has a high viscosity or low fluid motion; turbulent flow occurs when the fluid has a high Reynolds number or a low viscosity [83].

$$Re = \frac{\text{Inertial forces}}{\text{Viscous forces}} = \frac{\rho VL}{\mu} \quad (26)$$

The Reynolds number is useful for predicting flow patterns in a variety of fluid flow conditions. Laminar flow (fluid particles following smooth paths in layers) predominates at low Reynolds numbers. At high Reynolds numbers, flows tend to be turbulent [83].

Richardson number

The Richardson number (Ri) was named after Lewis Fry Richardson. It is the manifestation of mixed convection. It expresses the percentage of the buoyancy term to the flow gradient term as a dimensionless number. Ri represents the importance of natural convection in comparison to forced convection in thermal convection issues [87].

$$Ri = \frac{\text{buoyancy term}}{\text{flow gradient term}} = \frac{g\beta(T_{h\cap E} - T_{Ref})L}{v^2} = \frac{Gr}{Re^2} \quad (27)$$

II.2.2. Governing equations

The problems of fluid flow and heat transfer are solved by applying the fundamental laws of conservation of mass (continuity equations), conservation of momentum (momentum equations), and conservation of energy (energy equations), which collectively form a set of coupled, nonlinear partial differential equations. Moreover, it is assumed that the fluid flow is laminar, and that viscous heating dissipation is minimal [88].

The Boussinesq approximation assumes that the working fluid's physical parameters are constant. In all scenarios investigated, a uniform magnetic field (B_0) is used. The model is used to develop three- or two-dimensional laminar incompressible steady-state equations with a homogeneous magnetic field applied. The gravitational force (g) acts vertically downwards [88].

The following are the governing equations for heat transfer convection flow:

Continuity equation:

The continuity equation for the working fluid that is considered as incompressible maintains its original form [83].

$$\nabla \cdot \vec{q} = 0 \quad (28)$$

The vectorial expression represents the x, y, and z components of velocity as u, v, and w, respectively ($\vec{u} = u \cdot \vec{i} + v\vec{j} + w\vec{k}$).

When the flow is continuous, the individual particle trajectories appear as steady streamlines. The streamlines can be represented by the stream function equation $\psi(x,y) = \text{constant}$, where a distinct streamline is indicated by each value of the constant. Since streamlines are the paths that working fluid particles travel, the velocity vector (\vec{u}) is always perpendicular to them. So that, the continuity equation for 2D models can be expressed as [83]:

$$\frac{\partial u}{\partial x} + \frac{\partial v}{\partial y} = 0 \quad (29)$$

And for 3D:

$$\nabla \cdot \vec{u} = \frac{\partial u}{\partial x} + \frac{\partial v}{\partial y} + \frac{\partial w}{\partial z} = 0 \quad (30)$$

Momentum equation:

The Navier-Stokes equation defines the momentum equations. The fluid's movement is changed by the mechanical forces brought about by the magnetic field. The momentum equation for a 2D laminar incompressible steady fluid flow with a uniform magnetic field B_0 applied in the horizontal direction is as follows [83]:

In x-direction:

$$u \frac{\partial u}{\partial x} + v \frac{\partial u}{\partial y} = -\frac{1}{\rho} \frac{\partial P}{\partial x} + \nu \left(\frac{\partial^2 u}{\partial x^2} + \frac{\partial^2 u}{\partial y^2} \right) \quad (31)$$

In y-direction:

$$u \frac{\partial v}{\partial x} + v \frac{\partial v}{\partial y} = -\frac{1}{\rho} \frac{\partial P}{\partial y} + \nu \left(\frac{\partial^2 v}{\partial x^2} + \frac{\partial^2 v}{\partial y^2} \right) + g\beta(T - T_c) - \frac{\sigma B_0^2 v}{\rho} \quad (32)$$

Energy equation:

The first law of thermodynamics is utilized to derive this equation. The application of this law provides the following statement: under steady-state conditions, heat flow (In) equals heat flow (Out) [83].

$$u \frac{\partial T}{\partial x} + v \frac{\partial T}{\partial y} = \frac{k}{\rho c_p} \left(\frac{\partial^2 T}{\partial x^2} + \frac{\partial^2 T}{\partial y^2} \right) \quad (33)$$

Where $\alpha = k/\rho c$ is the thermal diffusivity.

II.2.3. Governing equations for porous media

As previously stated, the existence of porous material is a significant consideration in convective heat transfer investigations. Many of the examined geometries were assumed to be fully or partially porous media.

To simplify the numerical computations, we assumed that the problems under investigation in the presence of porous media are stable and incompressible. The fluid flows through a homogenous porous matrix with constant porosity (ϵ) and permeability (K).

The governing equations for the porous medium area in the case of natural convection are given below using Darcy-Brinkman-Forchheimer generalized formulas [89]:

$$\frac{\partial u}{\partial x} + \frac{\partial v}{\partial y} = 0 \quad (29)$$

$$\frac{1}{\epsilon^2} (u \frac{\partial u}{\partial x} + v \frac{\partial v}{\partial y}) = -\frac{1}{\rho_{nf}} \frac{\partial P}{\partial x} + \frac{\nu_{nf}}{\epsilon} (\frac{\partial^2 u}{\partial x^2} + \frac{\partial^2 u}{\partial y^2}) - \nu_{nf} \frac{u}{K} - \frac{F_c}{\sqrt{K}} u|u| \quad (34)$$

$$\frac{1}{\epsilon^2} (u \frac{\partial u}{\partial x} + v \frac{\partial v}{\partial y}) = -\frac{1}{\rho_{nf}} \frac{\partial P}{\partial y} + \frac{\nu_{nf}}{\epsilon} (\frac{\partial^2 v}{\partial x^2} + \frac{\partial^2 v}{\partial y^2}) - \nu_{nf} \frac{v}{K} - \frac{F_c}{\sqrt{K}} v|u| + \beta_{nf} g(T - T_{ave}) + \frac{\sigma_{nf}}{\rho_{nf}} B_0^2 v \quad (35)$$

$$(\rho c_p)_{nf} (u \frac{\partial T}{\partial x} + v \frac{\partial T}{\partial y}) = k_{nf} (\frac{\partial^2 T}{\partial x^2} + \frac{\partial^2 T}{\partial y^2}) \quad (36)$$

II.2.4. Boundary Conditions

To determine the temperature distribution in a medium, solve the appropriate form of the heat equation. However, such a solution is subject to the physical circumstances that exist at the medium's limits.

The numerical model of any of the analyzed scenarios must be solved using proper boundary conditions. All instances' boundary conditions are stated for the computational domain. In general, the examined geometry consists of adiabatic walls, walls subjected to high temperatures (T_H), and others subjected to low or cold temperatures (T_C) [89].

In global, the boundary conditions for the natural heat convection issue with uniform temperatures are as follows [89]:

For hot walls: $u = v = 0$ and $T = T_H$.

For cold walls: $u = v = 0$ and $T = T_C$.

For adiabatic walls: $u = v = 0$, $\frac{\partial T}{\partial n} = 0$.

II.2.5. Non-dimensional formulations

In addition to the dimensionless parameters described above, additional non-dimensional variables or integers are used to transform the governing equations and boundary conditions to dimensionless notation [83].

$$X = \frac{x}{L}, Y = \frac{y}{L}, U = \frac{u}{u_0}, V = \frac{v}{v_0}, \theta = \frac{T - T_L}{T_H - T_L}, C = \frac{c - c_L}{c_H - c_L}$$

II.3 Computational procedures

II.3.1. Computational Fluid Dynamics

The computational Fluid Dynamics (CFD) approach is gaining popularity for technical and scientific applications that do not require testing since it is both time-consuming and cost-effective for addressing fluid flow issues. The restricted flexibility of fluid dynamics made it difficult to conduct appropriate experimental research on temperature transfer and fluid movement. Because of the presence of complex geometric entities, many variables, various boundary shapes, and conditions, analytical solutions are insufficient. Numerical techniques are the most efficient way to solve realistic partial differential equations [88].

CFD is a computer-based simulation methodology used to address engineering issues with complicated geometry or important aspects that cannot be handled using conventional methods. CFD approximates a natural living system through the application of algebraic equations. Computational findings give information about a system's performance. Researchers employ CFD simulation tools with finite grids to generate realistic physical solutions with tolerable accuracy. Complex geometry's precise and accurate projections satisfy high dependability and economic difficulties. These behaviors are commonly noticed in CFD. Furthermore, CFD has been widely utilized to perform numerical fluid dynamics computations. It is currently effectively used to handle large-scale industrial problems, such as turbulent flow [88].

II.3.2. Discretization Approaches

Numerical discretization is the first stage in the solution process for a mathematical model of a physical phenomenon. This means that each component of a differential equation is turned into a numerical analog, which is then represented on a computer and processed using algorithm-based computer software. A variety of discretization approaches exist for high-performance numerical computation in CFD, including the boundary element method (BEM), the boundary volume method (BVM), the finite element method (FEM), the finite difference method (FDM), and the finite volume method (FVM) [88].

II.3.3. Finite Element Method

When other methods fail, finite element modeling (FEM) can handle complex geometric bodies and boundaries. This approach has the benefit of taking the body's disintegration into consideration [90].

The Galerkin weighted residual finite element approach was used in the current numerical computation. It is the most effective numerical computing approach for determining the approximate solutions to a system of PDEs. FEM is becoming increasingly popular as a solution to fluid dynamics difficulties. This approach is sufficiently global to handle time-dependent and nonlinear flow difficulties in irregular domains. The mathematical model is formed by bringing together the local approximations of the phenomena under study, which is an important component of FEM. The ability of FEM to accommodate any intricate geometry is a significant advantage. Furthermore, the grid is easily reconfigurable, and each component may be simply separated. The equations for each component are derived independently of the other components using FEM. The interactions between elements are only examined once the equations have been generated and combined into a global matrix.

Most computing processes rely on FEM to achieve these ideal properties. When the elements' sides are properly aligned and have the same nodes as the neighboring components, there are no restrictions on how they can be joined in FEM. Due of its versatility, we can express incredibly complex geometries [90].

A persistent physical problem is transferred to a discretized restricted element problem with unknown nodal values. To solve a linear issue, a system of linear algebraic equations has to be solved. Values stored in finite elements can be recovered using nodal values. Important steps in the FEM of a typical issue are as follows [90]:

- Mesh construction involves discretizing a domain into a finite number of components.
- Analyze a differential equation with weak formulation or weighted integral.
- The problem's FEM is created with the weak or weighted integral form.
- Developed a form function for elements.
- To create a global system of algebraic equations, combine the finite elements.
- Setting boundaries and constraints.
- An equation's solution and interest amount after computation.

II.3.4. Mesh Generation

FEM mesh or grid generation splits a domain into finite components. Mesh cells are used to discretize a local approximation derived from a large region. The aim is to create a mesh that accurately reflects the input domain geometry, has high-quality (well-shaped) cells, and isn't so dense that further computations become impossible. To enable accurate computations, the mesh should include fine, tiny components in strategic locations. Meshes are used for both computer screen rendering and physical simulation, which includes FEM and CFD [90].

Three-dimensional meshes using tetrahedra, pyramids, prisms, or hexahedra are required for finite element analysis. They are used in the finite volume technique and can be any form of polyhedra. Finite difference approaches use multi-block structured meshes, also known as piecewise structured arrays of hexahedra. The computational domain will be discretized into unstructured triangles utilizing the existing numerical methods by applying the Delaunay triangular method. The Delaunay triangulation is a geometric structure that became quite popular while mesh generation research was just being started. The goal of a two-dimensional Delaunay triangulation of a vertex set is to maximize the shortest angle among all feasible triangulations of that vertex set [90].

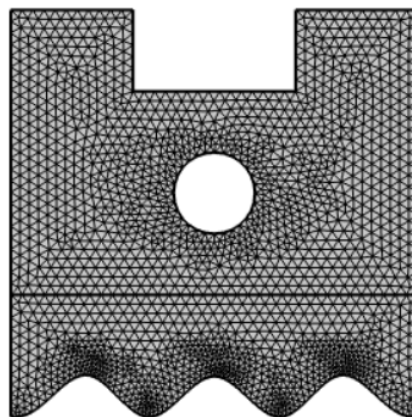


Figure II. 2: Example of FME discretization

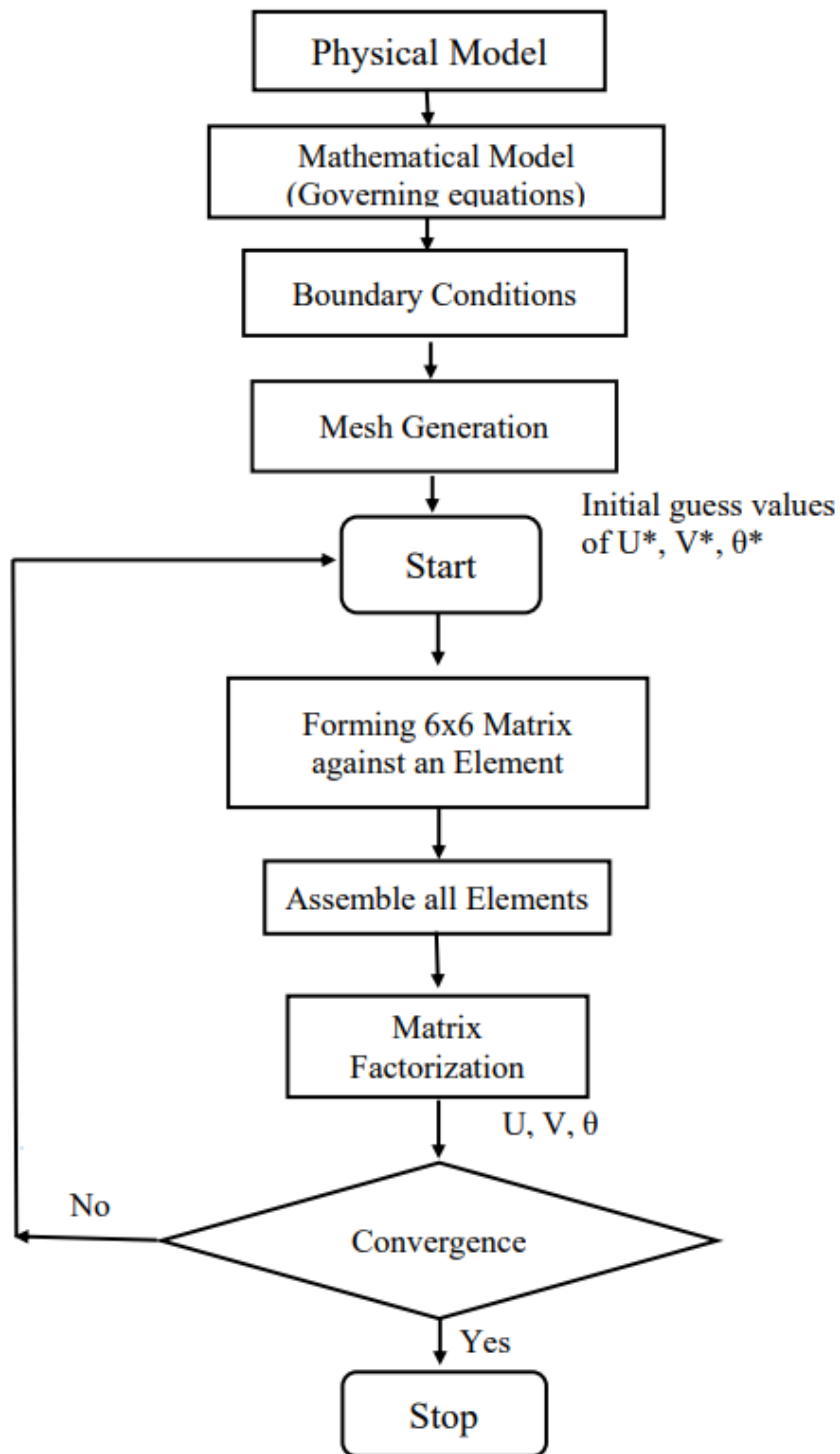


Figure II. 3: Flow diagram illustrating FEM computational process [91].

Chapter III

Influence of the thermos-physical properties of nanofluids and hybrid-nanofluids

Chapter III: Influence of the thermos-physical properties of nanofluids and hybrid-nanofluids

III.1 Introduction

Nanofluids are used to improve the thermal conductivity of common fluids including water, ethylene glycol, and propylene glycol. They have a wide range of technical and biological applications, including cooling, cancer treatment, and process industries. The addition of solid particle suspensions to traditional heat transfer fluids to increase thermal conductivity is a recent advancement in engineering technology. These suspensions increase the coefficient of heat transfer. Since solid metals have a greater thermal conductivity than base fluids, suspended particles can improve thermal conductivity and heat transfer performance [92].

Nanofluids have several advantages, including greater stability, a direct influence on viscosity due to nanoparticle properties, and better wetting, spreading, and dispersion capabilities on solid surfaces, even at low concentrations [92].

In this chapter, we investigate the effect of the added nanoparticles' thermophysical characteristics on the augmentation of heat transfer when exposed to MHD convective heat phenomena. The findings will be provided as streamlines, isotherm contours, and the output of the Nusselt number, as well as sensitivity to geometrical and porous media characteristics. This section will focus on two situations. The first one depicts a triangular form with an Ag-MgO/water hybrid nanofluid [92]. The second is a C-shaped container filled with Ag-water nanofluid [94].

III.2 Case 01: MHD natural convection of a hybrid nanofluid involved in a complex triangular enclosure [92].

III.2.1 Abstract

The current study looked at the behavior of a triangular cavity filled with Ag-MgO/water nanofluid under MHD natural convection and equipped with a rotating circular barrier, while the right-angled corner was outfitted with a quarter-circle porous medium and held at a constant high temperature T_h . Several characteristics are evaluated, including the Rayleigh number ($10^3 \leq Ra \leq 10^6$), Hartmann number ($0 \leq Ha \leq 80$), and Darcy number ($10^{-5} \leq Da \leq 0.15$). The findings indicate that Ra has an amplifying impact, and that the magnetic parameter regulates heat transport.

III.2.2 Characterization of problem

The current case employed a right-angled triangle enclosure with an Ag-MgO/water nanofluid and a porous medium quarter-circle shape at the right-angled corner. The permeable region's borders have been preserved at T_h . This hole also has a spinning circular barrier with a radius (r_{ob}). The heated sections are held at a constant hot temperature (T_h), while the remaining plates are adiabatic. The porous medium region resembles a quarter circle, with the radius (r_p) located at the right angle of the triangle enclosing.

The numerical simulation equation overlooks several factors, including viscosity dissipative, radiation, and the Joule effect. The hybrid nanofluid is predicted to be laminar, incompressible, and time independent.

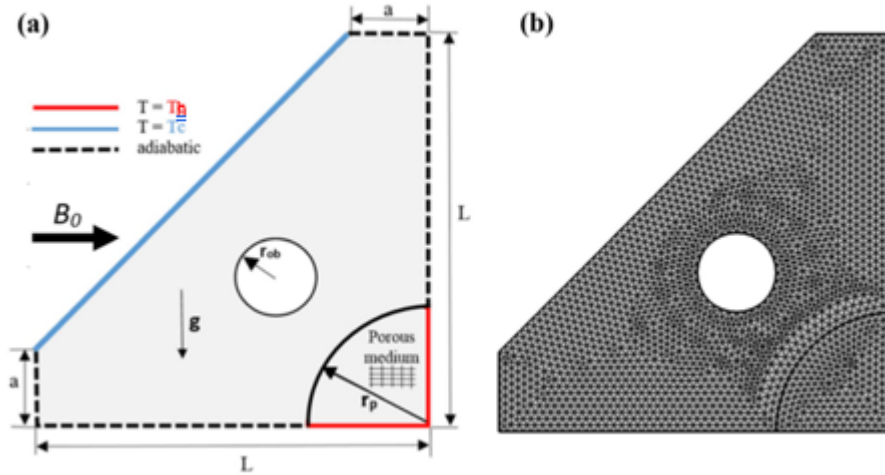


Figure. III. 1: A schematic representation (a) of the physical scheme and grid distribution (b) of the calculational domain

III.2.3 Formulation of the Mathematical Model

III.2.3.1 Mathematical Formulation

The main conservation equations in the hybrid nanofluid region of the 2D cavity fluid domain are as follows:

$$\frac{\partial u}{\partial x} + \frac{\partial v}{\partial y} = 0 \quad (29)$$

$$\left(u \frac{\partial u}{\partial x} + v \frac{\partial v}{\partial y}\right) = -\frac{1}{\rho_{hnf}} \frac{\partial P}{\partial x} + \nu_{hnf} \left(\frac{\partial^2 u}{\partial x^2} + \frac{\partial^2 u}{\partial y^2}\right) \quad (37)$$

$$\left(u \frac{\partial u}{\partial x} + v \frac{\partial v}{\partial y}\right) = -\frac{1}{\rho_{hnf}} \frac{\partial P}{\partial y} + \nu_{hnf} \left(\frac{\partial^2 v}{\partial x^2} + \frac{\partial^2 v}{\partial y^2}\right) + \beta_{hnf} g (T - T_{ave}) + \frac{\sigma_{hnf}}{\rho_{hnf}} B_0^2 v \quad (38)$$

$$(\rho c_p)_{hnf} \left(u \frac{\partial T}{\partial x} + v \frac{\partial T}{\partial y}\right) = k_{hnf} \left(\frac{\partial^2 T}{\partial x^2} + \frac{\partial^2 T}{\partial y^2}\right) \quad (39)$$

The Darcy-Brinkmann-Forchheimer generalized equation outlines the governing formulas for the porous area in case of hybrid nanofluid as follows:

$$\frac{\partial u}{\partial x} + \frac{\partial v}{\partial y} = 0 \quad (29)$$

$$\frac{1}{\varepsilon^2} \left(u \frac{\partial u}{\partial x} + v \frac{\partial v}{\partial y}\right) = -\frac{1}{\rho_{hnf}} \frac{\partial P}{\partial x} + \frac{\nu_{hnf}}{\varepsilon} \left(\frac{\partial^2 u}{\partial x^2} + \frac{\partial^2 u}{\partial y^2}\right) - \nu_{hnf} \frac{u}{K} - \frac{F_c}{\sqrt{K}} u |u| \quad (40)$$

$$\frac{1}{\varepsilon^2} \left(u \frac{\partial u}{\partial x} + v \frac{\partial v}{\partial y} \right) = -\frac{1}{\rho_{hnf}} \frac{\partial P}{\partial x} + \frac{\nu_{hnf}}{\varepsilon} \left(\frac{\partial^2 v}{\partial x^2} + \frac{\partial^2 v}{\partial y^2} \right) - \nu_{hnf} \frac{v}{K} - \frac{Fc}{\sqrt{K}} v |u| + \beta_{hnf} g (T - T_{ave}) + \frac{\sigma_{hnf}}{\rho_{hnf}} B_0^2 v \quad (41)$$

$$(\rho c_p)_{hnf} \left(u \frac{\partial T}{\partial x} + v \frac{\partial T}{\partial y} \right) = k_{hnf} \left(\frac{\partial^2 T}{\partial x^2} + \frac{\partial^2 T}{\partial y^2} \right) \quad (42)$$

The non-dimensional boundary constraints and control formulas are created using the following parameters.

$$x = \bar{x}/L, \quad y = \bar{y}/L, \quad u = \bar{u}/U_0, \quad v = \bar{v}/V_0.$$

$$\theta = (T - T_0)/(T_h - T_c), \quad \psi = \bar{\psi}/(U_0 L), \quad P = \frac{\bar{p}}{\rho_{hnf} u_0^2}, \quad Da = \frac{K}{L^2}.$$

The dimensionless equations can be given as follows:

$$\frac{\partial U}{\partial X} + \frac{\partial V}{\partial Y} = 0 \quad (43)$$

$$\frac{1}{\varepsilon^2} \frac{\rho_{hnf}}{\rho_f} \left(U \frac{\partial U}{\partial X} + V \frac{\partial V}{\partial Y} \right) = -\frac{1}{\rho_{hnf}} \frac{\partial P}{\partial X} + \frac{1}{\varepsilon} \frac{\nu_{hnf}}{\nu_f} \frac{Pr}{\sqrt{Ra}} \left(\frac{\partial^2 U}{\partial X^2} + \frac{\partial^2 U}{\partial Y^2} \right) - \frac{\nu_{hnf}}{\nu_f} \frac{Pr}{Da \sqrt{Ra}} - \frac{Fc}{\sqrt{Da}} |U|U \quad (44)$$

$$\begin{aligned} \frac{1}{\varepsilon^2} \frac{\rho_{hnf}}{\rho_f} \left(U \frac{\partial U}{\partial X} + V \frac{\partial V}{\partial Y} \right) &= -\frac{1}{\rho_{hnf}} \frac{\partial P}{\partial Y} + \frac{1}{\varepsilon} \frac{\nu_{hnf}}{\nu_f} \frac{Pr}{\sqrt{Ra}} \left(\frac{\partial^2 V}{\partial X^2} + \frac{\partial^2 V}{\partial Y^2} \right) - \frac{\nu_{hnf}}{\nu_f} \frac{Pr}{Da \sqrt{Ra}} V - \frac{Fc}{\sqrt{Da}} |U|V + \\ Pr \frac{\beta_{hnf}}{\beta_f} g \theta &+ \frac{\sigma_f}{\rho_{hnf}} \frac{\rho_f}{\rho_{hnf}} \frac{Pr Ha^2}{\varepsilon \sqrt{Ra}} V \end{aligned} \quad (45)$$

$$U \frac{\partial \theta}{\partial X} + V \frac{\partial \theta}{\partial Y} = \frac{\sigma_{hnf}}{\sigma_f} \left(\frac{\partial^2 \theta}{\partial X^2} + \frac{\partial^2 \theta}{\partial Y^2} \right) \quad (46)$$

III.2.3.2 Thermo-physical Aspects of the working fluid

The following characteristics of Ag and MgO nanosolids utilized to elaborate the working fluid (Hybrid nanofluid):

$$\varphi = \varphi_{Ag} + \varphi_{MgO} \quad (47)$$

$$\rho_{np} = \frac{\varphi_{MgO} \rho_{MgO} + \varphi_{Ag} \rho_{Ag}}{\varphi} \quad (48)$$

$$(c_p)_{np} = \frac{\varphi_{MgO} (c_p)_{MgO} + \varphi_{Ag} (c_p)_{Ag}}{\varphi} \quad (49)$$

$$\beta_{np} = \frac{\varphi_{MgO} \beta_{MgO} + \varphi_{Ag} \beta_{Ag}}{\varphi} \quad (50)$$

$$k_{np} = \frac{\varphi_{MgO} k_{MgO} + \varphi_{Ag} k_{Ag}}{\varphi} \quad (51)$$

$$\sigma_{np} = \frac{\varphi_{Ag} \sigma_{Ag} + \varphi_{MgO} \sigma_{MgO}}{\varphi} \quad (52)$$

The mixture-nanofluid's density is represented by ρ_{hnf} , while its viscosity and thermal conductivity are represented by μ_{hnf} and k_{hnf} , respectively. The thermal expansion

coefficient of the hybrid-nanofluids is $c_{p,hmf}$, and the nanofluid thermal expansion factor is β_{hmf} .

$$\rho_{hmf} = (1 - \phi)\rho_f + \phi\rho_p \quad (53)$$

$$(\rho c_p)_{hmf} = (1 - \phi)(\rho c_p)_f + \phi(\rho c_p)_p \quad (54)$$

$$(\rho\beta)_{hmf} = (1 - \phi)(\rho\beta)_f + \phi(\rho\beta)_p \quad (55)$$

$$k_{hmf} = \frac{k_{np} + (n-1)k_f - (n-1)(k_f - k_{np})\phi}{k_{np} + (n-1)k_f + (k_f - k_{np})\phi} k_f \quad (56)$$

$$\mu_{hmf} = \frac{\mu_f}{(1-\phi)^{2.5}} \quad (57)$$

$$\frac{\sigma_{hmf}}{\sigma_f} = 1 + \frac{3(\sigma_{np} - \sigma_f)\phi}{(\sigma_{np} + 2\sigma_f) - (\sigma_{np} - \sigma_f)\phi} \quad (58)$$

In case of using a hybrid nanofluid, the following are the definitions of Ra , Ha , Pr , average and local Nusselt numbers Nu_{ave} , Nu_{loc} :

$$Ra = \frac{\beta_f g (T_h - T_c) L^3}{\alpha_f \nu_f} \quad (59)$$

$$Ha = B_0 L \sqrt{\frac{\sigma_{hmf}}{\rho_{hmf} \nu_f}} \quad (60)$$

$$Pr = \frac{\nu_{hmf}}{\alpha_{hmf}} \quad (61)$$

$$Nu_{loc} = \begin{cases} \frac{k_{hmf}}{k_f} \frac{\partial T}{\partial x} \\ \frac{k_{hmf}}{k_f} \frac{\partial T}{\partial y} \end{cases} \quad (62)$$

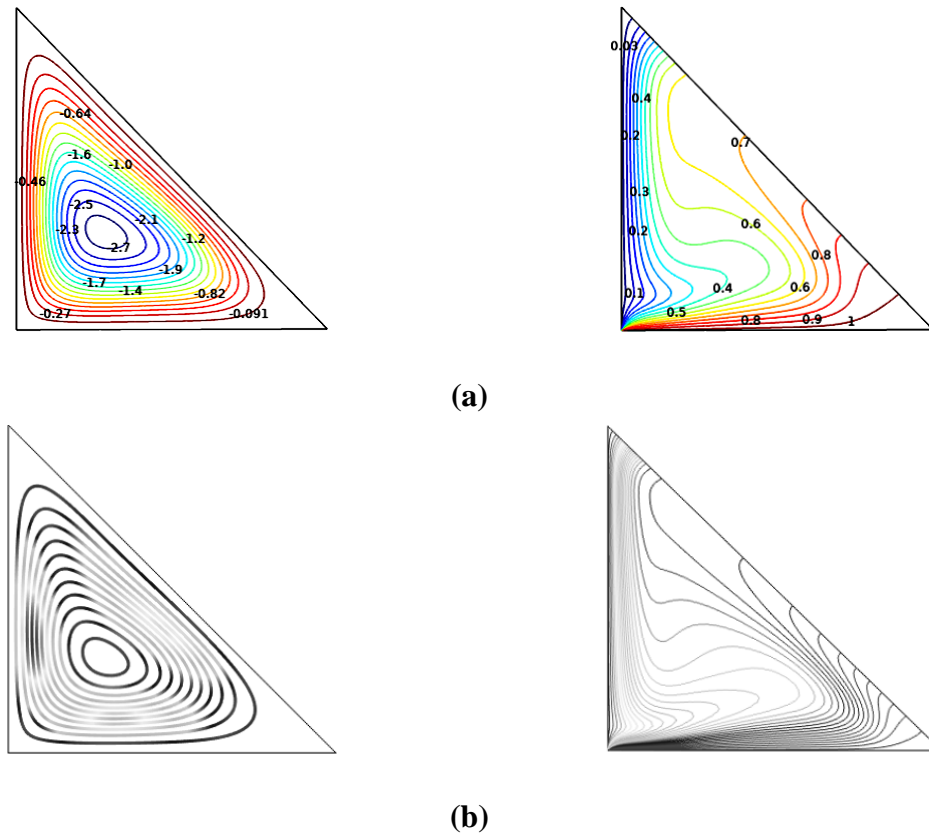
$$Nu_{avg} = \frac{1}{L} \int_0^L Nu_{loc} dL \quad (63)$$

III.2.3.3 Validation and test of mesh independency

To prove grid independence, the effect of the mesh scale on the average Nusselt number is explored for coarse, normal, fine, extra fine, and very fine mesh configurations. The extra fine grid (Gr05) with 4619 triangular elements was adopted in the current analysis.

Table III. 1. Effect of the mesh size on average Nusselt number with $Ra = 10^6$, $Ha = 0$, $\Phi = 0.02$, $\omega = 0$ rd/s, $r_p = 0.3L$ and $r_{ob} = 0.1L$.

Grid	01	02	03	04	05	06
Number of elements	298	633	852	1457	4619	17947
Nu_{avg}	1.692	1.6601	1.6493	1.6336	1.6086	1.5932

**Figure III. 2:** Comparison of current work (a) with Ref. [93] (b) at $Ra=10^5$ and $Ha=0$.

III.2.3.4 Results discussion

The influence of the main regulating parameters is examined in the current case. Numerous physical characteristics of the studied hybrid nanofluid are evaluated, including Rayleigh ($10^3 \leq Ra \leq 10^6$), Hartman number ($0 \leq Ha \leq 80$), and the nanoparticles volume fraction within the fluid.

a- Influence of Rayleigh number

The contours of the streamlines (left-hand) and isotherms (right-hand) change with varying Ra for the nanoparticle volume fraction ($\Phi = 0.02$) and rotation speed ($\omega = 0$ rd/s), as shown in Fig. III.3.a. The results show that as Ra values increase, the streamline and isotherm

distributions improve. It is noted that the isotherm lines appear stratified for lower values of Ra. This suggests that conduction has a greater role in the movement of heat.

The parallel shape of the isotherms and the low streamline values at the lower Ra ($Ra=10^3$) suggest that there is not enough convective fluid motion within the enclosure. Ra increases the relative importance of the convection method of heat transfer. Better heat dissipation within the hollow is shown by the more distorted isotherm lines. Higher values of Ra are preferable for convective fluid movement because of the increased buoyant forces.



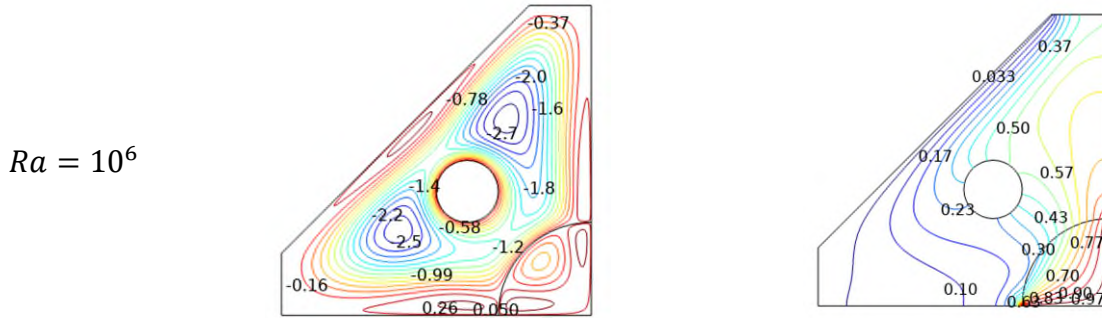


Figure III.3.a: Evolution of the ψ_{max} , and T for multiple amounts of Ra , $Ha = 20$, $\Phi = 0.02$, $r_p = 0.3L$, $r_{ob}=0.1L$ and $\omega = 0$ rd/s.

Figure III. 3.b depicts the results of Ra for various values of Ha . The average Nusselt number is reported to increase dramatically with Ra due to buoyant forces. For $Ra \geq 10^5$, this effect is clearly observable, and it is more intense in the absence of a magnetic field.

Figures III.3.c and III.3.d demonstrate that when the characteristics of the porous medium improve, Ra has a higher influence on heat transfer efficiency. The greatest Nu_{avg} is seen at the highest values of Darcy number ($Da=0.15$) and porosity ($\epsilon=0.5$). Furthermore, as demonstrated in Fig. III.3.e, a smaller porous medium radius ($r_p=0.1L$) has a stronger favorable influence on boosting Ra .

Figure III.3.f depicts the influence of Ra on different circular obstacle radiuses (r_{ob}) within the cavity when the rotational speed is zero ($\omega=0$ rd/s). According to the findings, there is no obvious variation in the average Nusselt as the obstruction dimensions rise in this situation. $Ra \leq 10^5$ produces a little impression of fluctuation. Figure III.3.g shows how increasing the obstacle's rotating velocity (ω) positively improves heat transfer efficiency (0 rd/s $\leq \omega \leq +2000$ rd/s). The inverse impact happens when the rotation speeds up in the negative direction (-2000 rd/s $\leq \omega \leq 0$ rd/s).

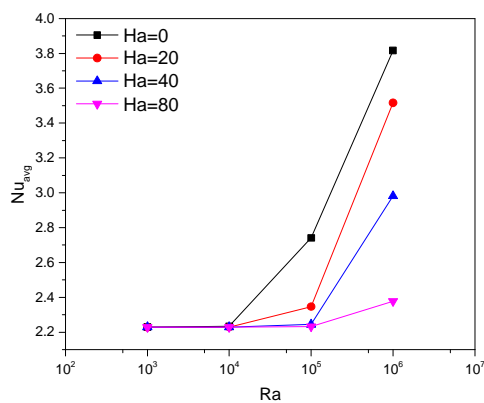


Figure. III.3.b. Evolution of Nu_{avg} with Ra for diverse Ha , $\Phi = 0.02$, $r_p = 0.3L$, $r_{ob} = 0.1L$ and $\omega = 0$ rd/s.

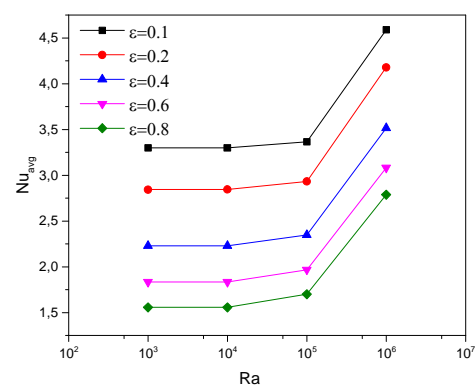


Figure. III. 3.c. Evolution of Nu_{avg} with Ra for diverse ϵ , $Ha = 20$, $r_p = 0.3L$, $r_{ob} = 0.1L$ and $\omega = 0$ rd/s.

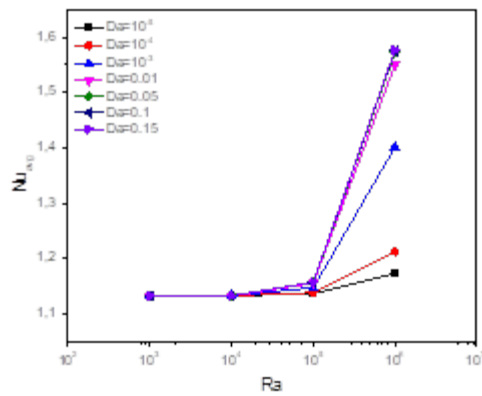


Figure. III.3.d. Evolution of Nu_{avg} with Ra for diverse Da , $Ha = 20$, $r_p = 0.3L$, $r_{ob} = 0.1L$ and $\omega = 0$ rd/s .

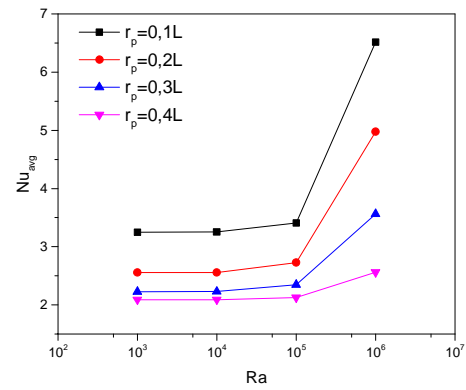


Figure. III.3.e. Evolution of Nu_{avg} with Ra for diverse r_p , $Ha = 20$, $\Phi = 0.02$, $r_{ob} = 0.1L$ and $\omega = 0$ rd/s .

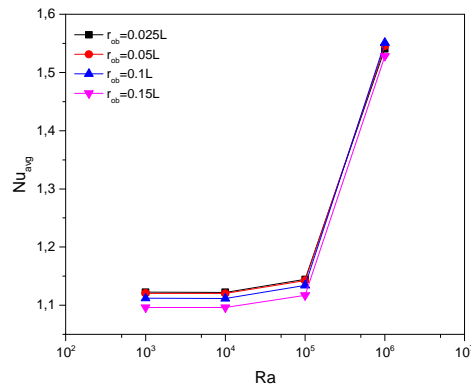


Figure. III.3.g. Evolution of Nu_{avg} with Ra for diverse r_{ob} , $Ha = 20$, $r_p = 0.3L$, $\Phi = 0.02$, $r_{ob} = 0.1L$ and $\omega = 0$ rd/s .

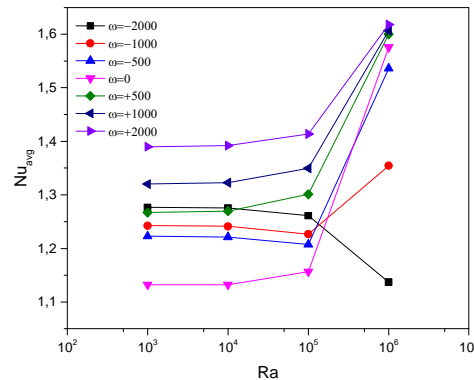


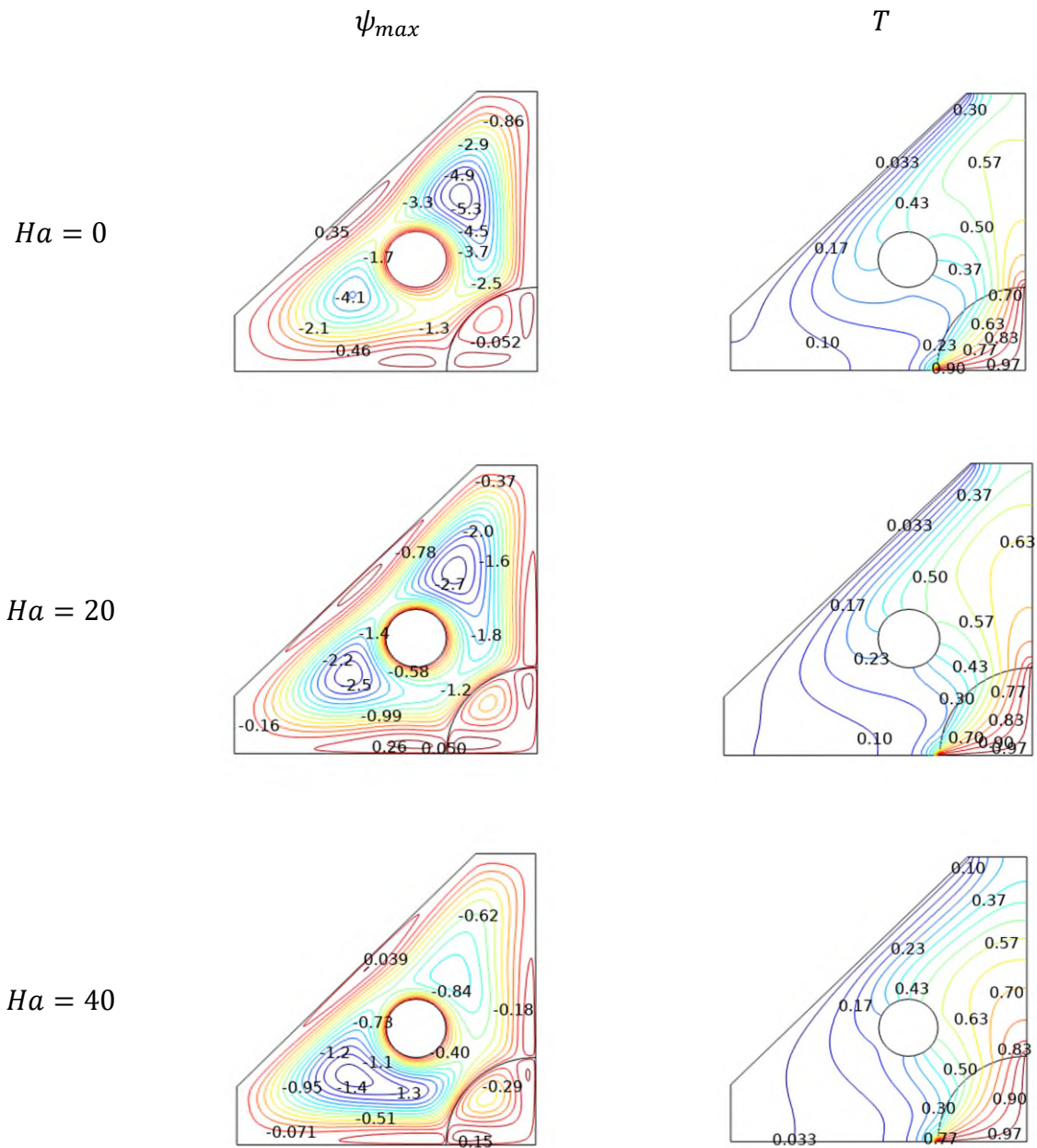
Figure. III.3.f. Evolution of Nu_{avg} with Ra for diverse ω , $Ha = 20$, $r_p = 0.3L$, $\Phi = 0.02$, and $r_{ob} = 0.1L$.

b- Influence of Hartmann number

Using the results of streamlines and isotherm outlines, numerical calculations are carried out to evaluate the impact of different quantities of Ha ($0 \leq Ha \leq 80$) on heat transfer efficiency. When Ha is changed, there are noticeable variations in the temperature field, as seen in Fig. III. 4.a. Increasing Ha lowers the concentration of isothermal lines. Moreover, the flowing area and vortex's velocity both decrease as Ha rises.

The Hartmann number acts as a characterization of the homogeneous magnetic field influence. Increases in Ha show variations in flux and thermal pattern. Increased Ha concentrations result in decreased fluid flow. In addition, A greater magnetic field reduces fluid mobility, resulting in a reduced concentration of isotherm lines near the warmed walls at the right-angled corner. These findings show the relationship between Ha and T and ψ_{max} .

Streamlines degrade with increasing Ha amount. But when Ha increases, isotherm profiles cover most of the hollow. Put another way, the magnetic field affects the cavity's heat transfer efficiency. Conversely, when Ha rises, so does the contribution from heat conduction.



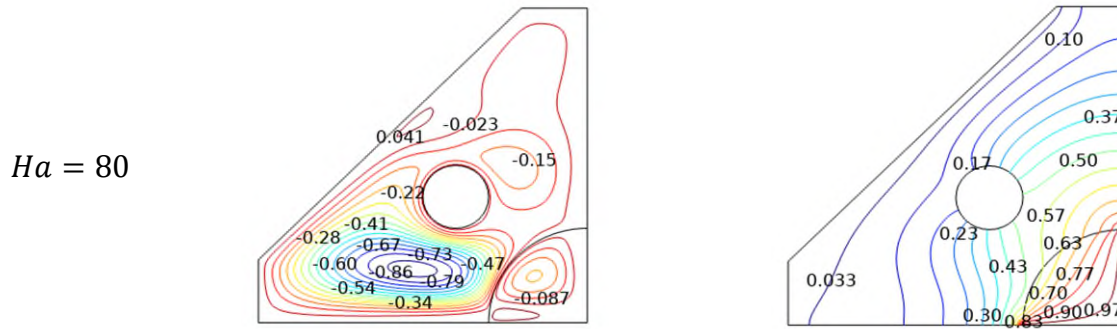


Figure III.4. a. Evolution of ψ_{max} and T for various Ha , $Ra = 10^6$, $\Phi = 0.02$, $r_p = 0.3L$, $r_{ob} = 0.1L$ and $\omega = 0$ rd/s .

Figure III.4.b demonstrates that Nu_{avg} declines with increasing Ha for all $Da \geq 0.01$ values. This answer is somewhat modified for small values ($Da \leq 10^{-3}$). Furthermore, boosting Da improves the efficacy of heat transport. Otherwise, when the Darcy number rises from $Da=0.1$ to $Da=0.15$, the increase in Nu_{avg} is insignificant.

Fig. III. 4.c shows the dependence of Ha on Nu_{avg} for various degrees of porosity (ϵ) in porous media. It is found that when the magnetic parameter dominates inside the enclosure, Ha rises, Nu_{avg} decreases, and convection flowing is significantly reduced. Furthermore, it is evident that increasing porosity improves the heat transfer response. Figure 4.d, which shows the fluctuation of Nu_{avg} for various diameters of the porous medium radius (r_p), exhibits the similar impact of Ha . It is discovered that raising r_p produces the greatest values of Nu_{avg} .

Figure III.4.e illustrates how Ha affects thermal efficiency at various nanoparticle concentrations (Φ). The graph demonstrates that when Ha increases, the strength of heat transportation convections decreases for all Φ values. Furthermore, the highest volume percentages of nanoparticles correspond with the highest values of Nu_{avg} .

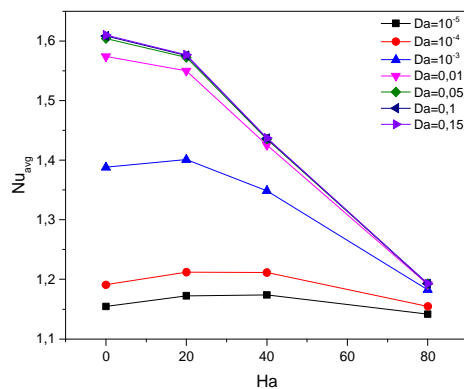


Fig.III.4. b. Evolution of Nu_{avg} with Ha for various Da , $Ra = 10^6$, $r_p = 0.3L$, $r_{ob} = 0.1L$ and $\omega = 0$ rd/s .

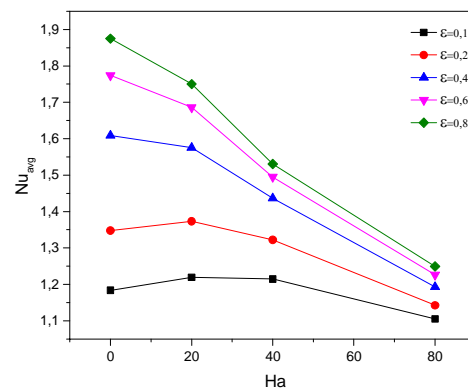


Fig.III.4. c. Evolution of Nu_{avg} with Ha for various ϵ , $Ra = 10^6$, $r_p = 0.3L$, $r_{ob} = 0.1L$ and $\omega = 0$ rd/s .

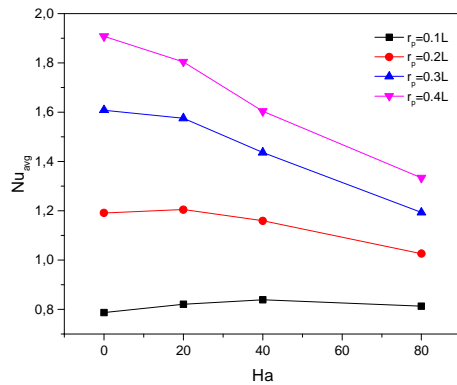


Fig.III.4. d. Evolution of Nu_{avg} with Ha for various r_p , $Ra = 10^6$, $\Phi = 0.02$, $r_{ob} = 0.1L$ and $\omega = 0$ rd/s .

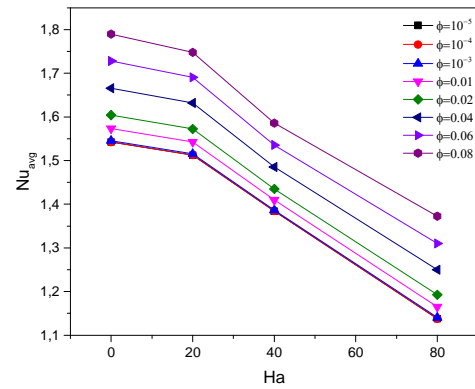


Fig.III.4. e. Evolution of Nu_{avg} with Ha for various Φ , $Ra = 10^6$, $r_p = 0.3L$, $r_{ob} = 0.1L$ and $\omega = 0$ rd/s .

III.3 Case 02: MHD natural convection of a nanofluid involved in a complex C-shaped enclosure [94].

III.3.1 Abstract

The MHD free convection heat of an Ag-Water nanofluid inside a porous C-shaped container is the main subject of this case study. This cavity is equipped with an elongating baffle that is kept at a cold temperature (T_c). On the bottom and left wall, non-uniform hot temperature (T_h) is also applied. This specific configuration has been used to investigate several thermophysical properties, such as Ra ($10^3 \leq Ra < 10^6$), Ha ($0 \leq Ha \leq 100$), and nanoparticle concentration ($0.01 \leq \Phi \leq 0.08$). FEM was used to do the computations with $Pr = 6.83$.

III.3.2 Characterization of problem

The present geometry consists of a porous C-shaped enclosure filled with Ag-H₂O nanofluid, as shown in the figure below. The bottom and left walls are heated to a non-uniform hot temperature (T_h), while the entire opposite side, including the undulating baffle, is maintained at a cold temperature (T_c). The upper side of the chamber is insulated.

The geometry under investigation is exposed to a constant magnetic field (B_0), and it is believed that the nanofluid within would flow lamarily and steadily and be Newtonian in nature.

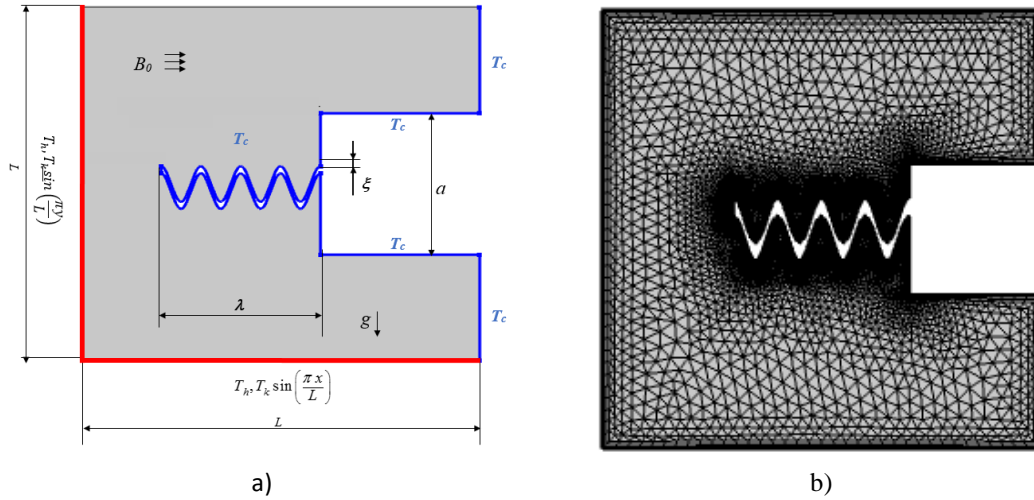


Figure.III.5 Graphic illustration of the mesh distribution (a) and physical model (b) of the studied geometry.

III.3.3 Formulation of the Mathematical Model

III.3.3.1 Mathematical formulation

The following is a list of the fundamental mathematical equations that control the nanofluid phase for the 2D cavity fluid area:

$$\frac{\partial u}{\partial x} + \frac{\partial v}{\partial y} = 0 \quad (29)$$

$$(u \frac{\partial u}{\partial x} + v \frac{\partial v}{\partial y}) = -\frac{1}{\rho_{nf}} \frac{\partial P}{\partial x} + \nu_{nf} (\frac{\partial^2 u}{\partial x^2} + \frac{\partial^2 u}{\partial y^2}) \quad (64)$$

$$(u \frac{\partial u}{\partial x} + v \frac{\partial v}{\partial y}) = -\frac{1}{\rho_{nf}} \frac{\partial P}{\partial y} + \nu_{nf} (\frac{\partial^2 v}{\partial x^2} + \frac{\partial^2 v}{\partial y^2}) + \beta_{nf} g (T - T_{ave}) + \frac{\sigma_{nf}}{\rho_{nf}} B_0^2 v \quad (65)$$

$$(\rho c_p)_{nf} (u \frac{\partial T}{\partial x} + v \frac{\partial T}{\partial y}) = k_{nf} (\frac{\partial^2 T}{\partial x^2} + \frac{\partial^2 T}{\partial y^2}) \quad (66)$$

The governing equations for the porous domain are as follows, based on the Darcy-Brinkmann-Forchheimer formula:

$$\frac{\partial u}{\partial x} + \frac{\partial v}{\partial y} = 0 \quad (29)$$

$$\frac{1}{\varepsilon^2} (u \frac{\partial u}{\partial x} + v \frac{\partial v}{\partial y}) = -\frac{1}{\rho_{nf}} \frac{\partial P}{\partial x} + \frac{\nu_{nf}}{\varepsilon} (\frac{\partial^2 u}{\partial x^2} + \frac{\partial^2 u}{\partial y^2}) - \nu_{nf} \frac{u}{K} - \frac{F_c}{\sqrt{K}} u |u| \quad (67)$$

$$\frac{1}{\varepsilon^2} (u \frac{\partial u}{\partial x} + v \frac{\partial v}{\partial y}) = -\frac{1}{\rho_{nf}} \frac{\partial P}{\partial y} + \frac{\nu_{nf}}{\varepsilon} (\frac{\partial^2 v}{\partial x^2} + \frac{\partial^2 v}{\partial y^2}) - \nu_{nf} \frac{v}{K} - \frac{F_c}{\sqrt{K}} v |v| + \beta_{nf} g (T - T_{ave}) + \frac{\sigma_{nf}}{\rho_{nf}} B_0^2 v \quad (68)$$

$$(\rho c_p)_{nf} (u \frac{\partial T}{\partial x} + v \frac{\partial T}{\partial y}) = k_{nf} (\frac{\partial^2 T}{\partial x^2} + \frac{\partial^2 T}{\partial y^2}) \quad (69)$$

Boundary conditions and dimensionless governing formulae are developed using the following parameters, which are:

$$x = \bar{x}/L, y = \bar{y}/L, u = \bar{u}/U_0, v = \bar{v}/V_0.$$

$$\theta = (T - T_0)/(T_h - T_c), \quad \psi = \bar{\psi}/(U_0L), \quad P = \frac{\bar{p}}{\rho_{nf}u_0^2}, \quad Da = \frac{K}{L^2}.$$

The main non-dimensional formulations are as follows:

$$\frac{\partial U}{\partial X} + \frac{\partial V}{\partial Y} = 0 \quad (43)$$

$$\frac{1}{\varepsilon^2} \frac{\rho_{nf}}{\rho_f} \left(U \frac{\partial U}{\partial X} + V \frac{\partial V}{\partial Y} \right) = - \frac{1}{\rho_{nf}} \frac{\partial P}{\partial X} + \frac{1}{\varepsilon} \frac{\nu_{nf}}{\nu_f} \frac{Pr}{\sqrt{Ra}} \left(\frac{\partial^2 U}{\partial X^2} + \frac{\partial^2 U}{\partial Y^2} \right) - \frac{\nu_{nf}}{\nu_f} \frac{Pr}{Da\sqrt{Ra}} - \frac{Fc}{\sqrt{Da}} |U|U \quad (70)$$

$$\frac{1}{\varepsilon^2} \frac{\rho_{nf}}{\rho_f} \left(U \frac{\partial U}{\partial X} + V \frac{\partial V}{\partial Y} \right) = - \frac{1}{\rho_{nf}} \frac{\partial P}{\partial Y} + \frac{1}{\varepsilon} \frac{\nu_{nf}}{\nu_f} \frac{Pr}{\sqrt{Ra}} \left(\frac{\partial^2 V}{\partial X^2} + \frac{\partial^2 V}{\partial Y^2} \right) - \frac{\nu_{nf}}{\nu_f} \frac{Pr}{Da\sqrt{Ra}} V - \frac{Fc}{\sqrt{Da}} |U|V +$$

$$Pr \frac{\beta_{nf}}{\beta_f} g\theta + \frac{\sigma_f}{\rho_{nf}} \frac{\rho_f}{\rho_{nf}} \frac{Pr Ha^2}{\varepsilon\sqrt{Ra}} V \quad (71)$$

$$U \frac{\partial \theta}{\partial X} + V \frac{\partial \theta}{\partial Y} = \frac{\sigma_{nf}}{\sigma_f} \left(\frac{\partial^2 \theta}{\partial X^2} + \frac{\partial^2 \theta}{\partial Y^2} \right) \quad (72)$$

III.3.3.2 Thermophysical characteristics of nanofluid

k_{nf} , μ_{nf} and ρ_{nf} indicate the density, viscosity, and the thermal conductivity of working fluid, respectively. β_{nf} is the thermal expansion coefficient of the nanofluid and $C_{p,nf}$ the thermal expansion coefficient.

$$\rho_{nf} = (1 - \phi)\rho_f + \phi\rho_p \quad (73)$$

$$(\rho c_p)_{nf} = (1 - \phi)(\rho c_p)_f + \phi(\rho c_p)_p \quad (74)$$

$$(\rho\beta)_{nf} = (1 - \phi)(\rho\beta)_f + \phi(\rho\beta)_p \quad (75)$$

$$k_{nf} = \frac{k_{np} + (n-1)k_f - (n-1)(k_f - k_{np})\phi}{k_{np} + (n-1)k_f + (k_f - k_{np})\phi} k_f \quad (76)$$

$$\mu_{nf} = \frac{\mu_f}{(1-\phi)^{2.5}} \quad (77)$$

$$\frac{\sigma_{nf}}{\sigma_f} = 1 + \frac{3(\sigma_{np} - \sigma_f)\phi}{(\sigma_{np} + 2\sigma_f) - (\sigma_{np} - \sigma_f)\phi} \quad (78)$$

The following are the definitions of the Rayleigh number (Ra), Hartmann number (Ha), and Prandtl number (Pr):

$$Ra = \frac{\beta_f g (T_h - T_c) L^3}{\alpha_f \nu_f} \quad (59)$$

$$Ha = B_0 L \sqrt{\frac{\rho_{nf}}{\rho_{nf} \nu_f}} \quad (79)$$

$$Pr = \frac{\nu_f}{\alpha_f} \quad (80)$$

Both Nusselt numbers, local and average are given as follows:

$$Nu_{avg} = \frac{1}{L} \int_0^L Nu_{loc} dL \quad (81)$$

$$Nu_{loc} = \begin{cases} \frac{k_{nf}}{k_f} \frac{\partial T}{\partial x} \\ \frac{k_{nf}}{k_f} \frac{\partial T}{\partial y} \end{cases} \quad (82)$$

III.3.3.3 Boundary conditions

The left and bottom sides of the C-shaped cavity are heated unevenly high (T_h). The cavity's upper side is insulated. In contrast, the undulating baffle and the whole right-sidewall maintain a constant cooling temperature (T_c).

The boundary conditions are as follows:

- Hot walls: $u = v = 0$,

$$\text{At the left wall: } T_h = T_k \sin\left(\frac{\pi y}{L}\right)$$

$$\text{At the bottom: } T_h = T_k \sin\left(\frac{\pi x}{L}\right)$$

- Cold walls and the undulated baffle: $u = v = 0$, $T = T_c$.

- Insulated upper wall: $u = v = 0$, $\frac{\partial T}{\partial n} = 0$.

III.3.3.4 Results discussion

This numerical research investigates the influence of several thermo-physical factors within a challenging geometry, such as Rayleigh number ($10^3 \leq Ra \leq 10^6$), Hartmann number ($0 \leq Ha \leq 100$), and the nanoparticles concentration ($0.01 \leq \Phi \leq 0.08$).

- a- Influence of Rayleigh number

Figure III.6 illustrates how the isotherms (right) and the streamlines (left) change as the Rayleigh number increases. As Ra grows, it can be noticed that the streamlines distribution improves and covers the whole geometry. Furthermore, the isotherm lines deform with

increasing Ra, indicating an elevation in heat loss within the cavity due to buoyancy forces and an increase in convective fluid motion.

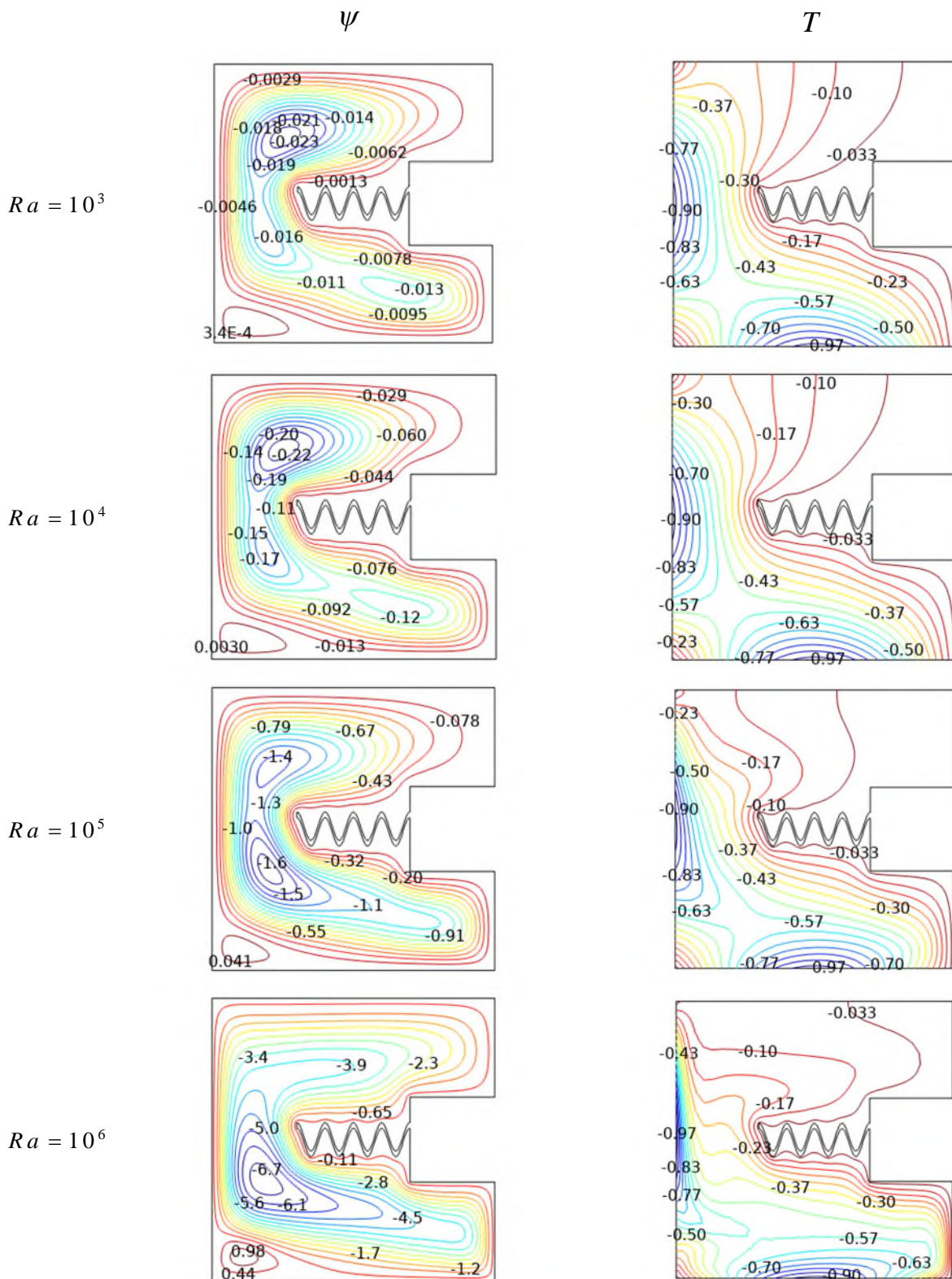


Figure.III.6.a Evolution of the streamlines and isotherms for multiple amounts of Ra, Ha=25, $\phi=0.01$, Da=0.01 and $\varepsilon = 0.4$

Figure III.6.b depicts the evolution of Nu_{avg} vs Ra for various Ha values. At lower values of Ha , Nu_{avg} increases with Ra . Ra has a greater effect when it is less than 10^4 . However, for higher Hartmann numbers ($Ha=100$), the effect of raising Ra is very minimal.

The impact of Ra on heat transfer efficiency when porosity and Da grow, respectively, is shown in Figures III.6.c and III.6.d. Increasing Da increases heat transfer efficiency and improves fluid flow inside the porous cavity. Moreover, permeability has a greater effect than porosity. As porosity increases, the average Nusselt number considerably lowers. As the number of empty spaces inside the cavity increases, the effective heat conductivity decreases, causing this response.

Convective heat transfer is much improved when the volume % of nanoparticles is increased, as Figure III.6.e demonstrates. This effect can be noticed for both high and low Rayleigh numbers. Figures III.7 f, g, and h show how the thickness (ζ), true horizontal length (λ), and undulation number (und) of an undulated baffle design affect Nu_{avg} response as Ra rises. It is found that increasing the baffle's length and thickness improves heat transmission efficiency. If not, there is no discernible difference when the number of undulations is increased.

The effects of changing the C-shaped cavity's empty section's size are seen in Figure III.6.i. Stated otherwise, modifying the length of a hollow square's sides (a). Nu_{avg} ($Ra \leq 10^5$) is significantly affected by length (a) increases when the Ra is large.

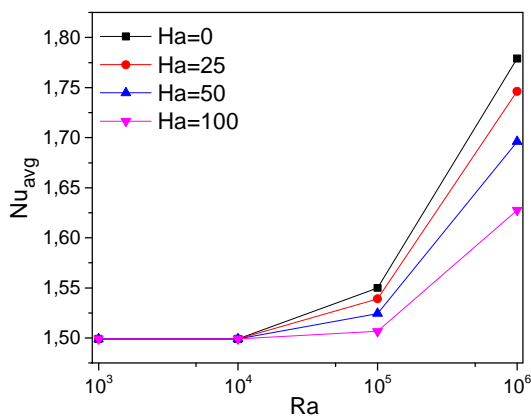


Figure. III.6.b Evolution of Nu_{avg} with Ra for different Ha values, $\phi=0.01$, $Da=0.01$ and $\epsilon=0.4$.

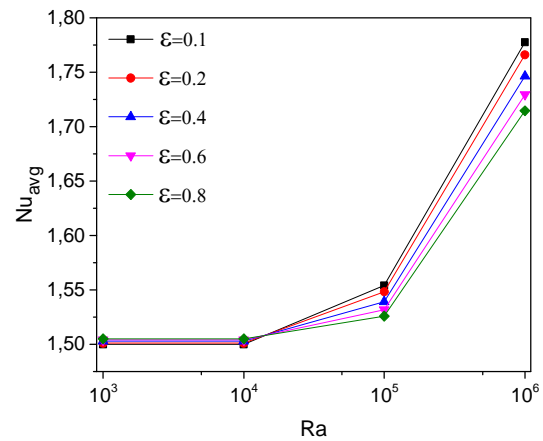


Figure. III.6.c Evolution of Nu_{avg} with Ra for different porosity values (ϵ), $Ha=25$, $\phi=0.01$ and $Da=0.01$.

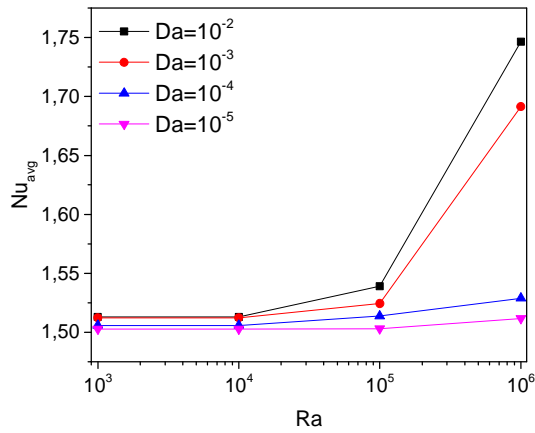


Figure. III.6.d Evolution of Nu_{avg} with Ra for different Da values, $Ha=25$, $\phi=0.01$ and $\varepsilon=0.4$.

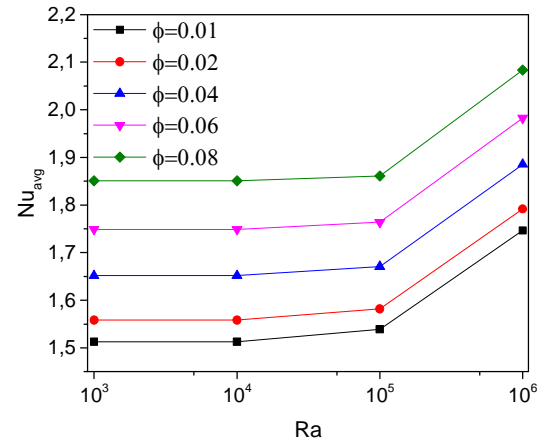


Figure. III.6.e Evolution of Nu_{avg} with Ra for various nanoparticles concentrations (ϕ), $Ha=25$, $\varepsilon=0.4$ and $Da=0.01$.

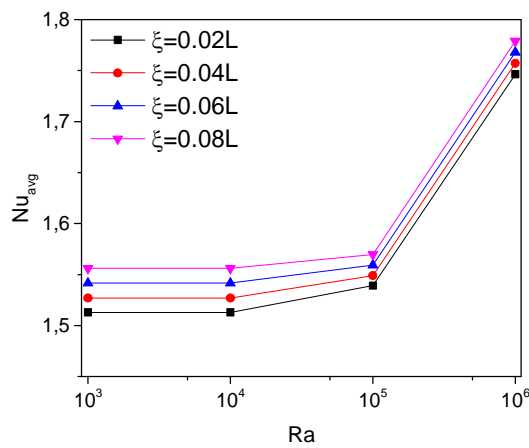


Figure. III.6.f Evolution of Nu_{avg} with Ra for different baffle thickness (ζ), $Ha=25$, $\phi=0.01$, $\varepsilon=0.4$ and $Da=0.01$.

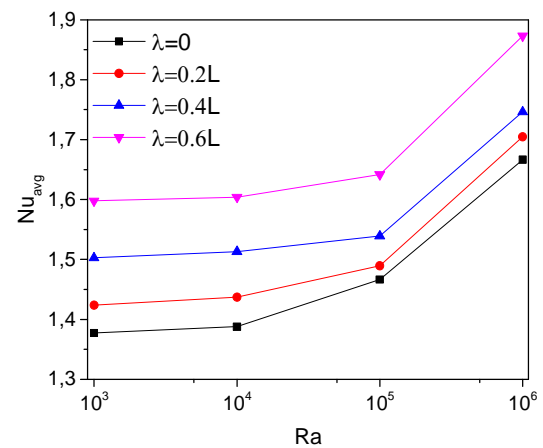


Figure. III.6.g Evolution of Nu_{avg} with Ra for for different baffle length (λ), $Ha=25$, $\phi=0.01$, $\varepsilon=0.4$, $Da=0.01$ and $\zeta=0.02L$.

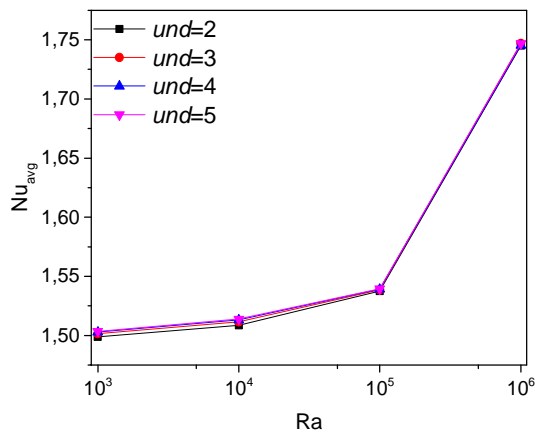


Figure. III.6.h Evolution of Nu_{avg} with Ra for different baffle undulation number (und), $Ha=25$, $\phi=0.01$, $\varepsilon=0.4$, $Da=0.01$, $\zeta=0.02L$ and $\lambda=0.4L$.

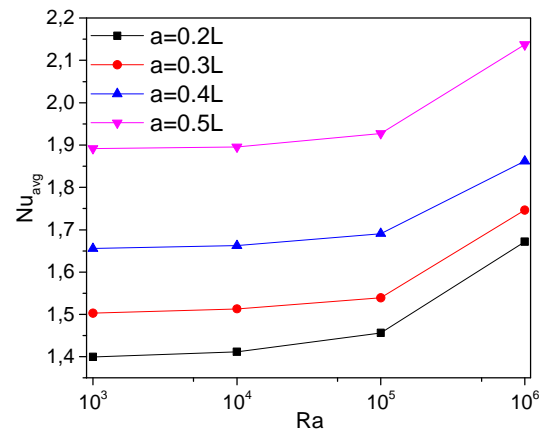
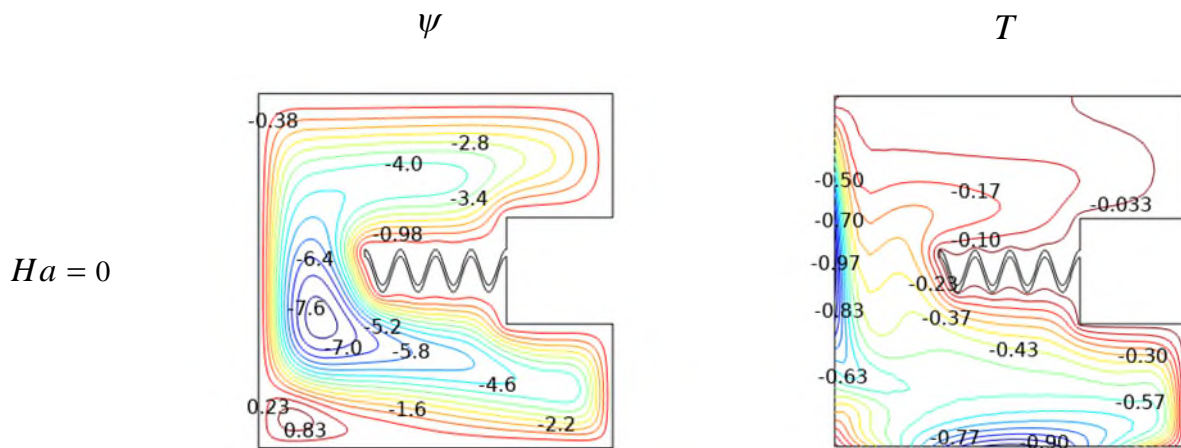


Figure. III.6.i Evolution of Nu_{avg} with Ra for different values of the empty square sides length (a), $Ha=25$, $\phi=0.01$, $\varepsilon=0.4$, $Da=0.01$, $\zeta=0.02L$, $\lambda=0.4L$ and $und=4$.

b- Influence of Hartmann number

Figure III.7.a exhibits isotherm contours and streamlines with Ha increments of $Ra=10^6$, $\phi=0.01$, $Da=0.01$, and $\varepsilon=0.4$. As Ha rises, streamline propagation decreases, indicating less convection flow circulation. In other words, when the magnetic field increases, heat transfer performance worsens due to the suppression effect of Lorentz forces. Furthermore, increasing Ha has a significant effect on the distribution of isotherms.



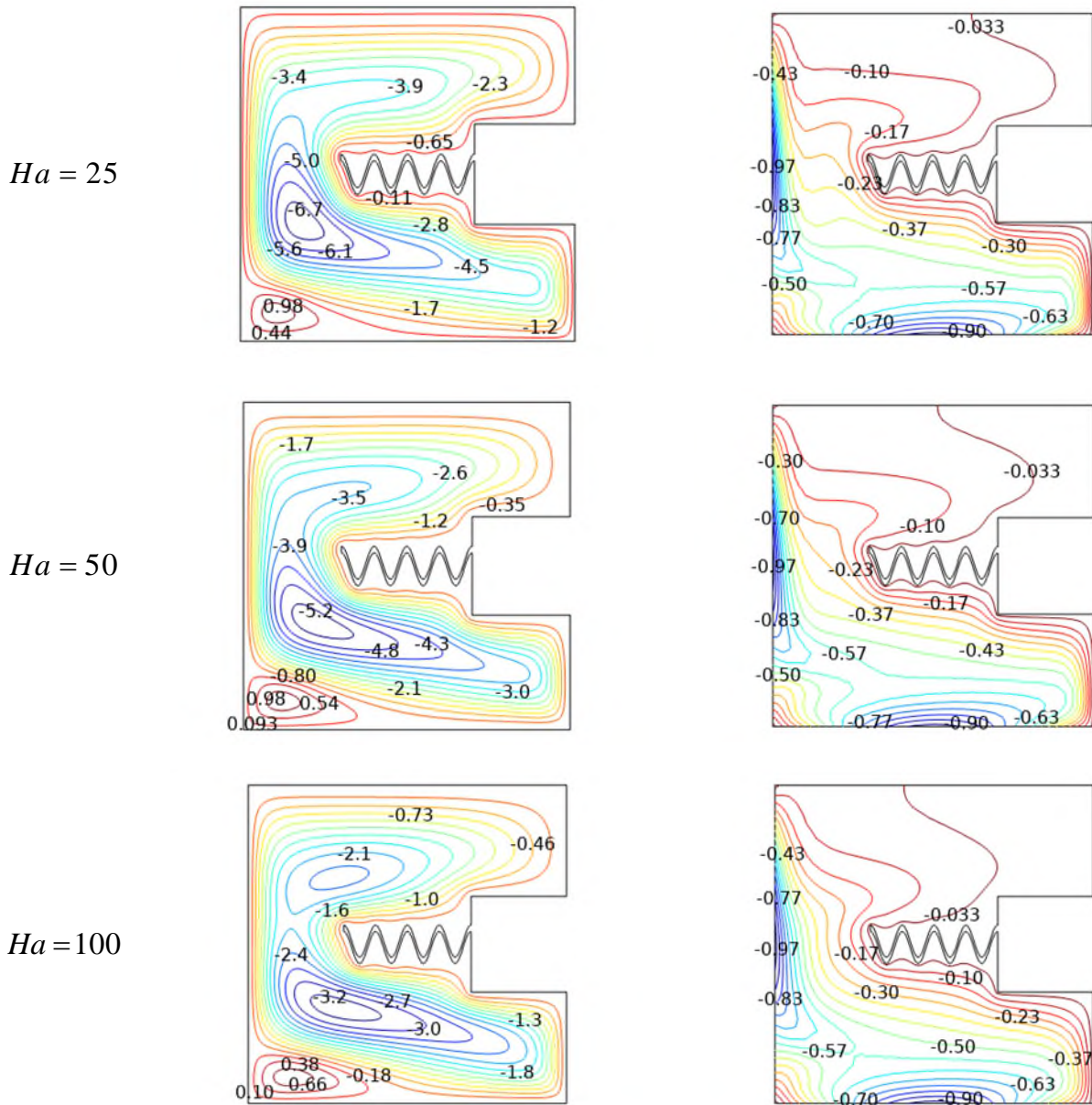


Figure III.7. a Evolution of the streamlines and isotherms for multiple amounts of Ha , $Ra=10^6$, $\phi=0.01$, $Da=0.01$ and $\varepsilon=0.4$

Figure III.7.b depicts the variability in Nu_{avg} against Ha at various porosity levels. At any porosity level, Nu_{avg} drops as the Ha increases, as expected. The decreasing impact becomes clearer as the magnetic field is more intensive ($Ha=100$) and porosity rises. ($\varepsilon=0.8$). Figure III.7.c demonstrates the heat transfer response to increasing magnetic field strength at various Darcy values. The presented graphs show that Nu_{avg} diminishes as Ha increases. Higher Darcy numbers have a significant impact, whereas lower ones ($Da < 10^{-4}$) have negligible effect.

Figure III.7.d compares Nu_{avg} response versus Ha variation at different nanoparticle concentrations. Nu_{avg} drops when the magnetic field intensity increases. As the volume percentage of nanoparticles in the base fluid rises, so does the convection heat transfer capacity.

Figures III.7.e and III.7.f relate Nu_{avg} to Ha for various thicknesses (ξ) and lengths (λ) values of the inner undulated baffle. Obviously, Nu_{avg} diminishes as Ha increases, regardless of baffle length or thickness. Furthermore, increasing the length or thickness leads to greater heat convection. Otherwise, increasing the baffle design's undulation number (*und*) has no influence on the declivity of Nu_{avg} versus Ha , as seen in Fig. III.7.g Figure III.7.h illustrates the effect of changing the length of the cavity's full C-shape. It has been established that increasing the sides length ($a = 0.5L$) with $Ha = 0$, resulted in a higher Nu_{avg} value.

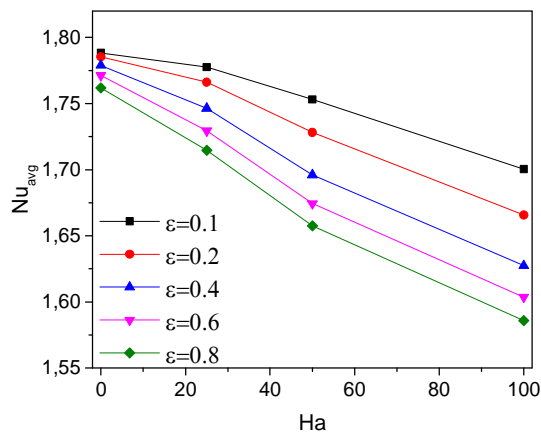


Figure.III.7. b Evolution of Nu_{avg} with Ha for different porosity values (ϵ), $Ra=10^6$, $\phi=0.01$ and $Da=0.01$.

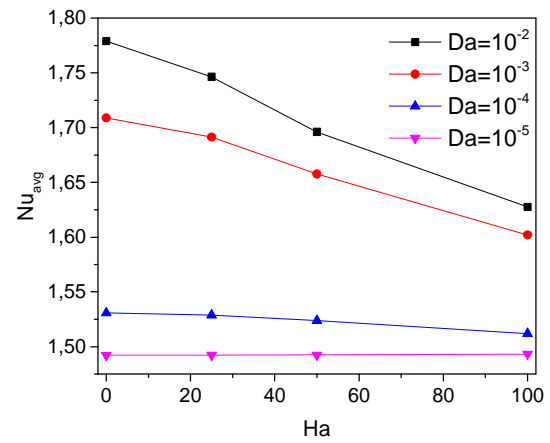


Figure.III.7. c Evolution of Nu_{avg} with Ha for different Da values, $Ra=10^6$, $\phi=0.01$ and $\epsilon=0.4$.

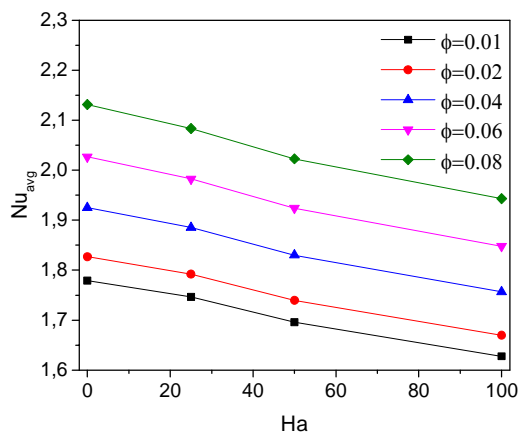


Figure.III.7. d Evolution of Nu_{avg} with Ha for different nanoparticles concentrations (ϕ), $Ra=10^6$, $\epsilon=0.4$ and $Da=0.01$.

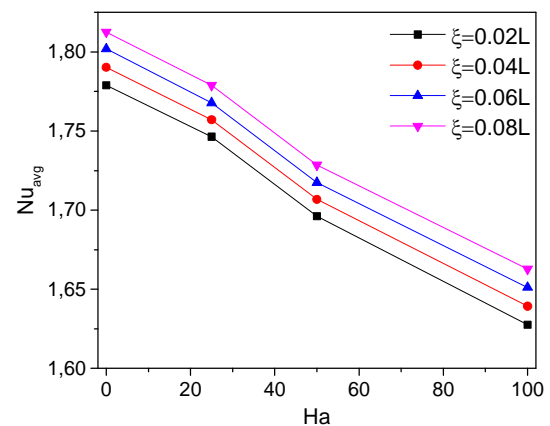


Figure.III.7. e Evolution of Nu_{avg} with Ha for different baffle thickness (ξ) at $Ra=10^6$, $\phi=0.01$, $\epsilon=0.4$ and $Da=0.01$.

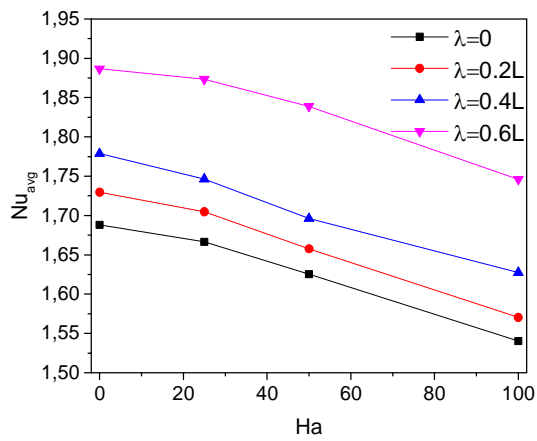


Figure.III.7. f Evolution of Nu_{avg} with Ha for different baffle length (b), $Ra=10^6$, $\phi=0.01$, $\varepsilon=0.4$, $Da=0.01$, $\xi=0.02L$.

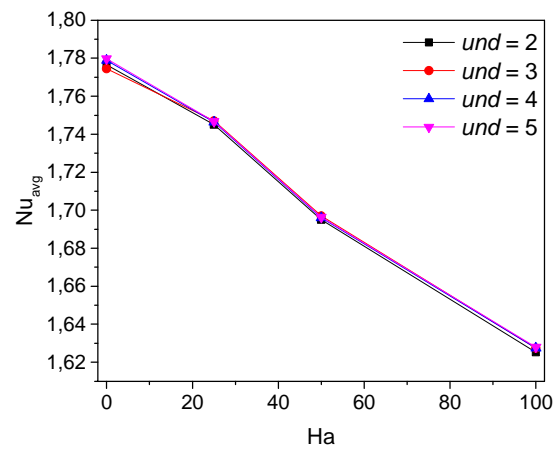


Figure.III.7. g Evolution of Nu_{avg} with Ha for different of the baffle undulation number (und), $Ra=10^6$, $\phi=0.01$, $\varepsilon=0.4$, $Da=0.01$, $\xi=0.02L$ and $\lambda=0.4L$.

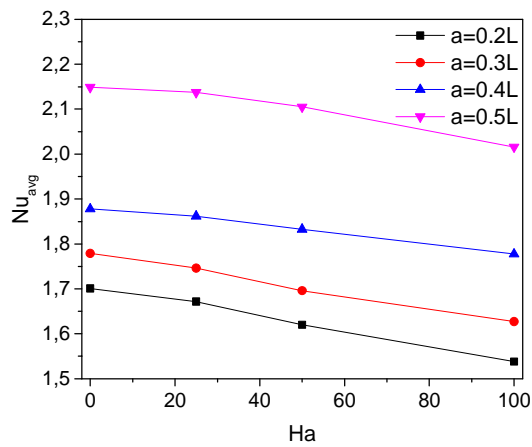


Figure.III.7. h Evolution of Nu_{avg} with Ha for different values of the empty square sides length (a), $Ra=10^6$, $\phi=0.01$, $\varepsilon=0.4$, $Da=0.01$, $\xi=0.02L$ and $\lambda=0.4L$. and $und=4$.

c- Influence of nanoparticles concentration

The graphs in Fig. III.8.a illustrate how the addition of the solid component in the base fluid influences the behavior of energy transmission within the cavity. Increasing the solid fraction enhances convection efficiency at any porosity level. Furthermore, it is obvious that all derived curves are almost straight with a noticeable slope. Figure III.8.b shows that Nu_{avg} improves when the solid fraction (ϕ) increases, independent of Darcy number. Furthermore, the greatest heat convection performance correlates to the highest Darcy number value ($Da = 10^{-2}$).

That relationship comes as a result of enhanced thermal conductivity of solid nanoparticles, which has a direct influence on the calculation of local and average Nusselt numbers. Raising Da also enhances the permeability of porous media, allowing fluid and solid particles to flow more easily.

As seen in Figs. III.8.c, III.8.d, and III.8.e, increasing the volume % of nanoparticles improves convection heat transfer at various geometrical adjustments, such as changing the undulated baffle thickness (ξ), baffle length (λ), and the parameter (a) related to the global shape of the geometry.

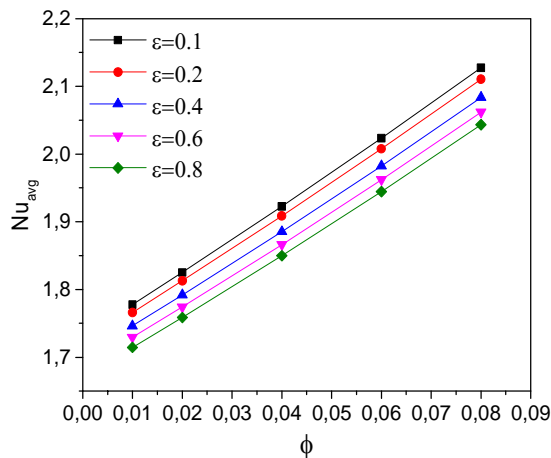


Figure.III.8. a Evolution of Nu_{avg} with the nanoparticles volume fraction (ϕ) for various values of porosity (ϵ), $Ra=10^6$, $Ha=25$, $Da=0.01$.

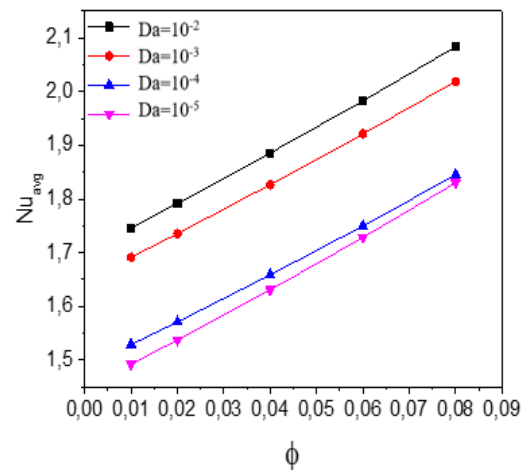


Figure.III.8. b Evolution of Nu_{avg} with the nanoparticles volume fraction (ϕ) for various values of Darcy number (Da), $Ra=10^6$, $Ha=25$, $\epsilon=0.4$.

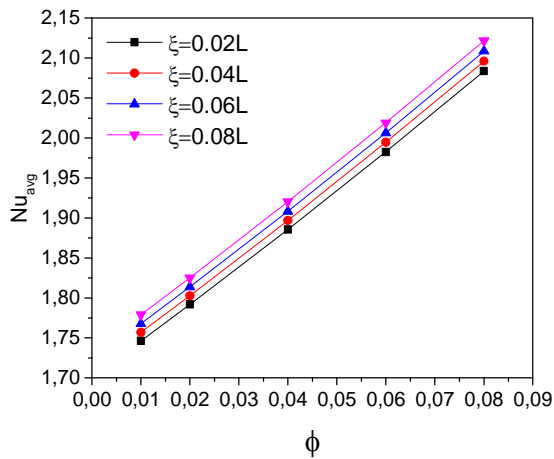


Figure.III.8.c Evolution of Nu_{avg} with the nanoparticles volume fraction (ϕ) for various values of baffle thickness (ξ), $Ra=10^6$, $Ha=25$, $\varepsilon=0.4$, $Da=0.01$.

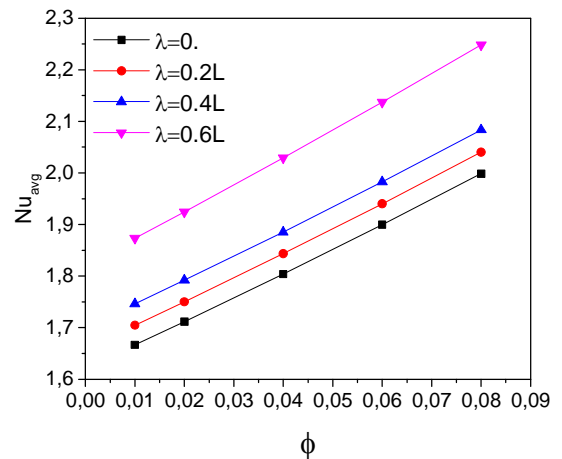


Figure.III.8.d Evolution of Nu_{avg} with the nanoparticles volume fraction (ϕ) for various values of baffle length (λ), $Ra=10^6$, $Ha=25$, $\varepsilon=0.4$, $Da=0.01$, $\xi=0.02L$.

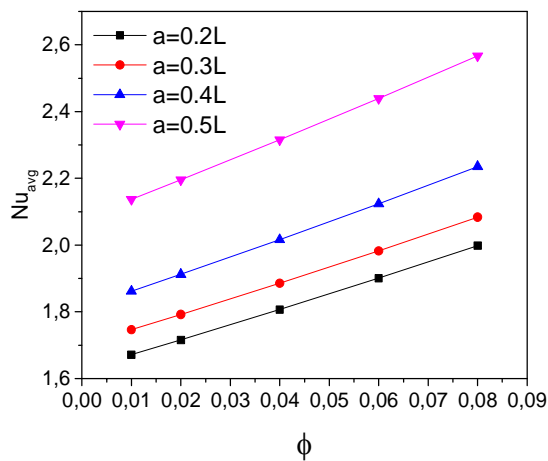


Figure.III.8.e Evolution of Nu_{avg} with the nanoparticles volume fraction (ϕ) for various values of the empty square sides length (a), $Ra=10^6$, $Ha=25$, $\varepsilon=0.4$, $Da=0.01$, $\xi=0.02L$, $\lambda=0.4L$ and $und=4$.

III.4 Conclusions

In this chapter, we discussed MHD free convection in a triangular cavity with partial presence of porous media and C-shaped chamber completely occupied by porous media. Both scenarios allow for the examination of the thermophysical behavior of the working fluid (nanofluids & hybrid nanofluid) inside enclosures, resulting in the following notable outcomes:

1. Increasing the Rayleigh number enhances heat transfer performance. An increase in buoyant forces results in better heat transfer efficiency and widespread nanofluid circulation within the enclosure.
- 2- Reducing nanoparticle velocity and monitoring the heat transfer response are achieved by increasing the magnetic field. Put another way, the Hartmann number indicates that convectonal heat transmission decreases as Lorentz powers rise.
- 3- Increased nanoparticle concentration enhances heat transfer efficiency within the cavity.

Chapter IV

Influence of the geometrical parameters of the cavity

Chapter IV: Influence of the geometrical parameters of the cavity.

IV.1 Introduction

This section will expand on the examination of the two scenarios from the previous chapter by examining how the geometry configuration affects the efficiency of MHD convection heat transfer. We'll look closely at the overall geometry, the form of the wall, the in-situ barriers in either a static or dynamic environment, and the existence of porous medium (including its size, permeability, and porosity).

IV.2 Case 01: MHD natural convection of a hybrid nanofluid involved in a complex triangular enclosure [92].

IV.2.1 Abstract

In this section, we will continue our investigation of the behavior of the Ag-MgO/Water hybrid nanofluid within the triangle hollow in response to certain geometrical input and modification, including the inclusion of porous media in one of its corners and a revolving cylinder in the center of the geometry.

The parameters of the porous medium, such as porosity and permeability, will be varied to determine the effect on heat transmission efficiency within the enclosure. Furthermore, the innovative findings in this work are based on establishing the boosting effect of increasing the thickness of the porous medium when it is related with the increase of the heated regions of the geometry. by increasing the radius's dimensions (r_p). Additionally, the circular obstacle's rotational velocity (ω) and radius (r_{ob}) are examined to determine their impact on energy flow within the cavity.

NB: The problem characterization, the mathematical model and the grid independency validation have been elaborated in the previous chapter (see: Chapter III).

IV.2.2 Results discussion

a- Influence of the porous medium proportion (r_p)

The triangular enclosure structure enables simultaneous modifications to the thickness of the porous medium and the length of the cavity's heated components. Such accuracy makes the analyzed cases more relevant. Figure IV.1. illustrates how the radius of the porous media (r_p) influences the variation in streamline and isotherm contours. According to the statistics, heat convection efficiency improves as (r_p) increases. Higher (r_p) values allow the streamlines to evaporate more effectively. Figure IV.2 depicts the comparable change in Nu_{avg} with varied circular barrier rotational velocity values (ω).

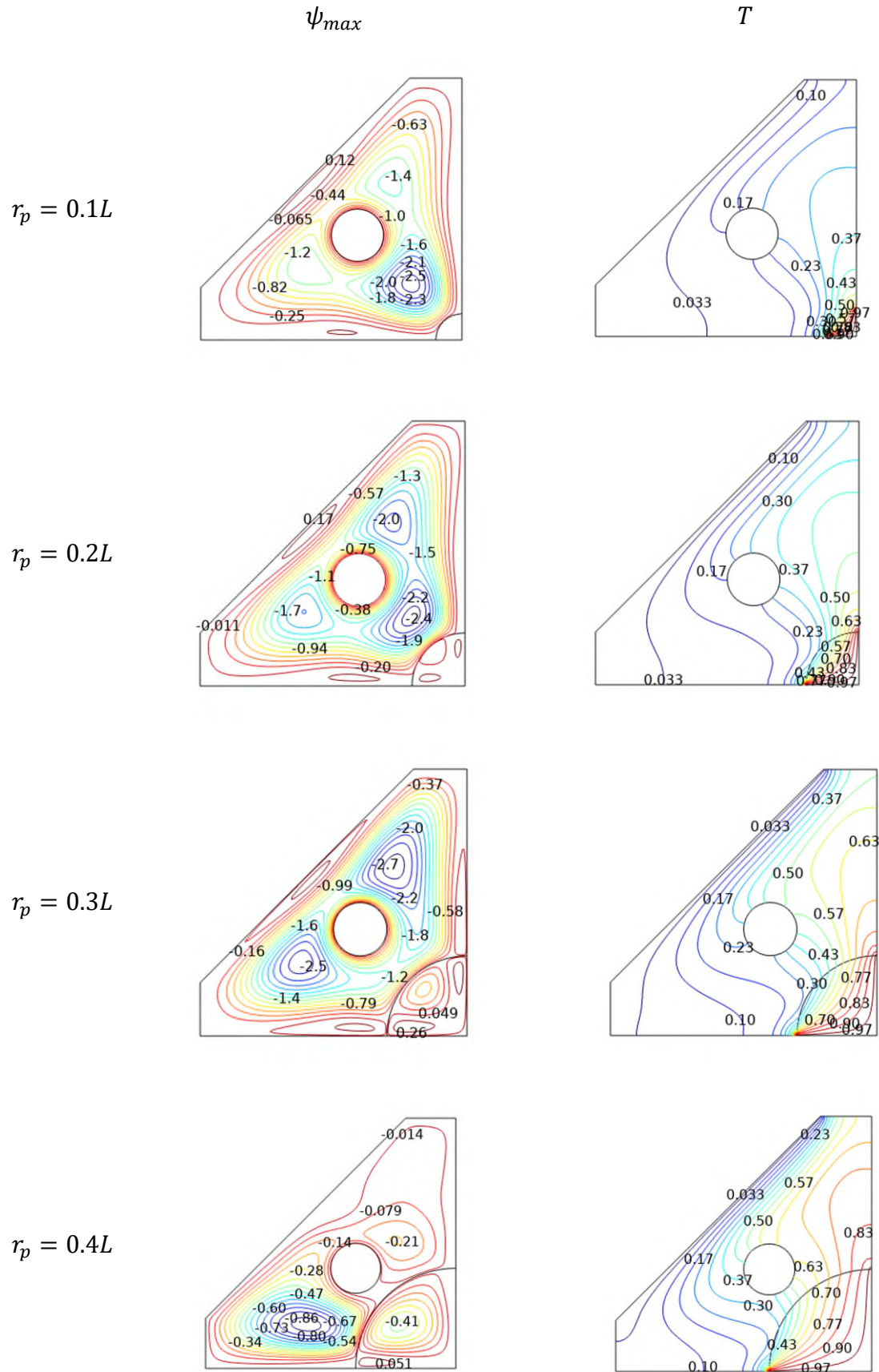


Figure. IV.1: Evolution of ψ_{max} and T for various r_p values, $Ra = 10^6$, $Ha = 20$, $\Phi = 0.02$, $r_{ob} = 0.1L$ and $\omega = 0$ rd/s .

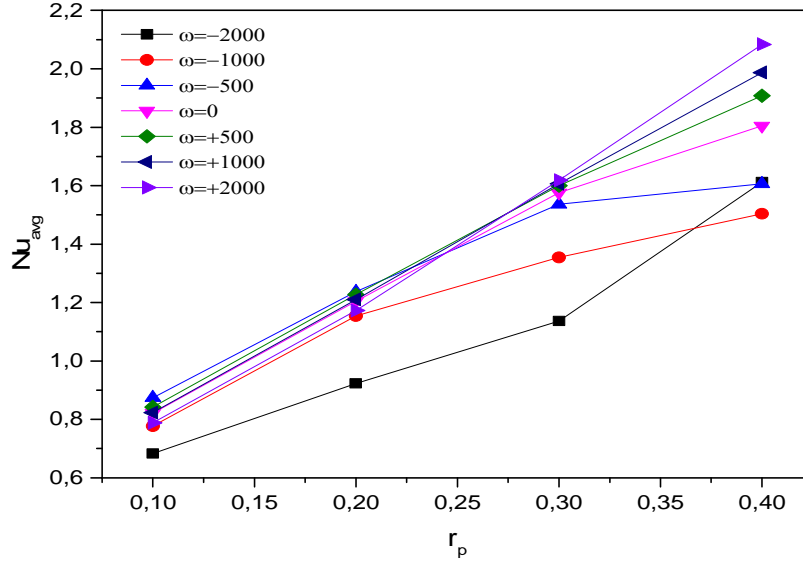


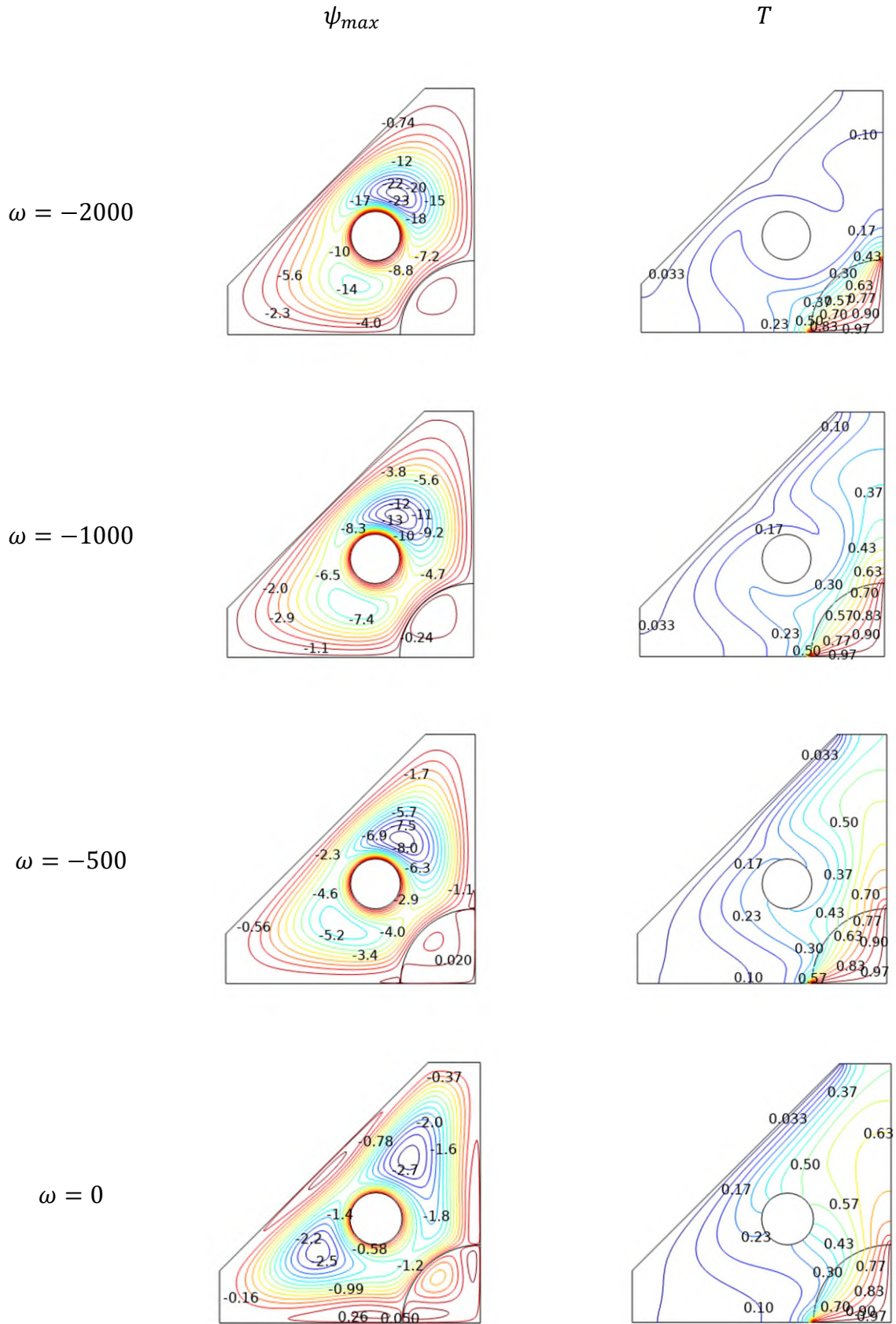
Figure. IV.2. Evolution of Nu_{avg} with r_p for various ω values, $Ra = 10^6$, $Ha = 20$, and $r_{ob} = 0.1L$.

b- Influence of the cylindrical barrier radius (r_{ob}) and its velocity (ω)

Figure IV.3.a depicts the fluctuation of ψ_{max} and T from different rotational velocity values ($-2000 \text{ rd/s} \leq \omega \leq +2000 \text{ rd/s}$), while Figure IV.3.b depicts the average Nusselt value variation for various circular barrier radius values ($0.025L \leq r_{ob} \leq 0.15L$). Increasing rotational velocity in the positive direction ($0 \leq \omega \leq +2000 \text{ rd/s}$) enhances heat transfer in enclosures with greater obstacle radius ($r_{ob} \leq 0.1L$).

Nevertheless, increasing ω in the negative direction ($-2000 \text{ rd/s} \leq \omega \leq 0$) causes the inverse effect. Furthermore, at the same rotating speed, higher radius values (r_{ob}) provide the largest Nu_{avg} value. Changing the barrier size ($0.025L \leq r_{ob} \leq 0.15L$) has no effect on Nu_{avg} if $\omega = 0 \text{ rd/s}$.

Figure IV.3.d shows isotherms and streamlines related to multiple obstacle radius lengths (r_{ob}) when $\omega = -2000 \text{ rd/s}$. The outcomes suggest that increasing the breadth of the rotating barrier and rotational motion in the positive direction may result in the best heat transfer performance.



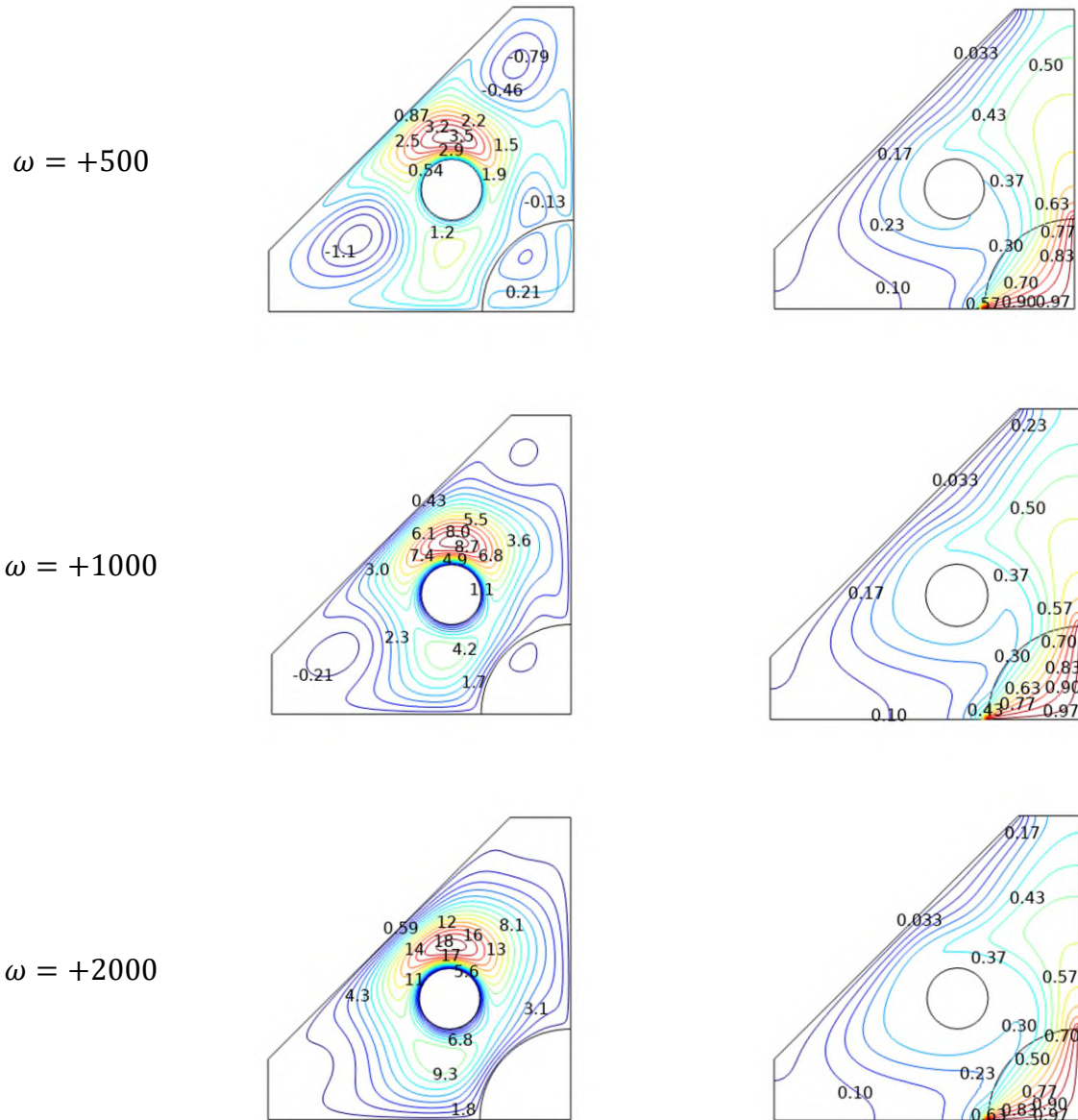


Figure. IV.3.a Evolution of ψ_{max} and T for multiple values of ω , $Ra = 10^6$, $Ha = 20$, $\Phi = 0.02$, $r_p = 0.3L$, and $r_{ob} = 0.1L$.

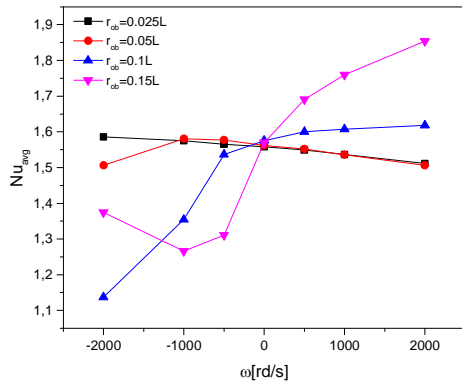


Figure. IV.3.b. Evolution of Nu_{avg} with ω for various values of r_{ob} , $Ra = 10^6$, $Ha = 20$, $\Phi = 0.02$ and $r_p = 0.3L$.

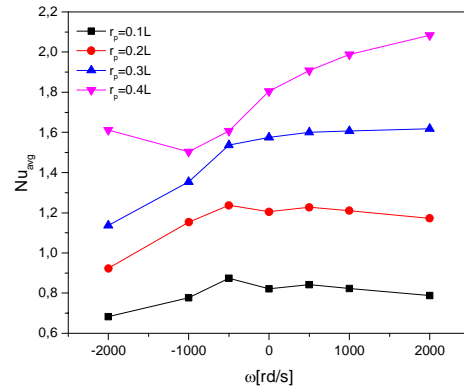
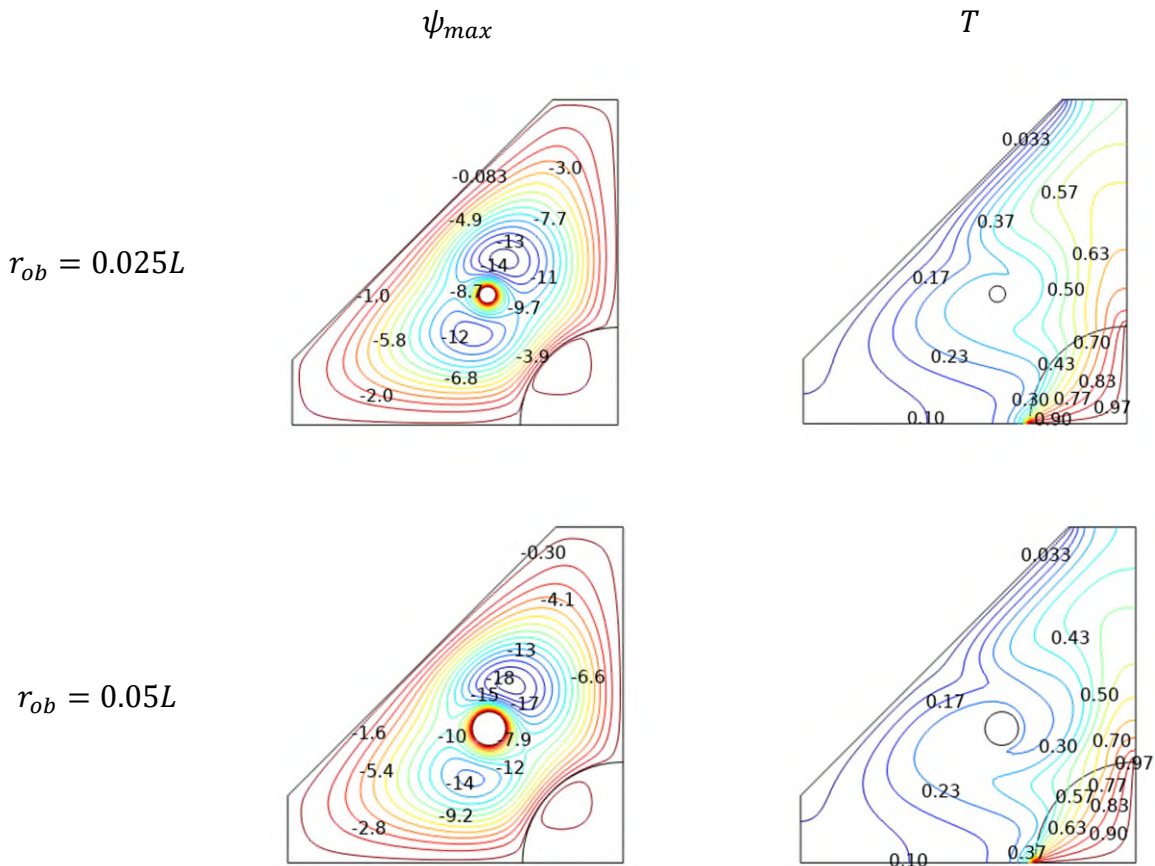


Figure. IV.3.c. Evolution of Nu_{avg} with ω for various values of r_p , $Ra = 10^6$, $Ha = 20$, $\Phi = 0.02$ and $r_{ob} = 0.1L$.



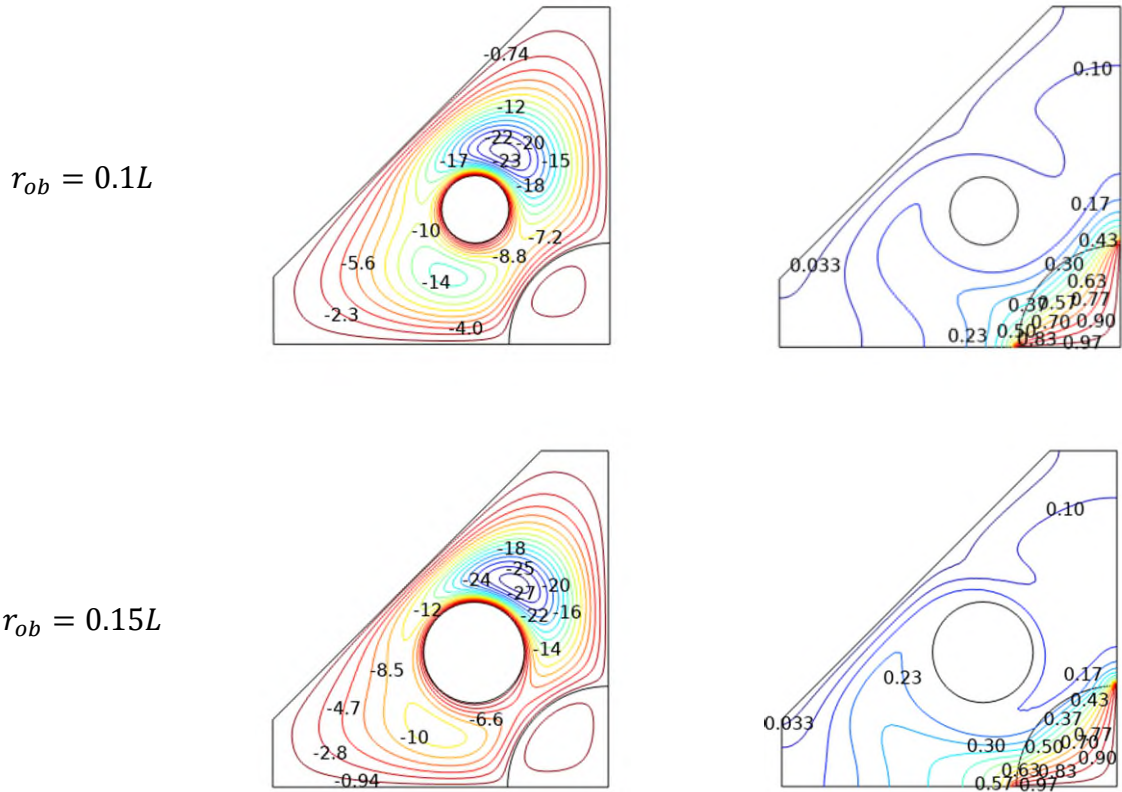
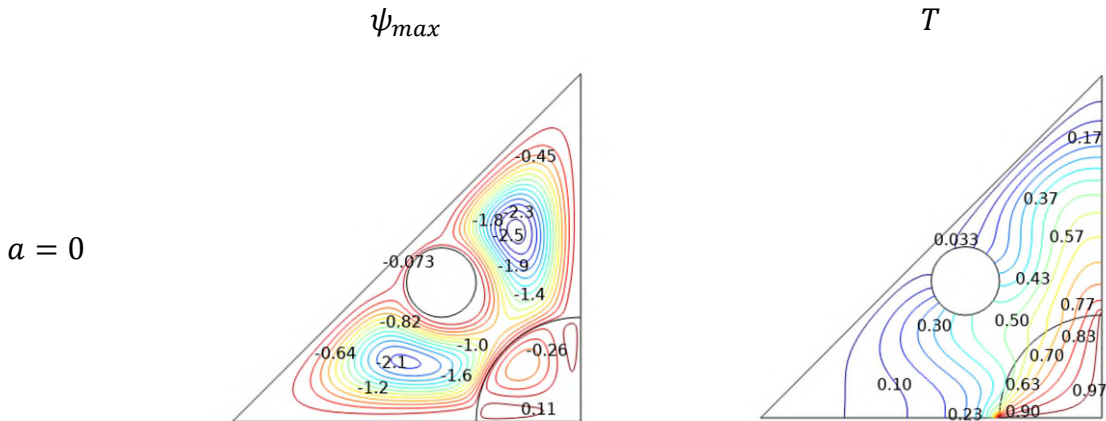


Figure. IV.3.d. Evolution of ψ_{max} and T for various values of r_{ob} , $Ra = 10^6$, $Ha = 20$, $\Phi = 0.02$, $r_p = 0.3L$ and $\omega = -2000 \text{ rd/s}$.

c- Influence of modifying the triangular cavity shape (a)

By adjusting the length (a), specific geometry change is done to get the ideal configuration for higher heat transfer efficiency. The streamlines and isotherms for various settings ($0 \leq a \leq 0.5L$) are shown in Figure IV.4.a. The effect of varying length (a) on heat transfer efficiency is seen in Figure IV.4.b. It has been observed that when dimension (a) increases, the cavity's heat rate decreases. Furthermore, when the length $a = 0$, Nu_{avg} is maximized.



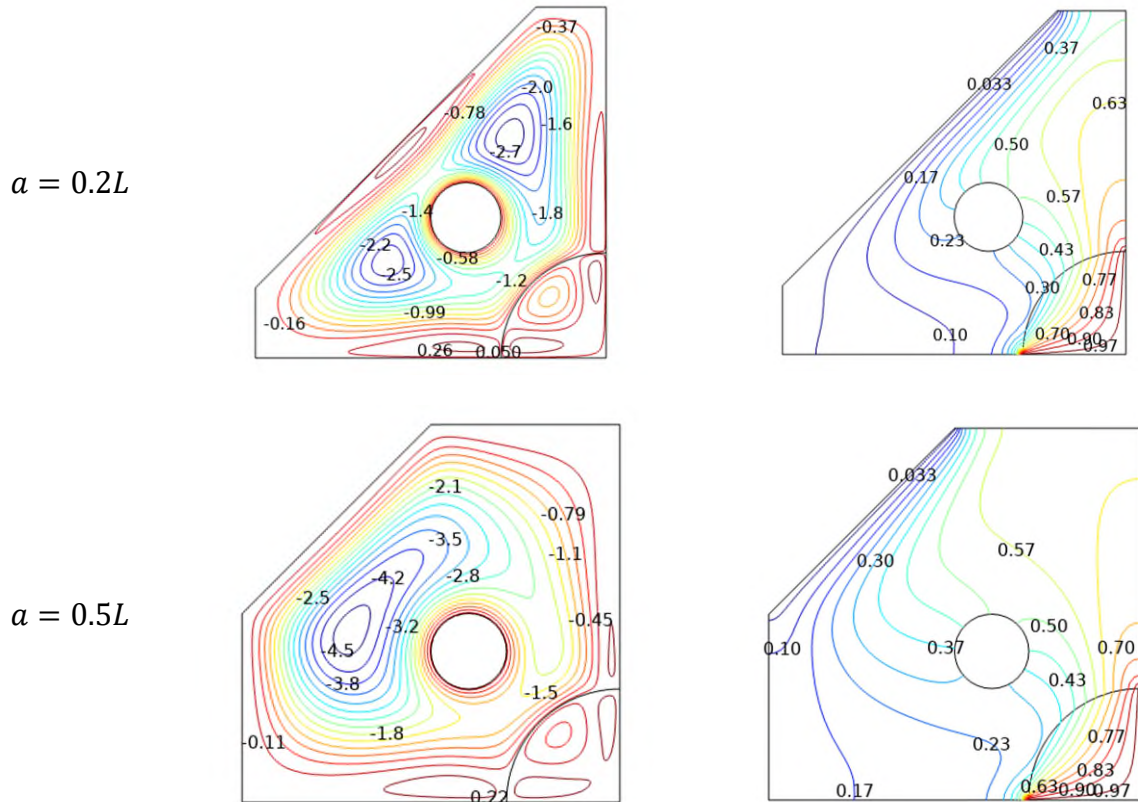


Figure. IV.4.a. Evolution of ψ_{max} and T for different values of the length (a), $Ra = 10^6$, $Ha = 20$, $\Phi = 0.02$, $r_p = 0.3L$, $r_{ob} = 0.1L$ and $\omega = -2000 \text{ rd/s}$.

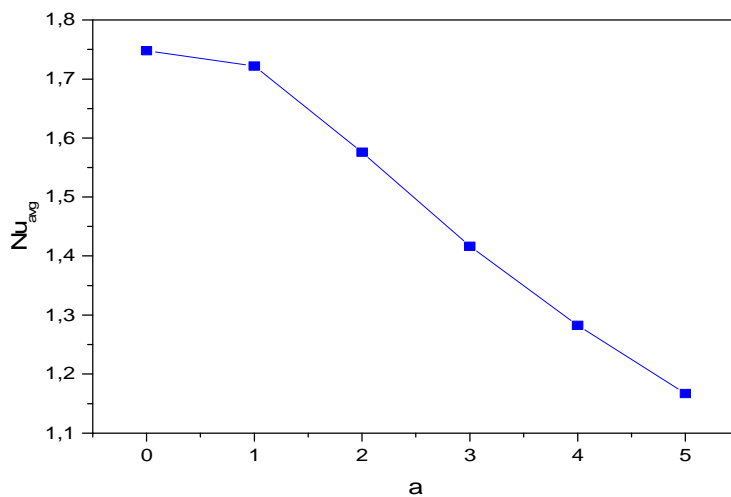


Figure. IV.4.b. Evolution of Nu_{avg} versus the length (a), $Ra = 10^6$, $Ha = 20$, $\Phi = 0.02$ and $r_p = 0.3L$, $r_{ob} = 0.1L$ and $\omega = 0 \text{ rd/s}$.

IV.3 Case 02: MHD natural convection of a nanofluid involved in a complex C-shaped enclosure [94].

IV.3.1 Abstract

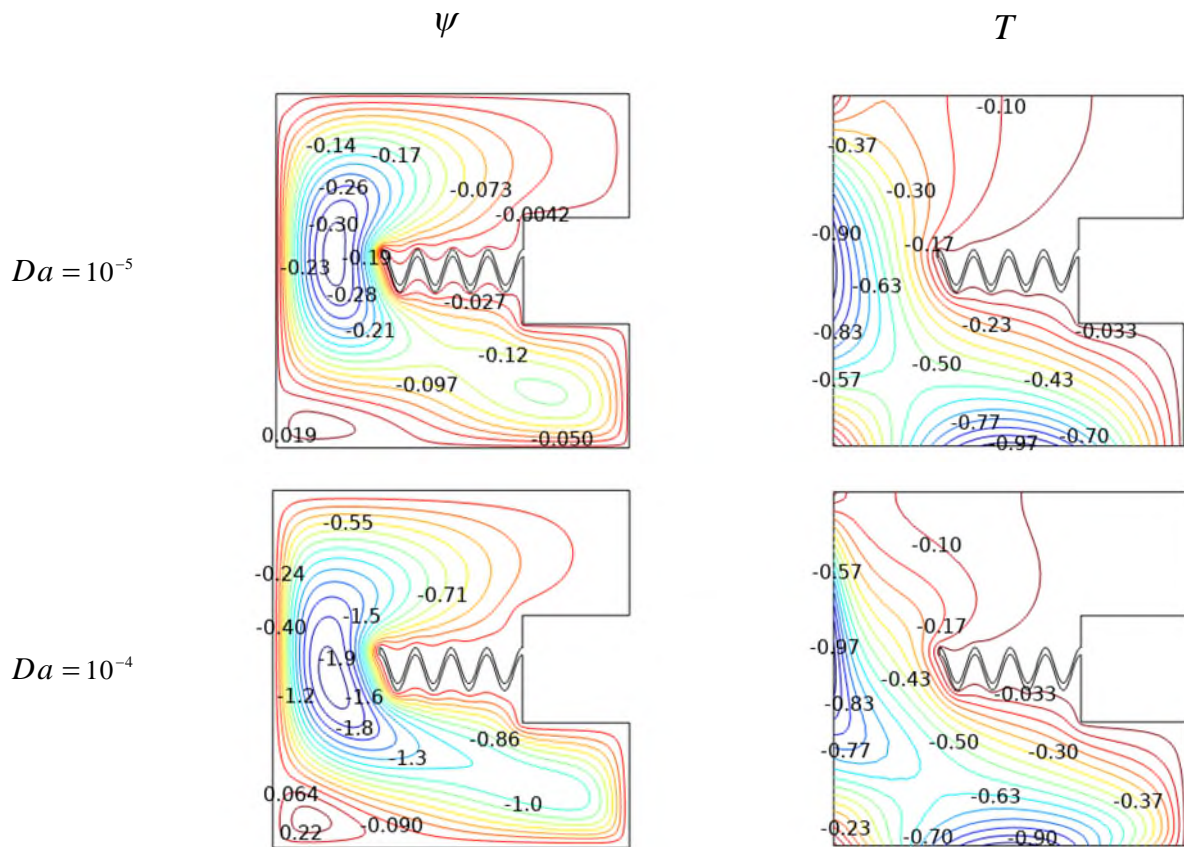
The second scenario demonstrates a C-shaped porous media container. In this situation, it was unfamiliar to install an inner baffle with a specific form within the cavity rather than usual ones, as well as calculate its optimal size. The study will examine how adapting the thickness (ζ) and length (λ) of the undulated baffle influence heat transmission efficacy.

NB: The problem characterization, the mathematical model and the grid independency validation have been elaborated in Chapter III.

IV.3.2 Results discussion

a- Influence of permeability (Da)

Figure VI.5 shows the difference in isotherms and streamlines for various Darcy number values at $Ra=10^6$ and $Ha=25$. The fluid flow has a decreased velocity at low Da due to the porous matrix's high resistance, as found. As a result, the streamline and isotherm distributions inside the cavity are greatly decreased. It may be concluded that raising Da greatly enhances the energy transmission.



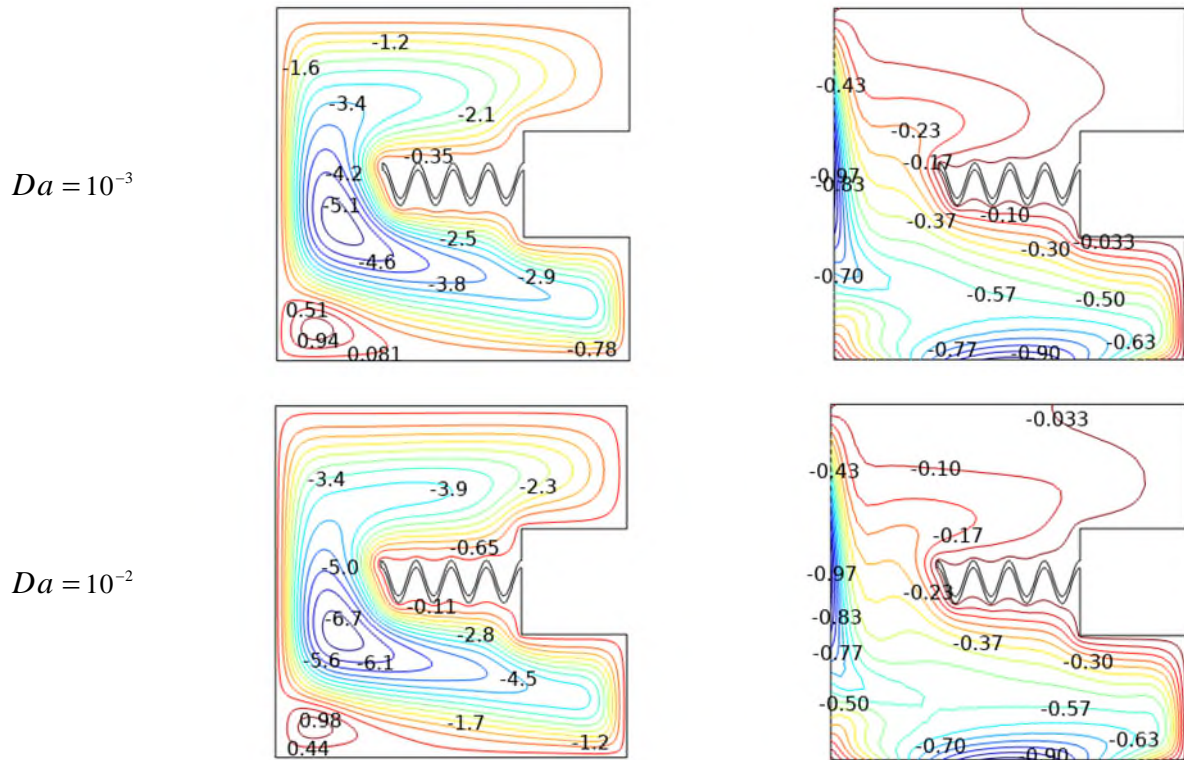


Figure IV.5. a Evolution of isotherms and streamlines for various values of Da , $Ra=10^6$, $Ha=25$, $\phi=0.01$ and $\varepsilon=0.4$.

Figure IV.5.b illustrates how raising Da enhances the energy transport performance for all nanoparticle concentrations. The greatest kicking impact happens when Da value is changed from 10^{-4} to 10^{-3} . Figure IV.5.c depicts the impact of changing porosity while raising the Darcy number on heat convection. It's vital to remember that increasing Da increases the average Nusselt number at all porosity levels. Improving permeability in smaller ranges ($10^{-5} \leq Da \leq 10^{-4}$) has a greater impact on lower porosity values than higher ones.

Figures IV.5.d and IV.5.e demonstrate how increasing the length and thickness of the baffle enhances its beneficial effect on heat convection. However, as Fig. IV.5.f illustrates, altering the baffle design by adding more undulations has little effect. The vacant spaces in the geometry expand with the length (a). Heat convection is significantly enhanced as a result, as seen in Fig. IV.5.g.

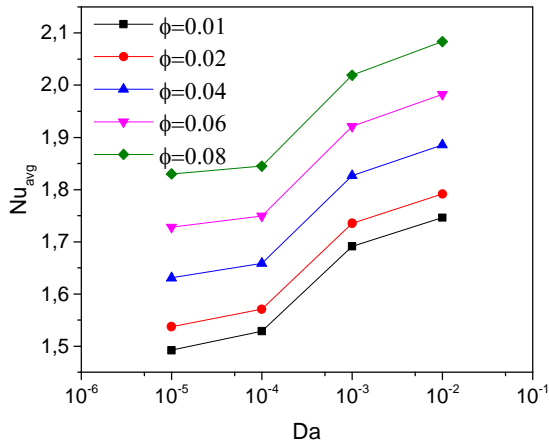


Figure.IV.5. b Evolution of Nu_{avg} with Da for different nanoparticles volume fraction values (ϕ), $Ra=10^6$, $Ha=25$, $\varepsilon=0.4$.

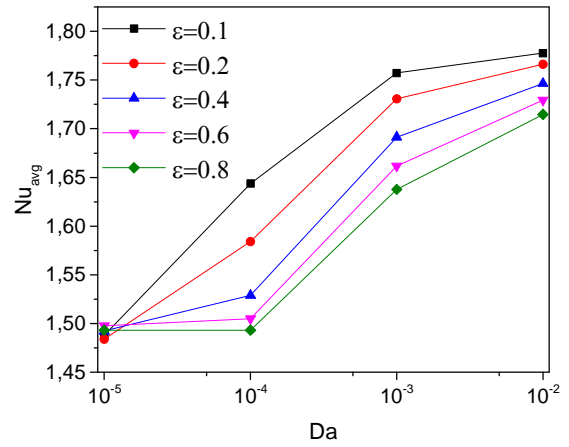


Figure.IV.5. c Evolution of Nu_{avg} with Da for different porosity values (ε), $Ra=10^6$, $Ha=25$, $\phi=0.01$.

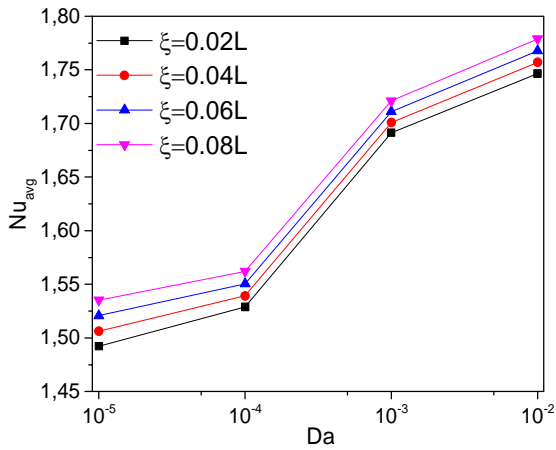


Figure.IV.5. d Evolution of Nu_{avg} with Da for different baffle thickness values (ζ), $Ra=10^6$, $Ha=25$, $\phi=0.01$, $\varepsilon=0.4$.

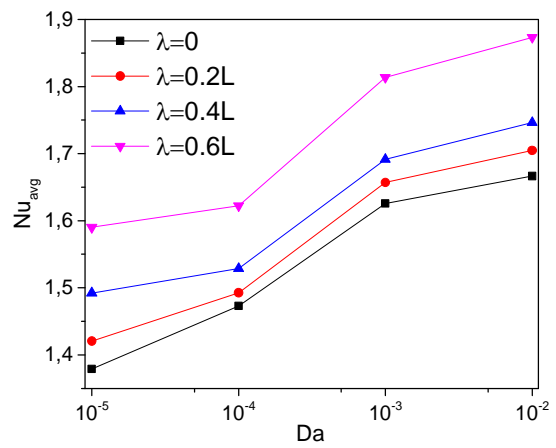


Figure.IV.5. e Evolution of Nu_{avg} with Da for different values of baffle length (λ), $Ra=10^6$, $Ha=25$, $\varepsilon=0.4$, $\phi=0.01$, $\zeta=0.02L$.

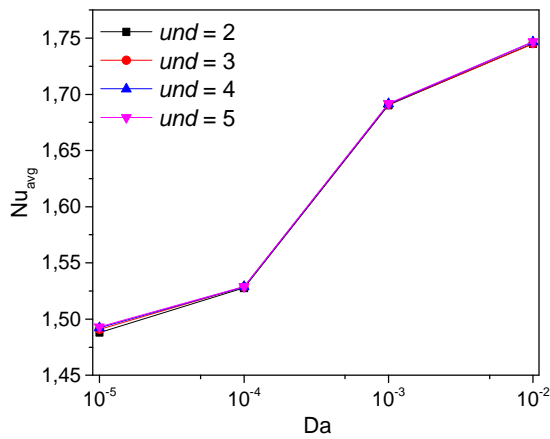


Figure.IV.5. f Evolution of Nu_{avg} with Da for different values of undulation number (und), $Ra=10^6$, $Ha=25$, $\varepsilon =0.4$, $\phi=0.01$, $\zeta=0.02L$ and $\lambda=0.4L$.

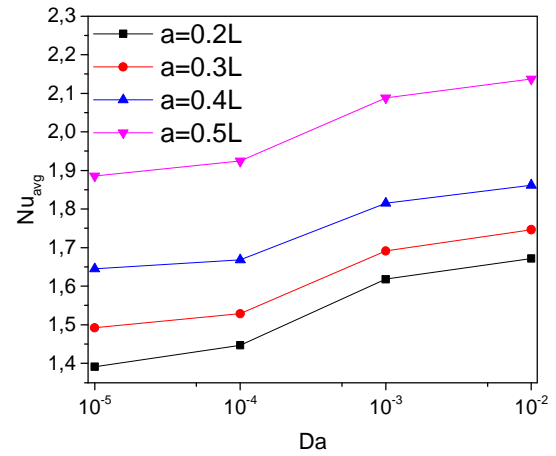
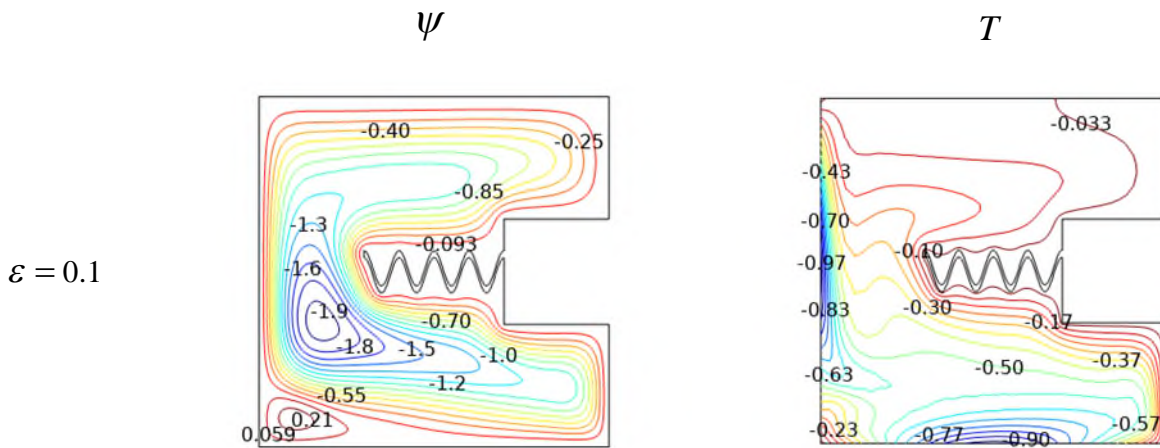


Figure.IV.5. g Evolution of Nu_{avg} with Da for different values of the empty square sides length (a), $Ra=10^6$, $Ha=25$, $\phi=0.01$, $\varepsilon =0.4$, $\phi=0.01$, $\zeta=0.02L$, $\lambda=0.4L$ and $und=4$.

b- Influence of porosity (ε)

Figure IV.6.a depicts the influence of varying the porosity (ε) on isotherms and streamlines distributions. Increasing porosity inhibits heat transport. This impact is directly related to the reduction in effective heat conductivity caused by the expansion of vacant spaces. In other words, as porosity increases, heat transmission reduces while inactive sections of the cavity grow.



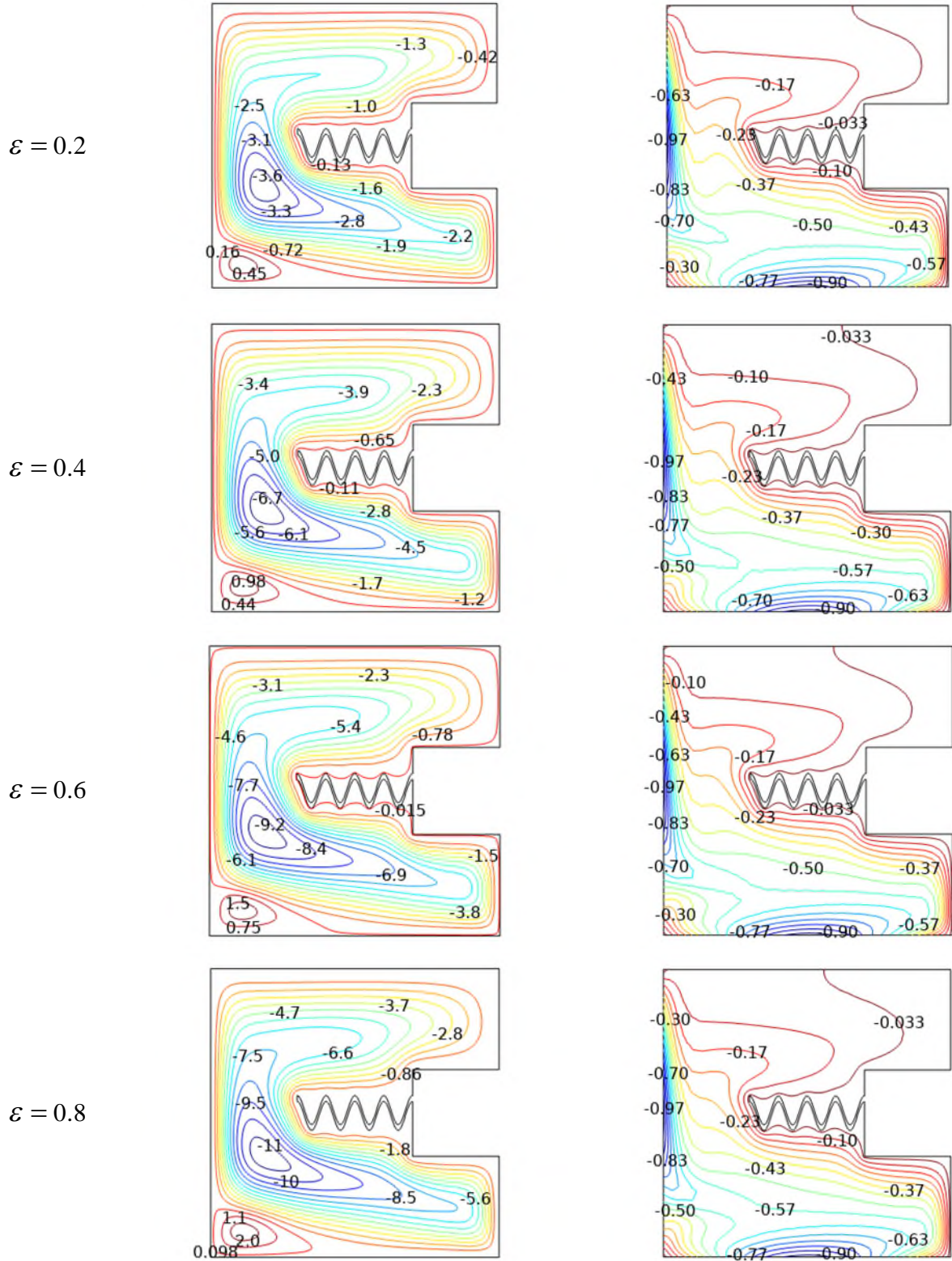


Figure.IV.6. a Evolution of the isotherms and streamlines for various values of porosity (ϵ), $Ra=10^6$, $Ha=25$, $\phi=0.01$ and $Da=0.01$.

Figure IV.6.b demonstrates how increasing porosity affects Nu_{avg} at different thicknesses of the inner obstacle. Nu_{avg} is shown to be greatly decreased when increased. Alternatively, when the baffle thickens, heat convection rises. Similarly, porosity reduces heat transmission for any length (λ), as seen in Figure IV.6.c. Furthermore, the lowest Nu_{avg} values match to the

scenario ($\lambda=0$), showing that the form totally suppresses the baffle. This highlights the advantages of using a baffle in the C-shaped cavity. However, modifying the baffle's undulation form has no influence on the porosity effects, as seen in Fig. IV.6.d.

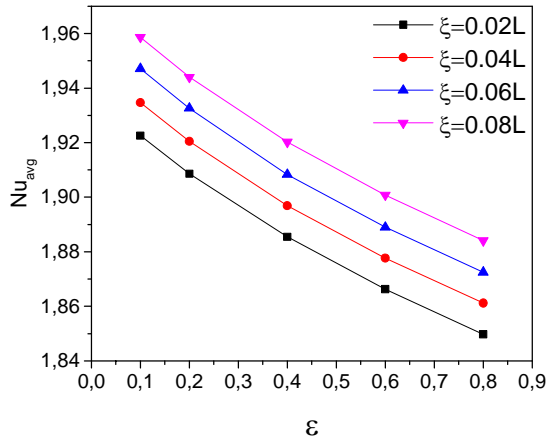


Figure.IV.6. b Evolution of Nu_{avg} with porosity (ϵ) for different values of baffle thickness (ξ), $Ra=10^6$, $Ha=25$, $\phi=0.01$, $Da=0.01$ and $\lambda=0.4L$.

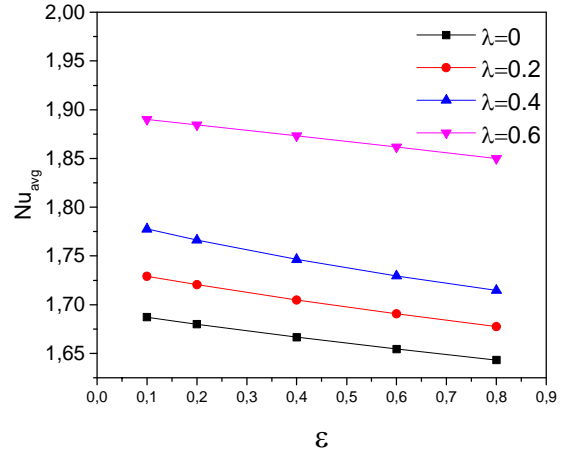


Figure.IV.6.c Evolution of Nu_{avg} with porosity (ϵ) for different values of baffle length (λ), $Ra=10^6$, $Ha=25$, $\phi=0.01$, $Da=0.01$ and $\zeta=0.02L$.

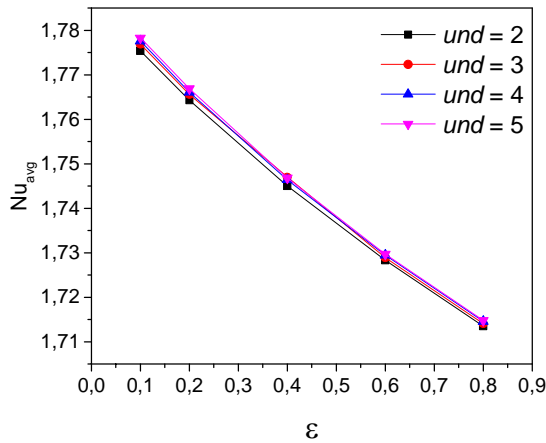


Figure.IV.6. d Evolution of Nu_{avg} with porosity (ϵ) for different values of undulation number (und), $Ra=10^6$, $Ha=25$, $\phi=0.01$, $Da=0.01$, $\zeta=0.02L$ and $\lambda=0.4L$.

VI.4 Conclusions

According to the two analyzed situations, the geometrical form, the installation of static or spinning barriers, and the existence of porous media can all have an influence on the quality of energy transmission in MHD convective heat transfer. The key results gained are summarized as follows:

1. Increasing the proportion of the porous medium within the cavity significantly affects the average Nusselt number and heat transmission efficiency.
2. An increase in the permeability of the porous medium improves heat transfer efficiency. This impact is more noticeable with higher Rayleigh and lower Hartmann values.
3. In the case of somewhat porous material, increasing its porosity significantly improves energy transmission inside the chamber.
4. Maximum Nu_{avg} values may be achieved by expanding the diameter of the revolving barrier inside the triangular cavity and speeding up its rotational velocity in the positive direction.
5. Adding a horizontal baffle inside the geometry improves the heat transfer response. This impact is amplified by increasing its thickness as well as real length.
6. Changing the inner baffle's undulation form did not show a valuable effect.
7. Modifying the geometrical layout of the triangular enclosure by modifying the length (a) has a substantial impact on convection performance. The optimal configuration is attained when $a=0$.
8. The heat transfer efficiency improves when the length of the C-shaped cavity surface is reduced.

Chapter V

Entropy generation analysis in case of MHD natural convection

Chapter V: Entropy generation analysis in case of MHD natural convection

V.1 Introduction

Entropy generation study is a strong method for investigating thermal system performance. Many researchers have investigated the entropy production of thermal systems to determine the optimal operating conditions [95][96][97].

Nanofluids have found several uses in consumer items, nanomedicine, energy conversion, and microsystem cooling [98]. The utilization of nanofluid flow to improve convective heat transfer and provide quick cooling of high heat-flux devices is particularly interesting [99] [100]. However, to properly optimize such thermal engineering systems in terms of design and operation, not only must heat transmission be maximized but also entropy creation be minimized.

This Chapter reviews the theoretical and computational contributions to entropy creation caused by hybrid nanofluid flow and heat transport in an example with complex geometry [101]. The thermal properties of the working fluid are investigated as well as the impact of the complexity of the geometry. Part of the outcomes of this study were presented in term of average Nusselt and entropy generation numbers.

V.2 Case study: Entropy generation in case of MHD natural convection within a complex cubic cavity filled with a hybrid nanofluid [101].

V.2.4 Abstract

In the present case, heat transfer by natural convection of an Ag-Al₂O₃/H₂O hybrid nanofluid loaded in a cubic enclosure provided with an undulated inner porous layer and a rotating cylinder exposed to a constant magnetic field is investigated. This complex geometry is used to investigate several thermophysical parameters, such as the concentration of nanoparticles [$0.02 \leq \Phi \leq 0.08$], Ra [$10^2 \leq Ra \leq 10^5$], and Ha [$0 \leq Ha \leq 100$]. Similarly, Da [$10^{-5} \leq Da \leq 10^{-2}$], which indicates the permeability of the porous medium, and the number of undulations [$0 \leq N \leq 4$] are studied together with the rotational speed [$-4000 \leq \omega \leq +4000$] and other characteristics of the porous layer.

With $Pr = 6.2$, the enclosed hybrid nanofluid is laminar, incompressible, stable, and Newtonian.

V.2.2 Characterization of problem

The explored geometry is shown in Figure V.1. Both 2D (a) and 3D (b) representations are shown. The walls at the top and bottom are insulated. There are also hot and cold areas on both sides, with the temperatures shown on the left and right walls as T_h and T_c , respectively. All cases have used the same (0.4H) heater and cooler component, which is symmetrical in the middle of the vertical walls. The remaining walls, however, are entirely insulated.

In the cavity at ($b = 0.35L$), an undulating vertical porous layer of thickness ($a = 0.1L$) has been placed.

In the center of the cavity, at ($c = 0.3L$) along the x-axis, revolves spinning cylinder with a diameter of ($d_m = 0.2L$). The cavity receives a uniform magnetic field in the x-direction. Ag/Al₂O₃-H₂O, a hybrid nanofluid with laminar flow, is incompressible, Newtonian, and free of viscous dissipation inside the cavity. Pr = 6.2 is the water Prandtl number.

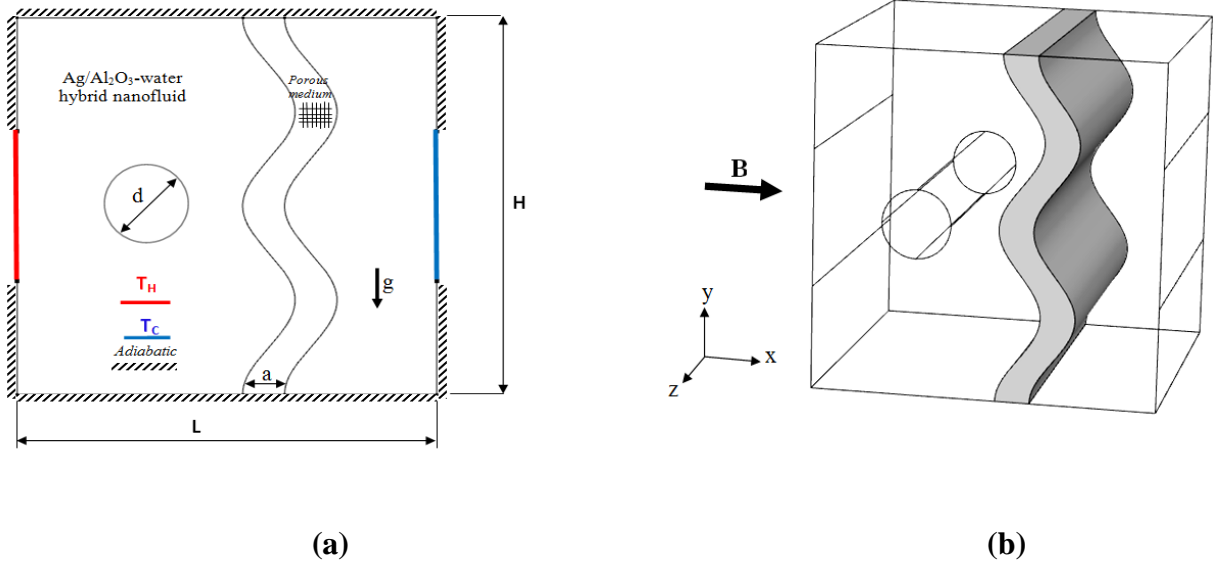


Figure.V.1 Graphical representation of the studied geometry in 2D (a) and 3D (b).

V.2.3 Formulation of the Mathematical Model

The same mathematical model and thermophysical basic definitions previously detailed in Chapter III – case 01 is considered in the present example.

The local entropy production measurement was derived by adding the conjugated fluxes and the forces produced. The non-dimensional local entropy formation in a convective process under the influence of a magnetic field is described as:

$$S_{gen} = \frac{k_{hnf}}{k_n} \left[\left(\frac{\partial \theta}{\partial x} \right)^2 + \left(\frac{\partial \theta}{\partial y} \right)^2 \right] + \chi \frac{\mu_{hnf}}{\mu_f} \left\{ (U^2 + V^2) + Da \left[2 \left(\frac{\partial U}{\partial x} \right)^2 + \left(\frac{\partial V}{\partial y} \right)^2 + \left(\frac{\partial U}{\partial y} + \frac{\partial V}{\partial x} \right)^2 \right] \right\} + \frac{\sigma_{hnf}}{\sigma_f} \chi Ha^2 V^2 \quad (83)$$

$$\text{With: } \chi = \frac{u_{hnf} T_{avg}}{k_f K} \left(\frac{\alpha_f}{L(T_h - T_c)} \right)^2 \quad \text{and} \quad T_{avg} = \frac{T_h + T_c}{2}$$

Regarding the boundary conditions pertaining to the walls of the hollow under study, the dimensional description is as follows:

- Cold walls: $T = T_c$, $u = v = 0$,
- Hot walls: $T = T_h$, $u = v = 0$,
- Insulated walls: $\frac{\partial T}{\partial n} = 0$, $u = v = 0$,

- Over the spinning cylinder:
$$\begin{cases} u = -\omega(y - y_0) \\ v = -\omega(x - x_0) \end{cases}$$

V.2.4 Results discussion

In the present section, we focused on understanding the entropy generation sensitivity to multiple thermos-physical and geometrical parameters such as Ra, Ha, Da, the inner cylinder velocity (ω) and the undulation form of the inner wall (N).

a- Entropy generation versus Rayleigh number

Figure V.2 shows that entropy generation (S_{gen}) appears to be activated at both heated ends of the cavity. A pair of contours develops at both ends, as well as enhanced entropy in the porous zone with a lower Rayleigh number, Ra. As Ra levels increase, this situation reverses itself.

The dual contours become single at both ends, with the hot end contour dragging down and the other claiming upward. For larger values of Ra, the porous section of the cavity can tolerate entropy change.

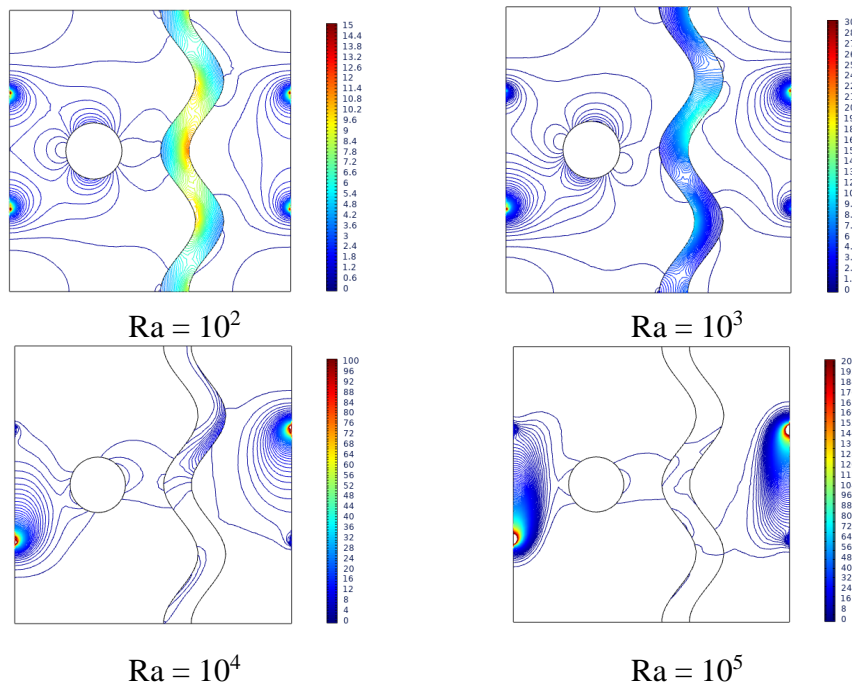


Figure V.2. Evolution of S_{gen} with various values of Ra, Ha = 0, N = 2, Da = 0.01, $\Phi = 0.02$, $\varepsilon = 0.2$, and $\omega = 0$.

b- Entropy generation versus Hartmann number

When compared Ha changing, the entropy generation behaves in the opposite way for variations in Rayleigh numbers. The contours start to appear from the two rear sides, as Fig. V.3 clearly illustrates. As the magnetic influence boosts, they displace concurrently towards the center of the enclosure, splitting into 02 contours on each side.

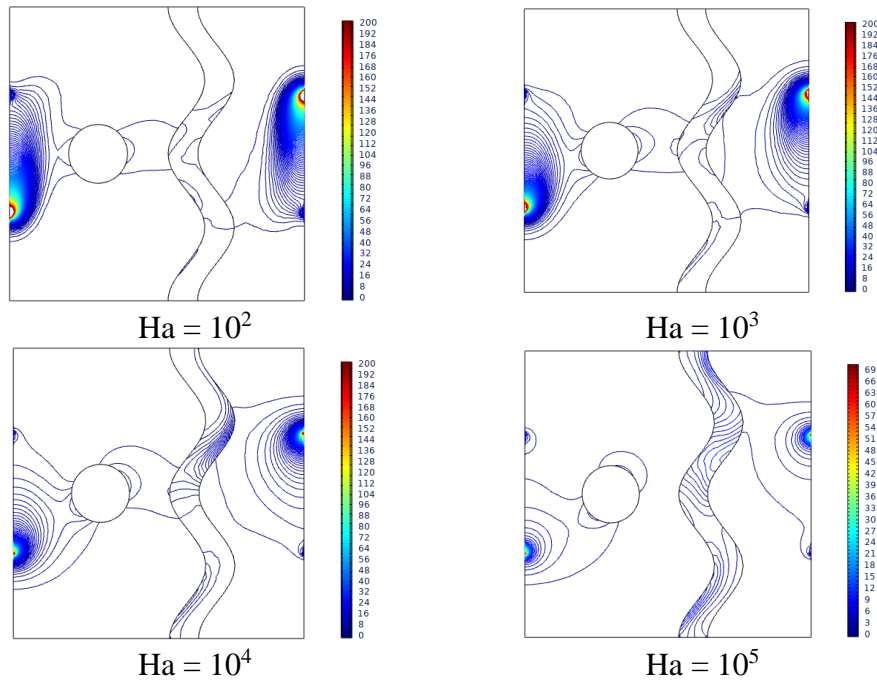
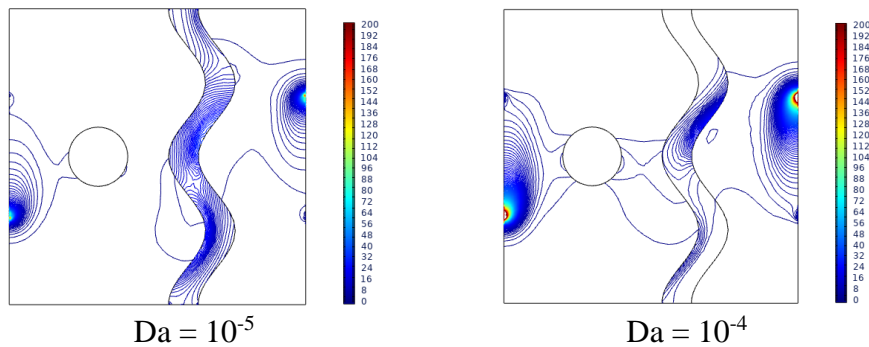


Figure V.3. Evolution of S_{gen} with various values of Ha , $Ra = 10^5$, $Da = 0.01$, $N = 2$, $\Phi = 0.02$, $\varepsilon = 0.2$ and $\omega = 0$.

c- Entropy generation versus Darcy number

Figure V.4 demonstrates that at lower Da values, the fluid struggles to pass through the porous medium, causing a buildup surrounding it. The graph of S_{gen} depicts the condition of entropy loss in fluid due to permeability restrictions across porous media. For higher permeability values, the flow penetrates the opposite side, leading to simply entropy losses in two areas of heat variation.



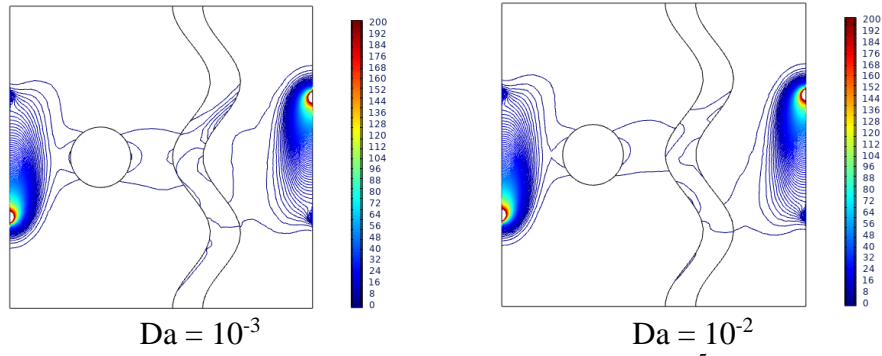


Figure V.4. Evolution of S_{gen} with various values of Da , $Ra = 10^5$, $Ha = 0$, $N = 2$, $\Phi = 0.02$, $\varepsilon = 0.2$ and $\omega = 0$.

d- Entropy generation versus the rotation speed of the inner cylinder

The velocity of the cylinder rotation (ω) was explored for positive and negative direction. Figure V.5 illustrates that when the rotation speed ω increases, the entropy production (S_{gen}) shifts from clockwise to anticlockwise in relation to the fluid's rotation direction inside the cavity.

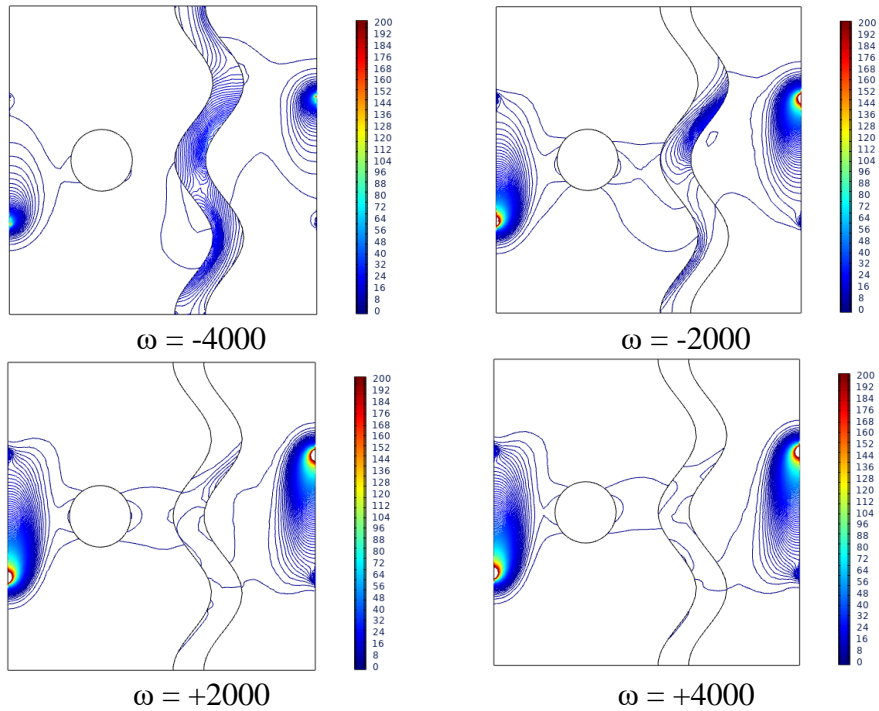


Figure V.5. Evolution of S_{gen} with various values of rotational speeds (ω) , $Ra = 10^5$, $Ha = 0$, $N = 2$, $\Phi = 0.02$, $\varepsilon = 0.4$ and $Da = 0.01$

e- Entropy generation versus undulation number

With respect to impact of the undulation parameter (N) depicted in Figure V.6, both S_{gen} and Nu_{avg} improve when $N = 2$. For higher values of N , both tend to fall, the Nusselt number falling more quickly than the entropy generation. Larger undulations complicate the flow and its nanoparticle suspension, which lowers heat transfer while simultaneously raising entropy generation and total entropy in the system.

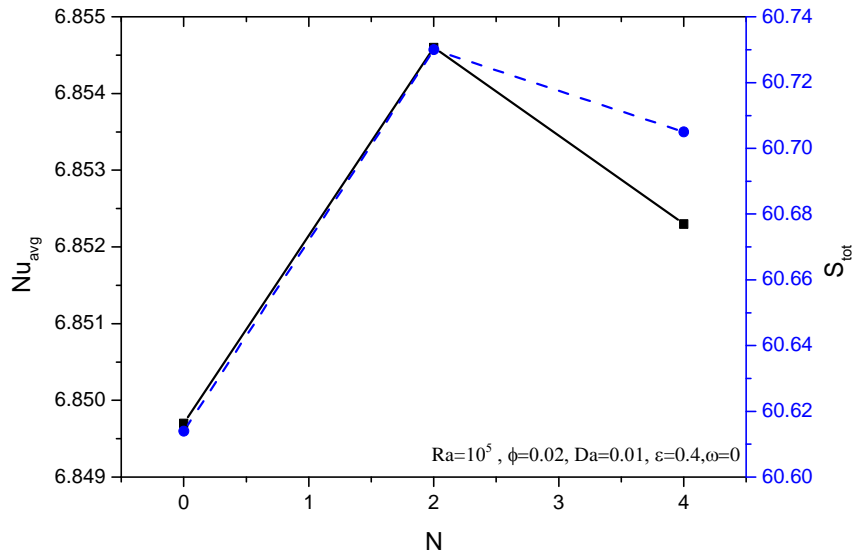


Figure V.6. Evolution of S_{gen} and Nu_{avg} for various values of undulation number (N), $Ra = 10^5$, $Ha = 0$, $\omega = 0$, $Da = 0.01$ and $\epsilon = 0.4$.

VI.3 Conclusions

A finite element investigation of the Ag/Al₂O₃-H₂O hybrid nanofluid inside a porous multilayer enclosure influenced by magnetic field over a revolving cylinder yielded the following conclusions:

- 1- Higher Rayleigh number and porosity values, as well as lower Hartmann numbers, were associated with increased entropy formation across the porous medium.
- 2- Despite a greater Hartmann number, an increased Rayleigh number, positive rotation speed, and rising Darcy number improved the heat transfer rate across the cavity.
- 3- The entropy generation S_{gen} shifted from clockwise to anticlockwise in relation to the fluid's rotation inside the cavity.
- 4- In the present case, entropy generation S_{gen} increases with the undulation of $N = 2$.

Chapter VI

Final conclusions & Way Forward

Chapter VI: Final conclusions & Way Forward

VI.1 Summary of major conclusions

The primary goal of this study was to use nanoparticles to perform MHD convection heat transfer, two-dimensional, laminar, viscous, incompressible convection flow, and optimize heat transmission. Brownian motion in several types of nanofluids and hybrid nanofluids with varying geometries where novel configurations were adopted and investigated. Because of the fluctuation in density caused by the temperature differential between the hot and cold walls, natural convection has been addressed. The thesis compares heating sources that are non-uniform and homogenous.

This state is made possible by the porous material that is present inside cavities. A cavity may include some porous material, or it may be entirely porous. Furthermore, a variety of in-situ barrier designs have been investigated, such as static baffles and spinning cylinders. To get a deeper comprehension of the natural convection heat transfer process, a variety of thermal boundary conditions were also investigated. The nondimensional form of the nonlinear governing partial differential equations was achieved using a set of similarity variables. A dependable partial differential equations solver program that employed the Galerkin weighted residual form finite element approach was utilized to simulate the dimensionless governing equations for the current issues.

The computational and experimental results highlighted in the literature analysis stand in excellent agreement. streamline contours and isothermal lines have been employed to demonstrate the structure and flow pattern of temperature transmission processes. After thorough analysis, the results corresponded to the appropriate average Nusselt number variations for a variety of physical model parameters, such as the Hartmann number (Ha), Rayleigh number (Ra), volume proportion of nanoparticles (ϕ), geometrical inputs, and requirements for porous media. Additionally, the variations of the entropy generation in the case of natural convection were the subject of a whole chapter at the end of the thesis.

The conclusions of this work can be summarized as follows:

- Increasing the Rayleigh number improves thermal performance and strengthens the flow field in the enclosure.
- Rayleigh number is a key amount in natural convection fluid flow and heat transfer, identifying the prevailing heat transfer mode in the computational area. Conduction heat transmission dominates at low Ra values, whereas buoyancy-induced convection heat transfer takes control at high Ra values.
- At moderate Hartmann number values, the streamline's shape tends to follow the enclosure's geometry and heat transmission is mostly diffusion dominated. In addition, the magnetic field can act as a flow controller by suppressing the flow within the enclosure.
- The magnetic field suppresses the flow in the enclosure thus it can serve as a flow controller.

- While the average Nu number has an inverse relationship with the Ha number, it has a direct relationship with the Ra and Da numbers.
- The streamlines and isotherms inside the enclosure are significantly altered by Ra, Da, and Ha. The impact of Hartmann and Darcy numbers on heat transfer is also noted, and the Nusselt number increases markedly at high convection strength.
- There is great potential for improving heat transmission in various thermal systems through the coupling of nanofluids with porous media, which also offers several chances for system development. This is caused by the porous medium's larger surface area/volume and the enhanced characteristics of the thermal properties of nanofluids.
- A fluid's thermal conductivity may be increased by adding nanoparticles but doing so may also increase its viscosity. Because viscosity has a major effect on convection, the effect of nanoparticles on enhancing thermal performance could be diminished as a result.
- Increased entropy formation was related to higher porosity and Rayleigh numbers, as well as lower Hartmann, across the porous medium.
- The heat transfer rate across the cavity was enhanced by a higher Rayleigh number, positive rotation speed, and increasing Darcy number, contrary to a higher Hartmann number.
- In accordance with the fluid's rotation inside the cavity, the entropy generation changed its behavior and direction.

VI.2 Further works & Way forward.

There are several prospects for this sort of research in the future. for the extensive and widespread use of nanofluids in several technical and environmental settings. There are several more mathematical models that may be used to illustrate these kinds of nanofluids. There are so several chances to pursue this investigation in novel directions. The current research can be further developed using the following recommendations.

- The enhancement of natural convection heat transmission is also significantly influenced by the shape, size, and composition of nanoparticles. As such, their impact must be considered while researching nanofluid natural convection.
- It is possible to expand the study by include the characteristics related to heat generation and absorption.
- It is possible to conduct investigations utilizing lid-driven mixed convection heat transmission.
- Future studies should involve more intricate and uncommon geometries. Blood cells, fuel cells, heat exchangers, contemporary solar collectors, elastic walled geometries, and microelectronic devices are examples of complex geometries.
- Future numerical studies could focus on radiation performance as well.

References

References:

- [1] BERGMAN, Theodore L. Fundamentals of heat and mass transfer. John Wiley & Sons, 2011.
- [2] JANNA, William S. Engineering heat transfer. CRC press, 2018.
- [3] MAXWELL, James Clerk. A treatise on electricity and magnetism. Oxford: Clarendon Press, 1873.
- [4] AHUJA, Avtar Singh. Augmentation of heat transport in laminar flow of polystyrene suspensions. I. Experiments and results. *Journal of Applied Physics*, 1975, 46.8: 3408-3416.
- [5] Choi, S.; Eastman, J. Enhancing Thermal Conductivity of Fluids with Nanoparticles (No. ANL/MSD/CP-84938; CONF-951135-29); Argonne National Lab.: Argonne, IL, USA, 1995.
- [6] GÜRDAL, Mehmet, et al. Effects of using nanofluid, applying a magnetic field, and placing turbulators in channels on the convective heat transfer: A comprehensive review. *Renewable and Sustainable Energy Reviews*, 2022, 162: 112453.
- [7] SELIMEFENDIGIL, Fatih, et al. A review on non-Newtonian nanofluid applications for convection in cavities under magnetic field. *Symmetry*, 2022, 15.1: 41.
- [8] ALSABERY, Ammar I., et al. Convection heat transfer in enclosures with inner bodies: a review on single and two-phase nanofluid models. *Renewable and Sustainable Energy Reviews*, 2023, 183: 113424.
- [9] ZARAKI, Abolfazl, et al. Theoretical analysis of natural convection boundary layer heat and mass transfer of nanofluids: effects of size, shape and type of nanoparticles, type of base fluid and working temperature. *Advanced Powder Technology*, 2015, 26.3: 935-946.
- [10] MENNI, Younes; CHAMKHA, Ali J.; AZZI, Ahmed. Nanofluid flow in complex geometries— a review. *Journal of Nanofluids*, 2019, 8.5: 893-916.
- [11] REDOUANE, Fares; HIDKI, Rachid. Conjugate local thermal non-equilibrium heat transfer in a porous medium-filled cavity with a rotating cylinder: Analysis and insights. *Numerical Heat Transfer, Part B: Fundamentals*, 2023, 1-19.
- [12] AISSANI, Abdelkader, et al. Analyzing heat transfer variations at specific locations in a cave filled with porous media, emphasizing non-equilibrium conditions. *Energy Sources, Part A: Recovery, Utilization, and Environmental Effects*, 2023, 45.4: 12711-12736.
- [13] BEJAN, Adrian. Convection heat transfer. John Wiley & Sons, 2013.
- [14] R.M. Fand, E.W. Morris, and M. Lum, "Natural convection heat transfer from horizontal cylinders to air, water and silicone oils for Rayleigh numbers between 300 and 200," *Int. J. Heat Mass Transf.*, Vol. 20, pp.1173–1184, 1977.
- [15] E. M. Sparrow and M. Charmcill, "Natural convection experiments in an inclosure between eccentric or concentric vertical cylinders of different height and diameter," vol. 26, no. I, pp. 133–143, 1983.
- [16] F. A. W. Hamad, "Experimental study of natural convection heat transfer in inclined cylindrical annulus," *Sol. Wind Technol.*, vol. 6, pp. 573–579, 1989.
- [17] K. Kitamura, Kami-iwa, F., and T. Misumi, "Heat transfer and fluid flow of natural convection around large horizontal cylinders," *Int. J. Heat Mass Transf.*, vol. 42, pp. 4093–4106, 1999.

-
- [18] S. A. Nada, "Experimental investigation of natural convection heat transfer in horizontal and inclined annular fluid layers," pp. 929–936, 2008.
- [19] G. Yesiloz and O. Aydin, "Natural convection in an inclined quadrantal cavity heated and cooled on adjacent walls," *Exp. Therm. Fluid Sci.*, vol. 35, no. 6, pp. 1169–1176, 2011.
- [20] H. Ghodsinezhad, M. Sharifur, J.P. Meyer, Experimental investigation on cavity flow natural convection of Al₂O₃-water nano-fluids, *Int. Commun. Heat Mass Tran.* 76 (2016) 316–324,
- [21] Torki, M.; Etesami, N. Experimental Investigation of Natural Convection Heat Transfer of SiO₂/Water Nanofluid inside Inclined Enclosure. *J. Therm. Anal. Calorim.*, 139, 1565–1574, 2020.
- [22] Abdulateef, A.M. Experimental Approach for Enhancing the Natural Convection Heat Transfer by Nanofluid in a Porous Heat Exchanger Unit. *Sustainability* 2023, 15, 2580.
- [23] Dey, Debashis, and Sukanta K. Dash. "An experimental investigation on the nanofluids in a cavity under natural convection with and without the rotary magnetic field." *Heliyon* 9.11 (2023).
- [24] SCOTT, T. O.; EWIM, D. R. E.; ELOKA-EBOKA, A. C. Experimental study on the influence of volume concentration on natural convection heat transfer with Al₂O₃-MWCNT/water hybrid nanofluids. *Materials Today: Proceedings*, 2023.
- [25] NAZARAHARI, Mahtab; GHASEMI ASL, Ramin; ARMAGHANI, Taher. Experimental study of nanofluids natural convection heat transfer in various shape pores of porous media. *Journal of Thermal Analysis and Calorimetry*, 2024, 1-19.
- [26] KEYHANI, M., et al. Free convection heat transfer from discrete heat sources in a vertical cavity. *Natural and Mixed Convection in Electronic Equipment Cooling*, ASME HTD, 1988, 100: 13-24.
- [27] AHMED, G. Refai; YOVANOVICH, M. M. Numerical study of natural convection from discrete heat sources in a vertical square enclosure. *Journal of thermophysics and heat transfer*, 1992, 6.1: 121-127.
- [28] KULKARNI, Ratnakar. *Natural convection in enclosures with localised heating and cooling*. 1998.
- [29] Kadhim, Hakim T., et al. "Numerical analysis of hybrid nanofluid natural convection in a wavy walled porous enclosure: local thermal non-equilibrium model." *International Journal of Thermofluids* 15 (2022): 100190.
- [30] Saleem, Khalid B., et al. "Natural convection heat transfer in a nanofluid filled l-shaped enclosure with time-periodic temperature boundary and magnetic field." *Alexandria Engineering Journal* 69 (2023): 177-191.
- [31] KHAN, Mumtaz, et al. Application of fractional derivatives in a Darcy medium natural convection flow of MHD nanofluid. *Ain Shams Engineering Journal*, 2023, 14.9: 102093.
- [32] ALBAIDANI, Mashael M., et al. Numerical analysis of magneto-radiated annular fin natural-convective heat transfer performance using advanced ternary nanofluid considering shape factors with heating source. *Case Studies in Thermal Engineering*, 2023, 44: 102825.
- [33] MISHRA, Vivek K., et al. Numerical analysis of forced convection heat transfer in a nuclear fuel storage vault. *International Journal of Thermal Sciences*, 2022, 173: 107429.

-
- [34] CIEŚLIŃSKI, Janusz T.; KOZAK, Przemysław. Experimental Investigations of Forced Convection of Nanofluids in Smooth, Horizontal, Round Tubes: A Review. *Energies*, 2023, 16.11: 4415.
- [35] B. C. Pak , Y. I. Cho , and H. G. Lorsch , Use of Advanced Low Temperature Heat Transfer Fluid for District Cooling Systems, Int. District Heating and Cooling System Conference , Virginia Beach , VA , vol. 85 , no. 269 , pp. 368 – 376 , 21–24 June 1989 .
- [36] XUAN, Yimin; LI, Qiang. Investigation on convective heat transfer and flow features of nanofluids. *J. Heat transfer*, 2003, 125.1: 151-155.
- [37] WEN, Dongsheng; DING, Yulong. Experimental investigation into convective heat transfer of nanofluids at the entrance region under laminar flow conditions. *International journal of heat and mass transfer*, 2004, 47.24: 5181-5188.
- [38] CHANDRASEKAR, M.; SURESH, S.; BOSE, A. Chandra. Experimental investigations and theoretical determination of thermal conductivity and viscosity of Al₂O₃/water nanofluid. *Experimental thermal and fluid science*, 2010, 34.2: 210-216.
- [39] FOTUKIAN, S. M.; ESFAHANY, M. Nasr. Experimental study of turbulent convective heat transfer and pressure drop of dilute CuO/water nanofluid inside a circular tube. *International communications in heat and mass transfer*, 2010, 37.2: 214-219.
- [40] KANJIRAKAT, Anoop; SADR, Reza. Heat transfer performance of SiO₂-water nanofluid in a plate heat exchanger. In: *Heat Transfer Summer Conference*. American Society of Mechanical Engineers, 2012. p. 267-272.
- [41] HO, C. J.; LIN, Y. J. Turbulent forced convection effectiveness of alumina–water nanofluid in a circular tube with elevated inlet fluid temperatures: An experimental study. *International Communications in Heat and Mass Transfer*, 2014, 57: 247-253.
- [42] GHASEMI, Seyed Ebrahim; RANJBAR, A. A.; HOSSEINI, M. J. Forced convective heat transfer of nanofluid as a coolant flowing through a heat sink: Experimental and numerical study. *Journal of Molecular Liquids*, 2017, 248: 264-270.
- [43] SALARI, Mehdi, et al. Experimental study on forced convection heat transfer of a nanofluid in a heat exchanger filled partially porous material. *Journal of Thermal Analysis and Calorimetry*, 2020, 1-15.
- [44] TALEBI, Mansour, et al. Experimental analysis of forced convection heat transfer of Hybrid Nanofluids in a vertical annulus with cosine heat flux. *Progress in Nuclear Energy*, 2022, 153: 104438.
- [45] SAGHIR, M. Ziad; RAHMAN, Mohammad M. Forced convection of Al₂O₃, Fe₃O₄, ND-Fe₃O₄, and (MWCNT-Fe₃O₄) mixtures in rectangular channels: Experimental and numerical results. *International Journal of Energy Research*, 2022, 46.8: 10002-10019.
- [46] ABDEL-LATIF, Salwa H., et al. Experimental and theoretical investigation of forced convection heat transfer with CNTs and CuO water based nano-fluids. *Kerntechnik*, 2022, 87.3: 336-350.
- [47] SINGH, Vinay, et al. Experimental investigations of thermophysical properties and convective heat transfer of Al₂O₃ and CuO nanofluids in a copper tube: Proposing new correlations. *Biointerface Research in Applied Chemistry*, 2023, 13.3: 229.

-
- [48] POURANFARD, Abdolrasoul, et al. Experimental and numerical study of forced convection heat transfer in a upward two-phase flow of air–water/SiO₂ nanofluid with slug flow regime. *Journal of Thermal Analysis and Calorimetry*, 2023, 148.13: 6501-6514.
- [49] CIEŚLIŃSKI, Janusz T. Numerical modelling of forced convection of nanofluids in smooth, round tubes: A review. *Energies*, 2022, 15.20: 7586.
- [50] MAIGA, Sidi El Becaye, et al. Heat transfer enhancement by using nanofluids in forced convection flows. *International journal of heat and fluid flow*, 2005, 26.4: 530-546.
- [51] Praveen K., et al. Numerical study of turbulent flow and heat transfer characteristics of nanofluids considering variable properties. *International journal of thermal sciences*, 2009, 48.2: 290-302.
- [52] VAJJHA, Ravikanth S.; DAS, Debendra K.; NAMBURU, Praveen K. Numerical study of fluid dynamic and heat transfer performance of Al₂O₃ and CuO nanofluids in the flat tubes of a radiator. *International Journal of Heat and fluid flow*, 2010, 31.4: 613-621.
- [53] CHOI, Jongwook; ZHANG, Yuwen. Numerical simulation of laminar forced convection heat transfer of Al₂O₃–water nanofluid in a pipe with return bend. *International Journal of Thermal Sciences*, 2012, 55: 90-102.
- [54] RAHIM MASHAEI, Payam, et al. Numerical investigation of nanofluid forced convection in channels with discrete heat sources. *Journal of Applied Mathematics*, 2012.
- [55] SELIMEFENDIGIL, Fatih; ÖZTOP, Hakan F. Corrugated conductive partition effects on MHD free convection of CNT-water nanofluid in a cavity. *International Journal of Heat and Mass Transfer*, 2019, 129: 265-277.
- [56] ALSABERY, A. I., et al. Impact of particles tracking model of nanofluid on forced convection heat transfer within a wavy horizontal channel. *International Communications in Heat and Mass Transfer*, 2021, 122: 105176.
- [57] JALILI, Bahram, et al. An investigation into a semi-porous channel's forced convection of nano fluid in the presence of a magnetic field as a result of heat radiation. *Scientific Reports*, 2023, 13.1: 18505.
- [58] SELIMEFENDIGIL, Fatih; ÖZTOP, Hakan F. Combined effects of using multiple porous cylinders and inclined magnetic field on the performance of hybrid nanofluid forced convection. *Journal of Magnetism and Magnetic Materials*, 2023, 565: 170137.
- [59] AKKURT, Nevzat, et al. Analysis of the forced convection via the turbulence transport of the hybrid mixture in three-dimensional L-shaped channel. *Case Studies in Thermal Engineering*, 2023, 41: 102558.
- [60] JAN, Ahmed; MUSHTAQ, Muhammad; HUSSAIN, Muzamil. Heat transfer enhancement of forced convection magnetized cross model ternary hybrid nanofluid flow over a stretching cylinder: Non-similar analysis. *International Journal of Heat and Fluid Flow*, 2024, 106: 109302.
- [61] POP, Ioan; INGHAM, Derek B. *Convective heat transfer: mathematical and computational modelling of viscous fluids and porous media*. Elsevier, 2001.
- [62] MERKIN, J. H. Mixed convection boundary layer flow on a vertical surface in a saturated porous medium. *Journal of Engineering Mathematics*, 1980, 14.4: 301-313.

-
- [63] OSBORNE, D. G.; INCROPERA, F. P. Laminar, mixed convection heat transfer for flow between horizontal parallel plates with asymmetric heating. *International journal of heat and mass transfer*, 1985, 28.1: 207-217.
- [64] ALDOSS, T. K., et al. Magnetohydrodynamic mixed convection from a vertical plate embedded in a porous medium. *Numerical Heat Transfer, Part A: Applications*, 1995, 28.5: 635-645.
- [65] YANG, Orhan Aydin, Wen-Jei. Mixed convection in cavities with a locally heated lower wall and moving sidewalls. *Numerical Heat Transfer: Part A: Applications*, 2000, 37.7: 695-710.
- [66] ABU-MULAWEH, H. I. Turbulent mixed convection flow over a forward-facing step—the effect of step heights. *International Journal of Thermal Sciences*, 2005, 44.2: 155-162.
- [67] MIRMASOUMI, S.; BEHZADMEHR, A. Numerical study of laminar mixed convection of a nanofluid in a horizontal tube using two-phase mixture model. *Applied Thermal Engineering*, 2008, 28.7: 717-727.
- [68] MANSOUR, M. A., et al. Numerical simulation of mixed convection flows in a square lid-driven cavity partially heated from below using nanofluid. *International Communications in Heat and Mass Transfer*, 2010, 37.10: 1504-1512.
- [69] SOUTIJI, E., et al. Numerical analysis of mixed convection heat transfer of Al₂O₃-water nanofluid in a ventilated cavity considering different positions of the outlet port. *Powder Technology*, 2014, 262: 71-81.
- [70] SELIMEFENDIGIL, Fatih; ÖZTOP, Hakan F. MHD mixed convection and entropy generation of power law fluids in a cavity with a partial heater under the effect of a rotating cylinder. *International Journal of Heat and Mass Transfer*, 2016, 98: 40-51.
- [71] WAHID, Nur Syahirah, et al. MHD mixed convection flow of a hybrid nanofluid past a permeable vertical flat plate with thermal radiation effect. *Alexandria Engineering Journal*, 2022, 61.4: 3323-3333.
- [72] ISLAM, Saiful, et al. Numerical investigation with sensitivity study of MHD mixed convective hexagonal heat exchanger using TiO₂-H₂O nanofluid. *Results in Engineering*, 2023, 18: 101136.
- [73] YASIR, Muhammad, et al. Design and fabrication of TiO₂/Nd polyurethane nanofibers based photoreactor: A continuous flow kinetics study for Estriol degradation and mechanism. *Journal of Water Process Engineering*, 2023, 56: 104271.
- [74] HASAN, Md Jahid, et al. Analysis of mixed convection under radiation and magnetohydrodynamics utilizing Kerosene-CNT nanofluid in a lid-driven cavity. *International Journal of Thermofluids*, 2024, 21: 100528.
- [75] ABOOD, Falah A., et al. Enhancing Thermal Performance in a Magnetized Square Cavity: Novel Insights from Mixed Convection of Ag-MgO Nanofluid around a Rotating Cylinder. *International Journal of Thermofluids*, 2024, 100630.
- [76] MOLOKOV, Sergei S.; MOREAU, René; MOFFATT, H. Keith (ed.). *Magnetohydrodynamics: Historical evolution and trends*. Springer Science & Business Media, 2007.
- [77] KEPLER, JOHANNES. *Introduction to Magnetohydrodynamics*. 2016.

-
- [78] MUNSON, Bruce R., et al. *Fundamentals of Fluid Mechanics*, John Wiley & Sons. Inc., USA, 2006.
- [79] SAFI, Safia; BENISSAAD, Smail. Heat and mass transfer in anisotropic porous media. *Advanced in Theoretical and Applied Mechanics*, 2012, 5: 15-26.
- [80] BEJAN, Adrian. *Porous and complex flow structures in modern technologies*. Springer Science & Business Media, 2004.
- [81] CHUNG, T. J. *Computational fluid dynamics*. Cambridge university press, 2002.
- [82] FERZIGER, Joel H.; PERIĆ, Milovan; STREET, Robert L. *Computational methods for fluid dynamics*. Springer, 2019.
- [83] YUNUS, A. Cengel, et al. *Heat transfer: a practical approach*. MacGraw Hill, New York, 2003, 210.
- [84] DOMBEK, Grzegorz; NADOLNY, Zbigniew; MARCINKOWSKA, Agnieszka. Effects of nanoparticles materials on heat transfer in electro-insulating liquids. *Applied Sciences*, 2018, 8.12: 2538.
- [85] X. Shan and D. Montgomery, "On the role of the Hartmann number in magnetohydrodynamic activity," *Plasma Phys. Control. fusion*, vol. 35, no. 5, p. 619, 1993.
- [86] MARTIN, Holger. Nusselt's Fundamental Law of Heat Transfer—Revisited. *Heat transfer engineering*, 2014, 35.3: 246-250.
- [87] MAZUMDER, B. S.; ELDHO, T. I. *An Introduction to Advanced Fluid Dynamics and Fluvial Processes*. CRC Press, 2023.
- [88] ANDERSON, Dale, et al. *Computational fluid mechanics and heat transfer*. CRC press, 2020.
- [89] BHANVASE, Bharat; BARAI, Divya. *Nanofluids for heat and mass transfer: Fundamentals, sustainable manufacturing and applications*. Academic Press, 2021.
- [90] LIU, Gui-Rong; QUEK, Siu Sin. *The finite element method: a practical course*. Butterworth-Heinemann, 2013.
- [91] AKHTER, Rowsanara, et al. Hybrid-nanofluid mixed convection in square cavity subjected to oriented magnetic field and multiple rotating rough cylinders. *Results in Engineering*, 2023, 18: 101100.
- [92] AMINE, Belhadj Mahammed, et al. Magnetohydrodynamics natural convection of a triangular cavity involving Ag-MgO/water hybrid nanofluid and provided with rotating circular barrier and a quarter circular porous medium at its right-angled corner. *Arabian Journal for Science and Engineering*, 2021, 46.12: 12573-12597.
- [93] ISLAM, Tarikul; AKTER, Nahida; JAHAN, Nusrat. MHD free convective heat transfer in a triangular enclosure filled with copper-water nanofluid. *Int. J. Mat. Math. Sci*, 2020, 2.2: 29-38.
- [94] BELHADJ MAHAMMED, Amine, et al. Thermal management of magnetohydrodynamic nanofluid within porous C-shaped cavity with undulated baffle. *Journal of Thermophysics and Heat Transfer*, 2022, 36.3: 594-611.

- [95] GHALI, Djellouli, et al. Mathematical entropy analysis of natural convection of MWCNT—Fe₃O₄/water hybrid nanofluid with parallel magnetic field via Galerkin finite element process. *Symmetry*, 2022, 14.11: 2312.
- [96] REDOUANE, Fares, et al. Entropy study of hybrid (Al₂O₃–Cu/H₂O) Nano-fluid in a cylindrical cavity with wavy sides under the effect of a parallel magnetic field. *Journal of Nanofluids*, 2023, 12.1: 231-241.
- [97] MEBAREK-LOUDINA, F., et al. Entropy and convection effect on magnetized hybrid nanofluid flow inside a trapezoidal cavity with zigzagged wall. *International Communications in Heat and Mass Transfer*, 2021, 125: 105279.
- [98] REDOUANE, Fares, et al. Heat flow saturate of Ag/MgO-water hybrid nanofluid in heated trigonal enclosure with rotate cylindrical cavity by using Galerkin finite element. *Scientific reports*, 2022, 12.1: 2302.
- [99] KADA, Benhanifia, et al. Numerical investigation of forced convection flow of a complex Bingham-Papanastasiou fluid between two concentric cylinders with a wavy inner wall. *Journal of Thermal Engineering*, 2024, 10.1.
- [100] MAHAMMED, Amine Belhadj; FARES, Redouane; LOUNIS, Mourad. Magnetohydrodynamics forced convection of a nanofluid-filled triangular vented cavity provided with a quarter circular porous medium at its right-angled corner. *collectors*, 2021, 1.5.
- [101] REDOUANE, Fares, et al. Influence of entropy on Brinkman–Forchheimer model of MHD hybrid nanofluid flowing in enclosure containing rotating cylinder and undulating porous stratum. *Scientific Reports*, 2021, 11.1: 24316.

ANNEX
&
PUBLICATIONS



Magneto hydrodynamics Natural Convection of a Triangular Cavity Involving Ag-MgO/Water Hybrid Nanofluid and Provided with Rotating Circular Barrier and a Quarter Circular Porous Medium at its Right-Angled Corner

Belhadj Mahammed Amine¹ · Fares Redouane¹ · Lounis Mourad¹ · Wasim Jamshed² · Mohamed R. Eid^{3,4} · Wael Al-Kouz⁵

Received: 13 February 2021 / Accepted: 14 July 2021
© King Fahd University of Petroleum & Minerals 2021

Abstract

The current paper studied the behavior of a triangular cavity occupied with Ag-MgO/water nanofluid under MHD natural convection and provided with a rotating circular barrier, while the right-angled corner is equipped with quarter-circle porous medium and maintained at a fixed hot temperature T_h . Several parameters are tested such as Rayleigh number ($10^3 \leq Ra \leq 10^6$), Hartmann number ($0 \leq Ha \leq 80$) and Darcy number ($10^{-5} \leq Da \leq 0.15$). The obtained results depict the enhancing effect of Ra and the controlling role of the magnetic parameter on heat transport. Increasing the characteristics of the porous media such as the porosity and the permeability showed a substantial impact on the heat transport efficiency within the enclosure. Moreover, the novelty findings in this paper are principally illustrated in the boosting impact of raising the porous medium thickness when it is associated with the growing up of the heated parts of the geometry by increasing the dimension of the radius (r_p). Also, the rotational velocity (ω) and the radius (r_{ob}) of the circular obstacle are tested and showed an important influence on the energy transport within the cavity. Moreover, the obtained results by modifying the length (a) prove its pertinent influence on the heat transfer performance.

Keywords Triangular cavity · Heat transfer · Hybrid nanofluid · Porous medium · Rayleigh number · Hartmann number

Abbreviations

k	Thermal conductivity (W/m k)
L	Dimension of the cavity (m)
r_{ob}	Radius of cylinder (m)
R_p	Radius of porous media (m)
a	Length (m)
Ra	Rayleigh number

Ha	Hartmann number
Nu	Nusselt number
Nu_{ave}	Average Nusselt number
Nu_{loc}	Local Nusselt number
Pr	Prandtl number
Da	Darcy number
x, y	Coordinate (m)
X, Y	Dimensionless coordinate
u, v	Velocity components (m/s)
U, V	Non-dimensional velocity components
T	Temperature ($^{\circ}C$)
p	Pressure (N/m^2)
P	Dimensionless pressure
K	Permeability
g	Gravitational acceleration vector (m/s^2)
F_c	Forchheimer coefficient
B_0	Intensity of magnetic field

Greeks symbols

θ	Dimensionless temperature
ε	Porosity

✉ Fares Redouane
redouane.fares@univ-relizane.dz

¹ LGIDD, Ahmed ZABANA University, 48000 Relizane, Algeria

² Department of Mathematics, Capital University of Science and Technology (CUST), Islamabad 44000, Pakistan

³ Department of Mathematics, Faculty of Science, New Valley University, Al-Kharga, Al-Wadi Al-Gadid 72511, Egypt

⁴ Department of Mathematics, Faculty of Science, Northern Border University, Arar 1321, Saudi Arabia

⁵ Mechanical and Maintenance Engineering Department, German Jordanian University, Amman, Jordan



Thermal Management of Magneto hydrodynamic Nanofluid Within Porous C-Shaped Cavity with Undulated Baffle

Amine Belhadj Mohammed,*¹ Redouane Fares,[†] and Mourad Lounis[‡]
 Ahmed Zabana University, Relizane 48000, Algeria

Wasim Jamshed[§]

Capital University of Science and Technology, Islamabad 44000, Pakistan
 Syed M. Hussain[¶]

Islamic University of Madinah, Medina 42351, Saudi Arabia
 and

Mohamed R. Eid**

Northern Border University, Arar 1321, Saudi Arabia

<https://doi.org/10.2514/1.T6365>

The present work focuses on the Magneto hydrodynamic free convection heat of Ag–water nanofluid involved in a porous C-shaped enclosure equipped with an undulated baffle. Various thermophysical parameters are investigated through this specific configuration, such as Rayleigh number ($10^3 \leq Ra < 10^6$), Hartmann number ($0 \leq Ha \leq 100$), Darcy number ($10^{-5} \leq Da \leq 10^{-2}$), porosity ($0.1 \leq \epsilon \leq 0.8$), and nanoparticles concentration ($0.01 \leq \phi \leq 0.08$). The calculations were carried out through the finite element method for Prandtl number $Pr = 6.83$. The novelty in this paper was the implementation of an inner baffle with a special shape inside the cavity instead of conventional ones and the definition of its optimal dimensions. The uniqueness of this work is that it overcomes the previous research gap by investigating the influence of the specific shape of the cold corrugated baffle on heat flux inside a C-shaped porous chamber. The obtained results show the favorable impact of increasing the thickness ξ and the length λ of this undulated baffle on the heat transmission performance. However, the variation in the undulation number (und) presented a negligible impact.

Nomenclature

a	=	length of the empty side of C cavity, m
Da	=	Darcy number
Ha	=	Hartmann number
K	=	permeability, m^2
Nu	=	Nusselt number
Pr	=	Prandtl number
T	=	temperature, K
U, V	=	nondimensional velocity components
x, y	=	coordinates, m
α	=	thermal diffusivity, m^2/s
ϵ	=	porosity
θ	=	dimensionless temperature
μ	=	dynamic viscosity, $W \cdot m^{-1} \cdot K^{-1}$
ξ	=	baffle thickness, m
σ	=	electrical conductivity, $\Omega \cdot M$

Subscripts

avg	=	average
B_0	=	intensity of magnetic field

c	=	cold
Fc	=	Forchheimer coefficient
f	=	fluid
H	=	hot
k	=	thermal conductivity, $W \cdot m^{-1} \cdot K^{-1}$
L	=	height of cavity, m
loc	=	local
nf	=	nanofluid
np	=	solid particles
P	=	pressure, Pa
p	=	porous medium
Ra	=	Rayleigh number
u, v	=	velocity components, m/s
und	=	number of waves of the undulated baffle
β	=	thermal expansion coefficient, K^{-1}
λ	=	length of the baffle, m
ν	=	kinematic diffusivity, $m^2 \cdot s^{-1}$
ρ	=	density, $kg \cdot m^{-3}$
ϕ	=	solid volume fraction
ψ	=	dimensionless stream function

1. Introduction

IN RECENT years, heat transfer convection has achieved great importance due to its multiple applications in various domains, such as solar-heat systems, chemical processing, electronic devices cooling, heat exchangers, and even nuclear industry [1–10]. Magneto hydrodynamic convection, which represents one of the key topics in heat transfer, has been widely studied, principally after substituting the conventional fluids with nanofluids [11–24]. In terms of history, the first apparition of the term *nanofluids* was caused by Choi [25] to define fluids with suspended particles. Moreover, Hartmann [26] carried out the first study on magneto hydrodynamics. He explored the reaction of fluids between two parallel plates under a magnetic field.

Several types of research have been carried out to investigate the heat transfer behavior of nanofluid within cavities filled partially or entirely by porous media [27]. Chamkha et al. [28] examined the Magneto hydrodynamic convection heat response of Cu–water nano-

Received 27 April 2021; revision received 23 October 2021; accepted for publication 2 November 2021; published online 26 November 2021. Copyright © 2021 by the American Institute of Aeronautics and Astronautics, Inc. All rights reserved. All requests for copying and permission to reprint should be submitted to CCC at www.copyright.com; employ the eISSN 1533-6808 to initiate your request. See also AIAA Rights and Permissions www.aiaa.org/randp.

*Ph.D., Department Mechanical Engineering, Laboratory of Industrial Engineering and Sustainable Development; amine.belhadjmahammed@univ-relizane.dz (Corresponding Author).

[†]Doctor, Department Physics, Laboratory of Industrial Engineering and Sustainable Development.

[‡]Professor, Department Electrical Engineering, Laboratory of Industrial Engineering and Sustainable Development.

[§]Doctor, Department of Mathematics.

[¶]Assist Professor, Department of Mathematics, Faculty of Science.

**Doctor, Department of Mathematics, Faculty of Science.



OPEN

Influence of entropy on Brinkman–Forchheimer model of MHD hybrid nanofluid flowing in enclosure containing rotating cylinder and undulating porous stratum

Fares Redouane¹, Wasim Jamshed^{2,3}, S. Suriya Uma Devi³, Belhadj M. Amine¹, Rabia Safdar⁴, Khaled Al-Farhany⁵, Mohamed R. Eid^{6,7}, Kottakkaran Sooppy Nisar⁸, Abdel-Haleem Abdel-Aty^{9,10} & I. S. Yahia^{11,12,13}

The current article aims to discuss the natural convection heat transfer of Ag/Al₂O₃-water hybrid filled in an enclosure subjected to a uniform magnetic field and provided with a rotating cylinder and an inner undulated porous layer. The various thermo-physical parameters are investigated such as Rayleigh number ($100 \leq Ra \leq 100000$), Hartmann number ($0 \leq Ha \leq 100$), and the nanoparticles concentration ($0.02 \leq \phi \leq 0.08$). Likewise, the rotational speed of the cylinder ($-4000 \leq \omega \leq +4000$), as well as several characteristics related to the porous layer, are examined in its porosity ($0.2 \leq \varepsilon \leq 0.8$), Darcy number ($-100000 \leq Da \leq -100$) which indicates the porous medium permeability and the number of undulations ($0 \leq N \leq 4$). The calculations are carried out based on the Galerkin Finite element method (GFEM) to present the streamlines, isotherms, entropy generation, and average Nusselt numbers in details. The main results proved that increment of Rayleigh number and Darcy number enhances heat transfer convection within the enclosure. Whilst, the porosity presents a minimal impact. Also, the rotational speed in a positive direction has a favorable influence on the heat transfer dispersion across the cavity.

List of symbols

B_0	Intensity of magnetic field
d_m	Diameter of cylinder (m)
C_p	Heat capacitance (J/kg K)

¹LGIDD, Ahmed ZABANA University, Relizane, Algeria. ²Department of Mathematics, Capital University of Science and Technology (CUST), Islamabad 44000, Pakistan. ³Department of Mathematics, KPR Institute of Engineering and Technology, Coimbatore 641407, India. ⁴Department of Mathematics, Lahore College for Women University, Lahore 54000, Pakistan. ⁵Department of Mechanical Engineering, University of Al-Qadisiyah, Al-Qadisiyah 58001, Iraq. ⁶Department of Mathematics, Faculty of Science, New Valley University, Al-Kharga, Al-Wadi Al-Gadid 72511, Egypt. ⁷Department of Mathematics, Faculty of Science, Northern Border University, Arar 1321, Saudi Arabia. ⁸Department of Mathematics, College of Arts and Sciences, Prince Sattam Bin Abdulaziz University, Wadi Aldawaser 11991, Saudi Arabia. ⁹Department of Physics, College of Sciences, University of Bisha, P.O. Box 344, Bisha 61922, Saudi Arabia. ¹⁰Physics Department, Faculty of Science, Al-Azhar University, Assiut 71524, Egypt. ¹¹Laboratory of Nano-Smart Materials for Science and Technology (LNSMST), Department of Physics, Faculty of Science, King Khalid University, P.O. Box 9004, Abha 61413, Saudi Arabia. ¹²Research Center for Advanced Materials Science (RCAMS), King Khalid University, P.O. Box 9004, Abha 61413, Saudi Arabia. ¹³Nanoscience Laboratory for Environmental and Biomedical Applications (NLEBA), Semiconductor Lab., Department of Physics, Faculty of Education, Ain Shams University, Roxy, Cairo 11757, Egypt. ✉email: wasiktk@hotmail.com



Magnetohydrodynamics forced convection of a nanofluid-filled triangular vented cavity provided with a quarter circular porous medium at its right-angled corner

Amine Belhadj Mohammed^{1*}, Redouane Fares², Mourad Lounis³

¹Dept. mechanical engineering, Laboratory of Industrial Engineering and Sustainable Development (LGIDD), Ahmed Zabana University, Relizane, Algeria

²Dept. physics, Laboratory of Industrial Engineering and Sustainable Development (LGIDD), Ahmed Zabana University, Relizane, Algeria

³Dept. electrical engineering, Laboratory of Industrial Engineering and Sustainable Development (LGIDD), Ahmed Zabana University, Relizane, Algeria

*Corresponding author e-mail: amine.belhadjmahammed@cu-relizane.dz

Abstract – *The current study investigated the behavior of a triangular cavity filled with water-based Al_2O_3 nanofluid under a MHD forced convection while the right-angled corner is equipped with quarter circle porous medium and maintained at a uniform hot temperature T_h . Several parameters like Rayleigh number ($10^3 \leq Ra \leq 10^6$) and Hartmann number ($0 \leq Ha \leq 80$) are tested and the results are carried out for two different nanoparticles volume fraction ($\Phi=0.01$ and $\Phi=0.04$). The obtained results depict the enhancing effect of Rayleigh number and the controlling role of the magnetic field on the heat transfer. Moreover, the novelty findings in this paper are principally illustrated in the conjugate impact of adjusting the porous medium and the length of the heated parts of the enclosure by modifying the dimension of the radius(r)*

Keywords: Heat transfer, Magnetohydrodynamics, forced convection, Nanofluid, Porous medium, Rayleigh number, Hartmann number.

[Received: October, Accepted: January 2021]

List of symbols

k Thermal conductivity
 L Height of cavity
 Ra Rayleigh number
 Ha Hartmann number
 Nu Nusselt number
 Pr Prandtl number
 T Temperature

*Research Review of
Engineering and Technologies*



Entropy Study of Hybrid (Al₂O₃–Cu/H₂O) Nano-Fluid in a Cylindrical Cavity with Wavy Sides Under the Effect of a Parallel Magnetic Field

Fares Redouane^{1,*}, Wasim Jamshed², S. Suriya Uma Devi³, M. Prakash⁴, Amine Belhadj Mohammed¹, and Roubi Abdelhak⁵

¹LGIDD, Ahmed ZABANA University, Relizane, 48000, Algeria

²Department of Mathematics, Capital University of Science and Technology (CUST), Islamabad, 44000, Pakistan

³Department of Mathematics, KPR Institute of Engineering and Technology, Coimbatore, 641407, India

⁴Department of Mathematics, Dr. N.G.P Institute of Technology, Coimbatore, India

⁵Department of Mechanical, Laboratory of Industrial Technology Study and Research, University Saad Dahlab, Blida 1, Algeria

The convection and entropy of a hybrid nanofluid were investigated in a cylindrical chamber. Inside the cylinder, we have added a rectangular fin with a temperature of T_h . T_c applied on the right wavy wall. Insulation installed on both the top and bottom walls. The induction of a steady magnetic field is included in this research. Governing equations are resolved by Galerkin finite element method (GFEM) and it's utilized to treat the controlling equations obtained by giving different characteristics of fluid like The porosity, cylinder rayon and the size of the nano particles with Rayleigh, Hartmann and Darcy numbers. This information is crucial for controlling both fluid flow and the heat transfer rate for normal convection. The results of the solution demonstrate that Da influences the entropy and leads to a decrease in the generation of entropy. The Nusselt mean differs in a straight line with the dynamic. The domain of flows through the sublime modes while it acts contrary with the magnetic force. The use of a rectangular fin inside a cylindrical enclosure rather than traditional ones, as well as the evaluation of its optimal dimensions, was novel in this paper. Moreover, the novelty of this study is that it fills a research gap by looking into the effect of the specific shape of the walls of the porous chamber on heat flux.

KEYWORDS: Hybrid Nanofluid, Free Convection, Porous Cylindrical Chamber, Galerkin Finite Element Method.

1. INTRODUCTION

Heat transfer is used in various areas of industry, represented by solar and thermal energy complexes, thermal insulation, metal melting, petrochemicals, cooling electronic components, fiber insulation, etc. Given applications, there is a need for high thermal operation.^{1–9} Many studies were conducted on the subject of nanoparticles in the container and heat transfer rate under the influence of a magnetic field, which was the most important.^{10–15}

Chamkha¹⁶ investigated the hydrodynamic magnetic motion (MHD) and thermal exchange in a rotary device for graphene and graphene/graphene hybrid hybrids. Their results prove that the small parts of hybrid nanoparticles and radiation factors are growing, and thermal exchange

while decreasing with enhanced recycling and magnetic parameters. The findings they reached showed that the normal behavior of the number weighs promotes Riley's digital values, porosity ratio, and the proportion of Darcy. They also found that the increased rate of thermal conductivity in the cavity produced longer and stronger uniforms. Belhadj et al.¹⁷ performed a numerical study to evaluate the thermal behavior of a C-shaped cavity provided with an undulated baffle and filled with Ag/H₂O nanofluid. Their outcomes showed the advantageous effect of raising the dimensions of the waved baffle on the heat transfer performance. However, increasing the undulation number showed an insignificant impact. Dogonchi et al.¹⁸ investigated the impact of natural thermal pregnancy along the magnetic hybrid liquid is considered within a T-shaped dynamic cavity of the T-shaped dynamic cavity of Darcy-Forscheimer-Brenkman summary for long periods of the port. They found that the number of women had improved through the unlimited choices of the ratio and thermal

* Author to whom correspondence should be addressed.
Email: redouane.fares@univ-relizane.dz
Received: 27 February 2022
Accepted: 17 April 2022



OPEN

Heat flow saturate of Ag/MgO-water hybrid nanofluid in heated trigonal enclosure with rotate cylindrical cavity by using Galerkin finite element

Fares Redouane¹, Wasim Jamshed², S. Suriya Uma Devi³, M. Prakash⁴, Nor Ain Azeany Mohd Nasir⁵, Zakia Hammouch⁶, Mohamed R. Eid^{7,8}, Kottakkaran Sooppy Nisar⁹, A. Belhadj Mahammed¹, Abdel-Haleem Abdel-Aty^{10,11}, I. S. Yahia^{12,13,14} & Emad M. Eed¹⁵

MHD Natural convection, which is one of the principal types of convective heat transfer in numerous research of heat exchangers and geothermal energy systems, as well as nanofluids and hybrid nanofluids. This work focuses on the investigation of Natural convective heat transfer evaluation inside a porous triangular cavity filled with silver-magnesium oxide/water hybrid nanofluid [H₂O/Ag-MgO]^{hnf} under a consistent magnetic field. The laminar and incompressible nanofluid flow is taken to account while Darcy–Forchheimer model takes account of the advection inertia effect in the porous sheet. Controlled equations of the work have been approached nondimensional and resolved by Galerkin finite element technique. The numerical analyses were carried out by varying the Darcy, Hartmann, and Rayleigh numbers, porosity, and characteristics of solid volume fraction and flow fields. Further, the findings are reported in streamlines, isotherms and Nusselt numbers. For this work, the parametric impact may be categorized into two groups. One of them has an effect on the structural factors such as triangular form and scale on the physical characteristics of the important outputs such as fluidity and thermal transfer rates. The significant findings are the parameters like Rayleigh and slightly supported by Hartmann along with Darcy number, minimally assists by solid-particle size and rotating factor as clockwise assists the cooler flow at the center and anticlockwise direction assists the warmer flow. Clear raise in heat transporting rate can be obtained for increasing solid-particle size.

¹LGIDD, Ahmed ZABANA University, Relizane, Algeria. ²Department of Mathematics, Capital University of Science and Technology (CUST), Islamabad 44000, Pakistan. ³Department of Mathematics, KPR Institute of Engineering and Technology, Coimbatore 641407, India. ⁴Department of Mathematics, Dr. N.G.P Institute of Technology, Coimbatore, India. ⁵Department of Mathematics, Centre for Defence Foundation Studies, Universiti Pertahanan Nasional Malaysia, Kem Sungai Besi, 57000 Kuala Lumpur, Malaysia. ⁶Département Des Sciences, École Normale Supérieure, Moulay Ismail University of Meknès, 50000 Meknes, Morocco. ⁷Department of Mathematics, Faculty of Science, New Valley University, Al-Kharga, Al-Wadi Al-Gadid 72511, Egypt. ⁸Department of Mathematics, Faculty of Science, Northern Border University, Arar 1321, Saudi Arabia. ⁹Department of Mathematics, College of Arts and Sciences, Prince Sattam Bin Abdulaziz University, Wadi Aldawaser 11991, Saudi Arabia. ¹⁰Department of Physics, College of Sciences, University of Bisha, P.O. Box 344, Bisha 61922, Saudi Arabia. ¹¹Physics Department, Faculty of Science, Al-Azhar University, Assiut 71524, Egypt. ¹²Laboratory of Nano-Smart Materials for Science and Technology (LNSMST), Department of Physics, Faculty of Science, King Khalid University, P.O. Box 9004, Abha 61413, Saudi Arabia. ¹³Research Center for Advanced Materials Science (RCAMS), King Khalid University, P.O. Box 9004, Abha 61413, Saudi Arabia. ¹⁴Nanoscience Laboratory for Environmental and Biomedical Applications (NLEBA), Semiconductor Lab., Department of Physics, Faculty of Education, Ain Shams University, Roxy, Cairo 11757, Egypt. ¹⁵Department of Clinical Laboratory Sciences, College of Applied Medical Sciences, Taif University, P. O. Box 11099, Taif 21944, Saudi Arabia. ✉email: wasiktk@hotmail.com

Article

Mathematical Entropy Analysis of Natural Convection of MWCNT—Fe₃O₄/Water Hybrid Nanofluid with Parallel Magnetic Field via Galerkin Finite Element Process

Djellouli Ghali ¹, Fares Redouane ², Roubi Abdelhak ³, Amine Belhadj Mohammed ², Chikr Djaoutsi Zineb ², Wasim Jamshed ^{4,*}, Mohamed R. Eid ^{5,6}, Sayed M. Eldin ⁷, Awad Musa ^{8,9} and Nor Ain Azeany Mohd Nasir ¹⁰



Citation: Ghali, D.; Redouane, F.; Abdelhak, R.; Belhadj Mohammed, A.; Zineb, C.D.; Jamshed, W.; Eid, M.R.; Eldin, S.M.; Musa, A.; Mohd Nasir, N.A.A. Mathematical Entropy Analysis of Natural Convection of MWCNT—Fe₃O₄/Water Hybrid Nanofluid with Parallel Magnetic Field via Galerkin Finite Element Process. *Symmetry* **2022**, *14*, 2312. <https://doi.org/10.3390/sym14112312>

Academic Editor: Ghulam Rasool

Received: 23 September 2022

Accepted: 26 October 2022

Published: 3 November 2022

Publisher's Note: MDPI stays neutral with regard to jurisdictional claims in published maps and institutional affiliations.



Copyright: © 2022 by the authors. Licensee MDPI, Basel, Switzerland. This article is an open access article distributed under the terms and conditions of the Creative Commons Attribution (CC BY) license (<https://creativecommons.org/licenses/by/4.0/>).

- ¹ Laboratoire de Physique Plasmas des Matériaux Conducteur et Leur Applications—LPPMCA, University of Sciences and Technology of Oran (USTO-MB), Bir El Djir 31000, Algeria
 - ² Laboratory of Industrial Engineering and Sustainable Development—LGIDD, Ahmed Zabana University, Relizane 48000, Algeria
 - ³ Laboratory of Industrial Technology Study and Research, University Saad Dahlab, Blida 09000, Algeria
 - ⁴ Department of Mathematics, Capital University of Science and Technology (CUST), Islamabad 44000, Pakistan
 - ⁵ Department of Mathematics, Faculty of Science, New Valley University, Al-Kharga 72511, Al-Wadi Al-Gadid, Egypt
 - ⁶ Department of Mathematics, Faculty of Science, Northern Border University, Arar 1321, Saudi Arabia
 - ⁷ Center of Research, Faculty of Engineering, Future University in Egypt, New Cairo 11835, Egypt
 - ⁸ Department of Physics, College of Science and Humanities in Al-Aflaj, Prince Sattam bin Abdulaziz University, Al-Aflaj 11912, Saudi Arabia
 - ⁹ Department of Physics, College of Science, Sudan University of Science and Technology, Khartoum 11115, Sudan
 - ¹⁰ Department of Mathematics, Centre for Defense Foundation Studies, Universiti Pertahanan Nasional Malaysia, Kuala Lumpur 57000, Malaysia
- * Correspondence: wasiktk@hotmail.com

Abstract: Heat transfer in a symmetrical cavity with two semi-cylinders was explored in this study. Several parameters, such as ($10^3 \leq Ra \leq 10^6$), ($10^{-5} \leq Da \leq 10^{-2}$), ($0.02 \leq \phi \leq 0.08$), ($0.2 \leq \varepsilon \leq 0.8$), and ($0 \leq Ha \leq 100$) were selected and evaluated in this research. The outcome of the magnetic field and the temperature gradient on the nanofluid flow is considered. The geometric model is therefore described using a symmetry technique. The flow issue for the governing equations has been solved using the Galerkin finite element method (G-FEM), and these solutions are presented in dimensionless form. The equations for energy, motion, and continuity were solved using the application of the COMSOL Multiphysics® software computer package. According to the results, there is a difference in the occurrence of the magnetic parameter and an increase in heat transmission when the right wall is recessed inward. The heat transmission is also significantly reduced when the right wall is exposed to the outside. The number of Nusselt grows directly proportional to the number of nanofluids in the environment. In contrast, all porous media with low Darcy and Hartmann numbers, high porosity, and low volume fraction have high Nusselt numbers. It is found that double streamlines for the hot side and single cooling for Darcy, Rayleigh, and Hartmann numbers. A cold isotherm at various physical parameters is needed in the top cavity. Rayleigh's number and a solid volume fraction raise Darcy's number, increasing heat transmission inside the cavity and thermal entropy determines entropy components.

Keywords: hybrid nanofluid; symmetrical cavity; heat transfer; entropy; magnetic field; galerkin finite element method

1. Introduction

In recent years, experts have been intrigued by Magnetohydrodynamics (MHD) heat transfer due to its vast application in various industries. Boilers, cooling systems, thermal